CAKING OF GRANULAR MATERIALS: AN EXPERIMENTAL AND THEORETICAL STUDY

By

DAUNTEL WYNETTE SPECHT

A DISSERTATION PRESENTED TO THE GRADUATE SCHOOL
OF THE UNIVERSITY OF FLORIDA IN PARTIAL FULFILLMENT
OF THE REQUIREMENTS FOR THE DEGREE OF
DOCTOR OF PHILOSOPHY

UNIVERSITY OF FLORIDA

2006

Copyright 2006

by

Dauntel Wynette Specht

This document is dedicated to Momma, Daddy, Techia and Danyel.

ACKNOWLEDGMENTS

I would like to acknowledge my advisors, Dr. Kerry Johanson and Dr. Spyros Svoronos, for their constant guidance and support. Dr. Johanson's extensive experience in the field of particle technology served as a continuous source of knowledge throughout my studies. Dr. Svoronos's help in all aspects of my graduate studies has been indispensable.

I thank my committee members, Dr. Ray Bucklin and Dr. Oscar Crisalle, and all other faculty who provided useful suggestions for the advancement of my studies. I would also like to thank Dr. Brij Moudgil and the National Science Foundation's Engineering Research Center for Particle Science and Technology and our industrial partners for their financial support.

I gratefully acknowledge all of my group members, Brian Scarlett, Jennifer Curtis, Nicolaie Cristescu, Yakov Rabinovich, Olesya Zhupanska, Claudia Genovese, Ali Abdel-Hadi, Ecivit Bilgili, Mario Hubert, Dimitri Eskin, Nishanth Gopinathan, Madhavan Esayanur, Caner Yurteri, Rhye Hamey, Maria Palazuelos Jorganes, Stephen Tedeschi, Milorad Djomlija, Osama Saada, Julio Castro, Benjamin James, Mark Pepple, and Bill Ketterhagen, for their help with experiments and modeling. I also acknowledge my friends in Gainesville for ultimately making this experience an enjoyable one.

Lastly but certainly not least, I thank my family for their constant love and support. To Momma and Daddy, thanks for believing in me and teaching me that I can do anything that I set my mind to. To Techia and Danyel, thanks for being the best sisters

that a girl could ask for. To Marco, thanks for experiencing the world with me but most of all being my home away from home.

TABLE OF CONTENTS

LIST OF TABLES

LIST OF FIGURES

Abstract of Dissertation Presented to the Graduate School
of the University of Florida in Partial Fulfillment of the
Requirements for the Degree of Doctor of Philosophy

CAKING OF GRANULAR MATERIALS: AN EXPERIMENTAL AND THEORETICAL STUDY

By

Dauntel Wynette Specht

May 2006

Chair: Kerry Johanson
Cochair: Spyros Svoronos
Major Department: Chemical Engineering

Many industries such as food service, pharmaceutical, chemical, and agricultural handle and store materials in granular form. The processing of granular materials can pose many challenges. The materials can gain strength during storage creating flow problems in process equipment. This phenomenon is known as caking and is defined as the process by which free flowing material is transformed into lumps or agglomerates due to changes in environmental conditions. The strength of a cake is a function of various material properties and processing parameters such as temperature, relative humidity, particle size, moisture content, and consolidation stress. A fundamental understanding of the entire caking process is needed in order to predict a caking problem.

In this research, caking based on the mechanism of moisture migration through the particle bed is studied. The influence of moisture content, consolidation stress, particle size, and humidity are investigated. An increase in these variables causes an increase in the unconfined yield strength of the material. Theoretical models exist to describe the

function of particle size and moisture content on the yield strength. However, the consolidation stress is not included in these models. The trend is often qualitatively explained by an increase in the interparticle forces. Applying this theory to the current research yields an incorrect prediction of the unconfined yield strength. It is postulated that the increase in unconfined yield strength is attributed to an increase in the number of major force chains in the shear zone. An increase in the number of major force chains results in the increase of the yield strength of the material. Using the principles of fracture mechanics, a new equation is developed to evaluate the strength of powder cakes. An improvement of existing cake yield strength models is made by including the consolidation stress.

Moisture migration through the particle system and moisture uptake by the particles themselves are significant factors of caking. These processes are modeled using a finite element partial differential equation solver, COMSOL Multiphysics. The heat and mass transport of the system is described as well as the kinetics of the material. The model is used to predict the areas of caking within a given geometry and approximate the unconfined yield strength.

CHAPTER 1
INTRODUCTION

Storage and Handling of Granular Materials

Granular materials are common in all facets of life: from food to baby diapers to geological matter. They encompass the complete range of matter in the form of discrete solid particles. Granular materials are often referred to as bulk solids. Many industries must store and handle bulk solids due to their prevalence in a wide variety of products. In the chemical industry, it is estimated that one-half of the products and at least three quarters of the raw materials are in the form of bulk solids (Nedderman, 1992). With such a vast number of processes involving bulk solids there is a need for a fundamental understanding of the behavior of such materials.

Granular materials behave differently from any other form of matter—solids, liquids, or gases. They tend to exhibit complex behaviors sometimes resembling a solid and other times a liquid or gas (Jenike, 1964). Thus the characterization of granular materials presents a challenge unlike any other. It has been estimated that industries processing bulk solids total one trillion dollars a year in gross sales in the United States and they operate at only 63 percent of capacity. By comparison, industries that rely on fluid transport processes operate at 84 percent of design capacity (Merrow, 1988). Due to the often inadequate and unreliable design of particulate processes, there exists a significant discrepancy in the efficiency of particulate operations compared to fluid operations. Many of the problems in particulate operations deal with the flow of material through the process. Often times it is the lack of flow that creates additional problems

such as limited capacity of the process equipment and product degradation. One type of flow problem is caking. A caking event often occurs when a bulk solid does not flow and is allowed to remain stagnant over a period of time.

Caking in Industrial Processes

Bulk solids such as food powders, detergents, pharmaceuticals, feedstocks, fertilizers, and inorganic salts often gain strength during storage. The increase in strength is caused by particles bonding together at contact points through a cementing action. This phenomenon is known as caking and can be defined as the process by which free flowing materials are transformed into lumps and agglomerates due to changes in atmospheric or process conditions. More precisely, caking is the increase in bulk cohesive strength due to changes in interparticle forces.

Traditional interparticle forces such as the formation of liquid bridges, Van der Waals forces, or electrostatic forces can cause an increase in bulk cohesive strength. However, none of these phenomena alone cause caking. Caking occurs when the surface of the particle is modified over time to create interparticle bonds due to the formation of solid bridges between similar or dissimilar materials. Thus, the presence traditional interparticle forces may initiate the caking process, but the advent of caking requires some mechanism to change these forces into solid bridges.

Caking is the accumulation of smaller particles held together by solid bridges to produce a cluster of particles. This phenomenon is related to agglomeration. Agglomeration techniques are often used to improve the shape, appearance and handling properties of materials (Schubert, 1981). This can result in better flow characteristics, improved packing density, dust-free operations and faster dissolution in liquids (Aguilera *et al.*, 1995). However agglomeration is unwanted and unexpected in the case of caking.

This is attributed to the fact that the process of caking is uncontrolled and the outcome can be useless material. In the food and pharmaceutical industries, the effect of caking may be detrimental to the process and product. These problems often result in the loss of quality and function of a product (Purutyan *et al.*, 2005).

Regardless of the reason for caking, the presence of such agglomerates causes significant problems in process equipment (Johanson and Paul, 1996). Severe caking can result in the solidification of the entire mass within a silo as shown in Figure 1-1. Moreover, consumer products such as detergent and food powders can cake during storage both prior to purchase and after initial use. Hence, the problems of handling such products are often passed on to the consumers.

Figure 1-1. Top down view of a silo wall with a thick layer of caked material attached.

Currently, there are no predictive tools to forecast the likelihood of a caking event occurring. The industry must rely on empirical knowledge of caking to provide solutions to the problem. This ranges from controlling the process environment to maintaining a regular cleaning schedule. A common practice for minimizing the effects of caking is the maintenance of a controlled environment surrounding the process; i.e., the temperature and relative humidity are maintained at a level such that caking may not be induced. The

material response to temperature and relative humidity conditions are determined by measuring sorption isotherms. The isotherms give an indication of the hygroscopic nature of the material and the amount of moisture adsorbed at a specific temperature and relative humidity. In situations where controlling the environmental parameters is not feasible, flow aids are sometimes introduced into the product mixture. Flow aids act as a physical barrier or moisture barrier between particles that exhibit caking tendencies. However, when controlled environments and flow aids both fail, brute force is used to dislodge the cake from process equipment. These actions may result in damage to the equipment and personal injuries. Furthermore, if the caking continues to be a persistent problem, a regular cleaning schedule of the process equipment is established.

Aim and Outline of Dissertation

A fundamental knowledge of the caking phenomenon appears to be non-existent. Most of the studies on caking are experimental, focusing on empirical solutions to the problem. Many of these solutions are not universally applicable. There are few studies which concentrated on predicting the strength of caking and the moisture diffusion through the bulk. Often times these studies investigate ideal situations and are not suitable for real materials. As a consequence, when new products are developed it requires a great deal of time, effort, and money to diagnose and remedy a caking problem.

Caking is a problem that may be solved in two ways: before the initiation of an event or eliminated after its existence. The goal of this research is to understand the variables that are involved to induce caking. This will enable the prediction as well as the prevention of a caking problem. To accomplish this, a comprehensive knowledge base of the caking phenomenon must be established. With this knowledge it is then possible to

develop a model to predict the onset and strength of caking. The following objectives are proposed to achieve the goals of the research:

- Understand the mechanisms of caking as well as the material properties and process conditions necessary to induce a caking event.
- Measure the cake strength as a function of process variables.
- Quantify the hygroscopic nature of the bulk material by measuring adsorption isotherms.
- Develop a model to predict the onset of caking based on the moisture migration through the bulk.
- Develop a model to predict the strength of caking based on the process variables.

The research plan includes both an experimental and a theoretical investigation to fully describe the caking process. The experimental work involves measuring the bulk cohesive strength and the adsorption isotherms. In the theoretical studies various parameters from the experimental work will be used to develop a mathematical model of the caking process. In chapter 2 the reader is further introduced to caking and the material properties and process parameters influencing the strength of cakes. Included in this chapter are the possible mechanisms of caking and interparticle bond formation. Often times there are several mechanisms involved in a caking event. It is beyond the scope of this dissertation to investigate every mechanism. Therefore, the focus of this study is moisture migration caking. The various methods for quantifying cake strength are discussed as well as the testing apparatus suitable for this purpose. Experimental data of the bulk cohesive strength are presented and explained in regards to observations of other researchers.

In order for moisture migration caking to occur, the bulk material must possess a certain affinity for water (in the form of moisture). Hence the interactions between the

bulk solid and moisture in the system must be understood. This is accomplished by measuring the adsorption isotherms of the material. Chapter 3 provides a brief introduction into adsorption isotherms and presents experimental data as a function of temperature. The kinetics of sorption are also presented in this chapter.

Using the sorption kinetics the moisture migration through the bulk can be modeled. In chapter 4, finite element methods are employed to predict the migration of moisture using an improved model. Many of the existing models assume that the convection in the system is negligible. This research shows that the free convection enhances moisture migration, making it a significant contributor to caking.

Chapter 5 begins with a discussion of previous models for predicting the cake strength. These models do not adequately predict the strength and they are based on single process variables. A new model for predicting the strength is developed which incorporates all the significant parameters of caking. The novelty of the model is the inclusion of the consolidation stress to predict the strength of the material. The experimental data from chapter 2 are used to verify the model.

The final chapter summarizes the findings of this study and provides suggestions for future research in the study of caking.

CHAPTER 2
CAKING AND CAKING CONDITIONS

This chapter discusses the various mechanisms of caking along with the methods for quantifying bulk cohesive strength. The material properties and process parameters which influence the initiation of a caking event as well as the strength of caking are the focus of this chapter.

Mechanisms of Caking

A powder cake is formed by numerous solid bridges bonding particles together. The mechanisms of solid bridge formation are therefore the key to cake formation. There are several mechanisms for solid bridge formation. Throughout a single caking event more than one mechanism can contribute to the bulk cohesive strength. An understanding of all the mechanisms of solid bridge formation is essential for a thorough explanation of the caking process.

Rumpf (1958) was the first to propose several mechanisms for the formation of solid bridges. He named crystallization, sintering, chemical reaction, partial surface melting, and liquid binder solidification as causes for bridge formation. More recently other researchers (Noel *et al.*, 1990 and Farber *et al.*, 2003) have suggested that glass transition may be a potential caking mechanism. The following is a list of mechanisms and a short summary of each phenomenon.

- **Crystallization** – Materials that are soluble or slightly soluble are subject to this mechanism. This includes many chemicals and fertilizers. The moisture content of the solid increases as water vapor condenses onto the surface of the particle. A portion of the surface material dissolves and bridges are formed at contact points

between particles. A subsequent change in moisture content evaporates the liquid in the bridge leaving solid crystal bridges between particles.

- **Sintering** – Many useful products containing powder metals and ceramics are formed by this mechanism. The molecules or atoms of the material diffuse at the contact points of the particles to form solid bridges. Sintering usually takes place at 1/2 to 2/3 of the melting temperature. Direct reduction of iron ore is one example of a situation where this type of caking is undesired.

- **Chemical reaction** or **binder hardening** – The production of fiberboard from resin impregnated wood chips or flakes makes use of this mechanism. A reaction occurs between two different materials to form bridges between the particles much like mortar between bricks. Binder material may be used to form the bridges. Unlike crystallization, the binder liquid does not evaporate but is incorporated into the structure of the bridges either by chemical reaction or binder solidification.

- **Partial melting** – Ice crystals and snow are products of this mechanism. A pressure induced phase change or a temperature change caused by local friction between the particles at contact points causes the surface material to melt and consecutively solidify, thereby forming bridges.

- **Glass transition** – Many pharmaceuticals and food products are subject to this mechanism of caking. An increase in surface moisture causes a lowering of the glass transition temperature T_g of the solid material. As T_g lowers, particles are cemented together by plastic creep. The material changes from a hard crystalline phase into an amorphous plastic phase. A subsequent change in moisture content increases the glass transition temperature, solidifying the amorphous mass.

The mechanisms of glass transition and crystallization are dominant in the cases of undesired caking (Pietsch, 1969; Aguilera *et al*., 1995; Johanson *et al*., 1996; Hancock *et al*., 1998). In these situations, the formation of a cake is initiated from the condensation of moisture onto the surface of individual particles in a bulk assembly. The moisture adsorbs onto the particle surface and migrates through the bulk at particular process conditions such as temperature and relative humidity. A change in these parameters during storage acts as a driving force to induce periodic condensation and evaporation of moisture on a particle surface. Once the moisture is adsorbed it can absorb into the particle creating a layer of amorphous material in the case of glass transition. The

moisture can also remain at the surface causing the surface of the particle to dissolve and crystallize during desorption of the moisture.

The mechanism of crystallization and associated moisture migration are chosen as the focus of this caking research. This type of caking is prevalent in many industries that handle crystalline materials. Although the focus of this research is crystallization caking, the moisture migration analysis is applicable to all mechanisms involving the sorption of water vapor.

Model of Moisture Migration Caking

Solid bridge formation by crystallization is initiated by the presence of moisture in the environment or in the particle. Frequently, a change in process conditions such as an increase in temperature or relative humidity creates a moisture concentration gradient in the material. Moisture migrates through the interstitial voids of the bulk adsorbing on the surface of particles at the contact points to form liquid bridges. A local increase in the moisture content causes slight dissolution of the particles. A subsequent change in the local temperature or relative humidity causes the surface moisture to evaporate and the material at the contact points to crystallize and form a solid bridge. This process is influenced by process parameters (temperature, relative humidity, consolidation pressure, storage time) and material properties (initial moisture content and particle size). The bulk cohesive strength varies with the magnitude of these parameters. A systematic study of the caking strength with regard to the process parameters is required for a thorough understanding of this process. This includes the effect of moisture released or adsorbed by the particle and the number of temperature or humidity cycles during storage. From this information a model to predict and prevent caking can be developed.

Quantifying the Bulk Cohesive Strength of Caking

Several techniques have been employed to quantify caking and study the effects of properties influencing the bulk cohesive strength of a material. These methods include measuring the unconfined yield strength using direct shear testers, measuring tensile strength using tensile tests, and measuring yield stresses using penetration testing. In addition, measuring the thickness of a caked layer of material and classifying the degree of caking are used to characterize cake strength. A review of the available methods for testing bulk cohesive strength is given below.

Direct Shear Testers

Direct shear testers are used to characterize the flow of powders and granular materials. One characteristic of flow is the strength of the material or the unconfined yield strength f_c. This property is not directly measured. It is extrapolated from shear stress data by the construction of Mohr circles. The shear stress data are measured using direct shear testers. Direct shear testers are constructed of two parts: a stationary part and a moving part. The moving part is displaced relative to the stationary part such that the powder shears and a shear zone is created. Prior to shear the powders are consolidated to a predefined state by applying a load normal to the shear plane. The tester will, after a short transition state, deform the powder with a steady state shear force which is dependent on the applied normal load. The strength of the powder is a function of the applied normal load (or consolidation load). When the powder is in the steady state condition, the deformation is stopped. The normal load is decreased and the sample sheared to instant failure. This process is repeated several times with different failure normal loads. The steady state and failure data are used to construct Mohr circles. The Mohr circles define the state of stress of the powder in the τ-σ plane (shear stress vs.

normal stress). The unconfined yield strength can be determined from the Mohr circles. Figure 2-1 shows an example of Mohr circles. The failure points from the shear tests form the yield locus. The large (limiting) Mohr circle is tangent to this yield locus and includes the steady state condition. The Mohr circle intersects the x-axis at the major and minor principle stress, σ_3 and σ_1, respectively. The unconfined yield strength, f_c, is the major principle stress of the Mohr circle that is tangent to the yield locus and has a minor principle stress of zero (ASTM, 2002).

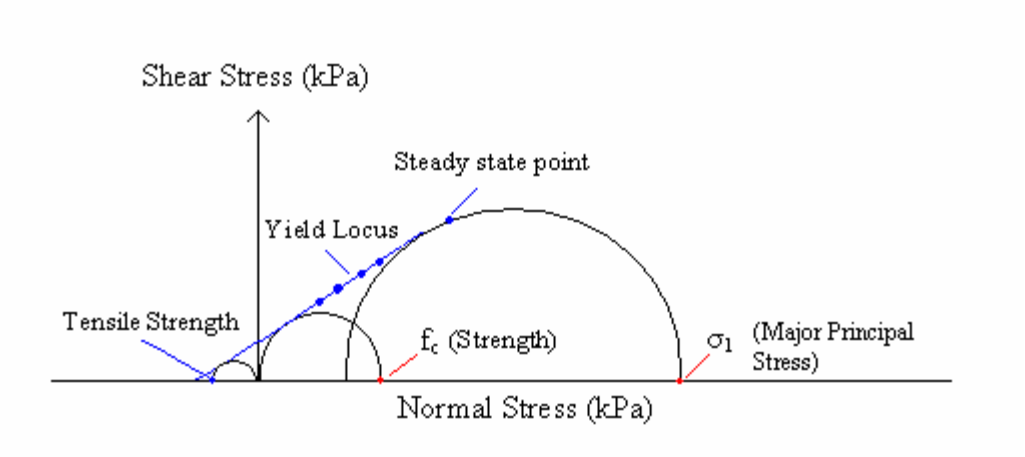

Figure 2-1. Representation of the two limiting Mohr circles, showing the major principal stress of the steady state condition σ_1 and the unconfined yield strength f_c.

Shear testers are very useful for designing equipment for the storage and handling of bulk materials. The disadvantage of using direct shear testers is that multiple experiments are required to find the unconfined yield strength. Using shear testers can be time consuming for measuring cake strength due to the time-induced nature of the caking process. An exception to this is the Johanson Indicizer® which estimates the unconfined yield strength with a single test. The measurement principles of this device are discussed in detail in a later section.

Tensile Testers

Tensile testers are used to determine the tensile strength of materials. From the test various mechanical properties, besides the tensile strength, can be deducted from the stress-strain curve. There are many types of tensile testers, two of which are the horizontal (Leaper *et al.*, 2003) and vertical testers (Pietsch, 1969a, and Schweiger *et al.*, 1999) used for measuring the strength of granular material. The horizontal tester consists of a cylindrical split cell with one part rigidly connected to a load cell and the other part moving. The tensile strength is measured by moving one half of the split cell away from the load cell until the sample breaks. For a vertical tester the sample is prepared outside of the tester. After the cake is formed, the sample is glued between two platens. The platens are moved in opposite directions until the sample breaks. For both types of testers, the force required to break the sample divided by the cross sectional area of the sample defines the tensile strength.

The difference between tensile testers and shear testers is the mechanism of breakage or shear. With shear testers, a shearing action is needed to break the cake. Tensile testers use a tensile force to break the cake. The most active force in the breakage of bonds between particles is often a shear force (Pietsch, 1969b). The tensile strength and the unconfined yield strength are defined by two different Mohr circles of the same yield locus. The tensile force is considered a negative force and the unconfined yield strength is a positive force. The tensile strength σ_t is the x-intercept of the yield locus as shown in Figure 2-1.

Penetration Testing

The bulk cohesive strength of a cake can be measured by cone penetration. This technique was adapted from soil mechanics where it has been used for years to measure

geotechnical parameters of soil. The measurement apparatus consists of a cone and a testing machine. Similar to tensile tests the caked samples are formed in a cylindrical die. The diameter of the die is large enough such that the walls are at a great enough distance from the failure plane that allows the assumption that the fail surface is unconfined. After the cakes are formed, a cone indents the surface to a defined depth and the penetration force is recorded as function of penetration depth. The penetration force at a given depth is proportional to the unconfined yield strength (Knight, 1988). Similar to shear tests the sample fails in shear but the cone only acts over a limited area of the cake. This technique does not require specialized equipment for evaluating the cake strength and the tests are not time-consuming.

Crushing Test or Uniaxial Compression

The crushing test is frequently used in the food industry to study the cohesion of various food powders (Down *et al.*, 1985 and Rennie *et al.*, 1999). The preparation of the caked sample is similar to that of tensile and penetration tests. The powders are consolidated into a cylindrical mold. After the cake is formed it is removed from the mold and placed between two platens of a compression testing machine. The sample is axially loaded until the cake fails. The stress at which the cake breaks is defined as the unconfined yield stress. The cake must be strong enough to withstand the removal from the mold. Thus the caked samples must exhibit a minimum strength for measurements to be possible. This measuring technique is directly related to the theory of the unconfined yield strength. Unlike the shear testers, the unconfined yield stress of the material is measured directly. For shear cell data, the unconfined yield strength is extrapolated using Mohr circles.

Choosing a Tester

Although there are many testers and numerous methods available to investigate the strength of caking, direct shear testers are used in this research to quantify the bulk cohesive stresses. This choice is partly due to the availability and access to direct shear cells but also because the important information related to caking is obtained in an efficient and accurate manner.

The Johanson Hang-Up Indicizer® and the Schulze shear cell are used in this study. The Indicizer® is used to measure the strength of the cakes as a function of temperature cycling, initial moisture content, consolidation load and particle size. The Schulze cell is used to measure the strength of the cakes as a function of temperature and relative humidity cycling, consolidation load, and time.

Johanson Indicizer

The Johanson Hang-Up Indicizer® is a powder flow tester used to measure material flow properties. The Indicizer® is chosen for its ability to estimate the unconfined yield strength from a single test. Many other shear testers indirectly measure the unconfined yield strength through a series of experiments. This requires the measurement of a yield locus and construction of Mohr circles to determine the unconfined yield strength. Due to the possible error introduced from inconsistent mixtures (cakes) it is advantageous to minimize this error by using a single experiment for the strength estimation.

The test cell used to estimate the unconfined yield strength with the Johanson Indicizer® is shown in Figure 2-2 (Johanson, 1992). The test cell consists of an inner piston, outer piston and lower piston. For the typical strength test, the sample is first consolidated to a known stress state. The consolidation load and the lower piston are removed after consolidation such that the sample is in an unconfined state. The inner

piston then moved downward to fail the sample. The diameter of the inner piston is smaller than that of the lower piston. This configuration allows the creation of an inverted conical shear zone during failure as shown in Figure 2-3. A force balance on the material displaced from the tester during failure is used to relate the shear stress and normal stress acting at the walls of this conical section to the force applied on the inner piston.

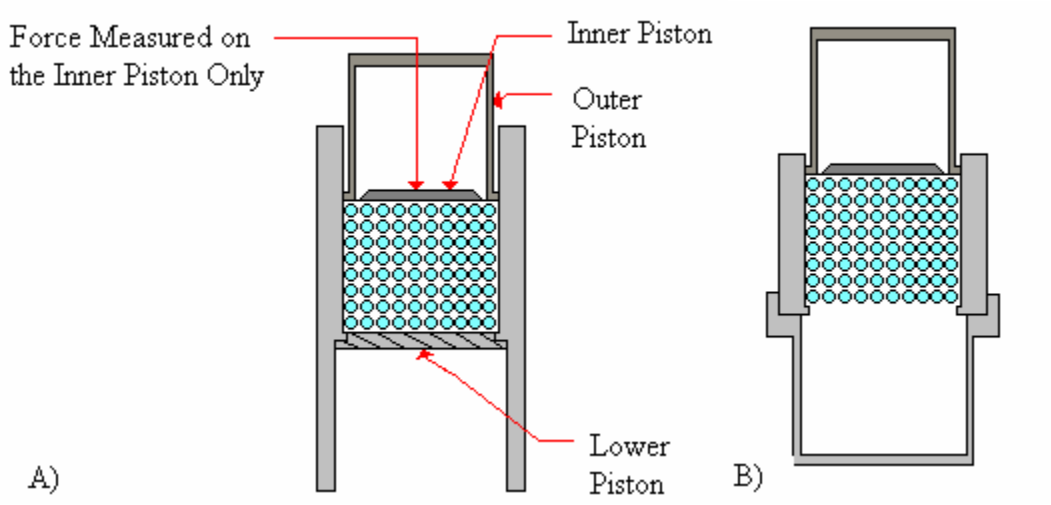

Figure 2-2. Johanson Indicizer test cell. A) the original test cell and B) modified test cell.

The force balance on the conical section is given in equation 2-1 where P is the consolidation load, V_s is the volume of the sample, ρ_b is the bulk density of the material and S is the surface area of the shear zone. The equation accounts for the force of the material within the inverted conical section on the inner piston, the weight of the material in this section, and the normal and shear stresses acting on the inverted conical section.

$$P + \rho_b g V_s = \tau \cdot S \cos\theta - \sigma \cdot S \sin\theta \qquad (2\text{-}1)$$

The diverging character of this failure zone (flow channel) makes it possible to estimate the unconfined yield strength. If it is assumed that the material in the test cell is in an unconfined state of stress and the piston is pushed through the material forming a shear plane. The unconfined Mohr circle in Figure 2-3 represents this unique state of

stress. The shear stress acting on the failure plane is τ as shown in Figure 2-3. The normal stress acting on the shear plane is σ as shown in the same figure. The geometry of the Mohr circle is used to relate the shear and normal stresses to the unconfined yield strength f_c and the internal friction angle ϕ. These relationships are given in equations 2-2 and 2-3.

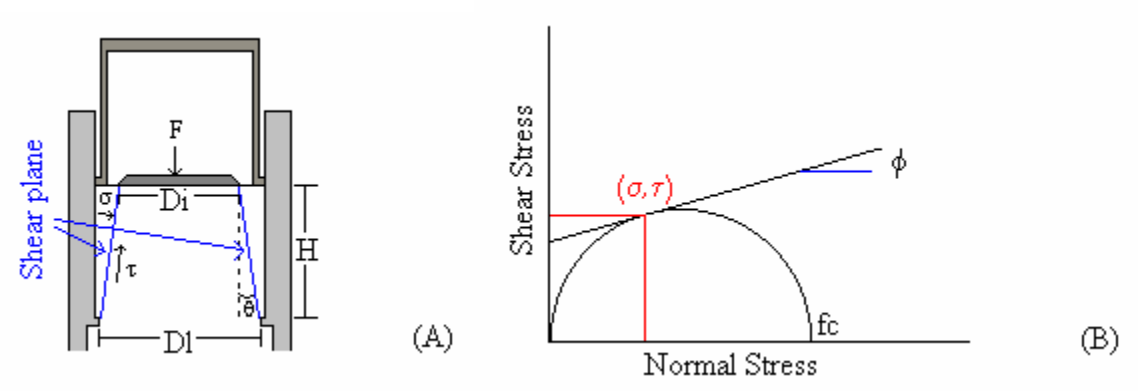

Figure 2-3. Schematic of the standard Indicizer® test cell (A) and Mohr circle used for calculation of the unconfined yield strength (B).

$$\sigma = \frac{1}{2} f_c \left(1 - \sin\phi\right) \tag{2-2}$$

$$\tau = \frac{1}{2} f_c \cos\phi \tag{2-3}$$

The volume of the material V_s that is displaced from the tester is given by

$$V_s = \frac{1}{12} \pi H \left(D_i^2 + D_i D_l + D_l^2\right) \tag{2-4}$$

where H is the height of the sample and D_i and D_l are the inner and lower diameters of the pistons, respectively.

The surface area of the shear zone is

$$S = \frac{1}{4} \pi \frac{D_l^2 - D_i^2}{\sin\theta} \tag{2-5}$$

The dimensions of the test cell define the angle θ of the shear zone.

$$\tan\theta = \frac{D_l - D_i}{2H} \tag{2-6}$$

The unconfined yield strength is calculated by substituting equations 2-2 through 2-6 into equation 2-1. This yields a value for the unconfined yield strength based on the dimensions of the test cell, bulk density and the force applied by the inner piston. It is assumed that the shear angle θ is small.

$$f_c = \frac{1}{3}\frac{\rho_b \pi H\left(D_i^2 + D_i D_l + D_l^2\right) + 12F}{\pi H \cos\phi\left(D_i + D_l\right)} \tag{2-7}$$

Failure with the Indicizer® is a two step process. First there is an increase in compaction stress, up to a set maximum value. The lower piston is moved downward causing the material to be supported by the lip. Then the inner piston moves at a steady rate to shear the material. After the initial failure, the shear stress and normal stress acting on the displaced material decrease to the conditions of steady flow. This value is associated with the shape of the flow channel formed after failure (inverted conical section). It is critical that the shear stress on the flow channel walls be less than the shear stress during failure to assure unconfined conditions. The test is invalid if this condition is not met. The diverging nature of the flow channel ensures that the normal stress is always greater that the confining wall stress.

The Johanson Indicizer® operates in two modes, normal and scientific. In the scientific mode, the sample can be sheared without consolidation and the user manually enters the consolidation load. For the cake strength measurements the tester is operating in the scientific mode. The consolidation load applied automatically by the tester is not required because the cakes are consolidated before the strength measurements. Pre-

consolidation is performed on a consolidation bench external to the tester and these samples are placed in the Johanson Indicizer® for failure. The test cell was modified as shown in Figure 2-2 for the cake strength measurements. The modified cell consists of two parts and the lower piston becomes inoperable.

The cakes are formed on a consolidation bench as shown in Figure 2-4. The bench is housed in an environmental chamber where the temperature and relative humidity of the surroundings are controlled. The bench is equipped with a strip heater to control the temperature, position transducers to monitor the axial strain, and load cells to monitor radial stress on the powder. The powder sample is contained in a 3" diameter cylindrical cell. The cell is constructed from phenolic, an insulating material, to prevent dissipation of heat through the cylinder walls.

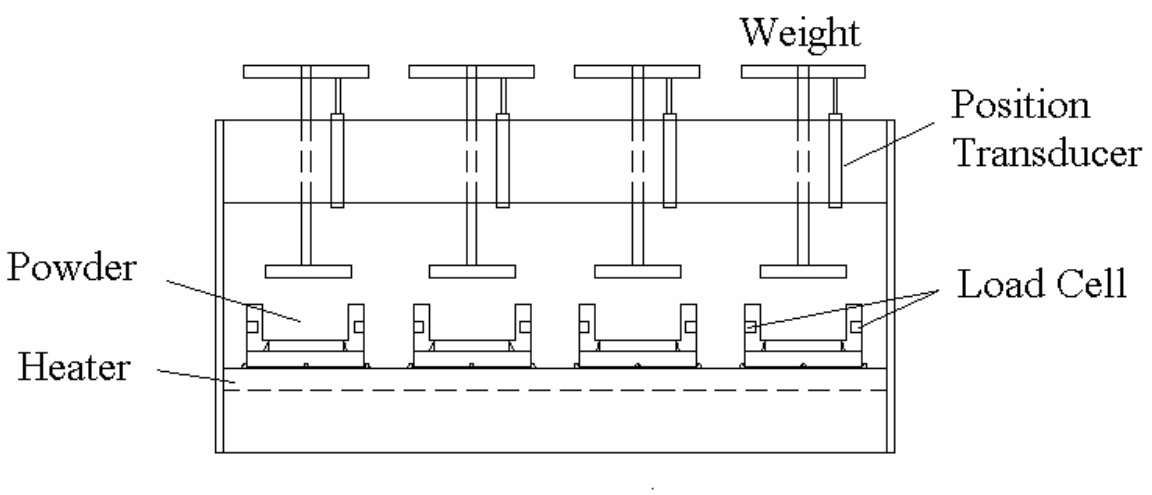

Figure 2-4. Consolidation bench used for making the caked samples.

The procedure for making the cakes and measuring the strength is given in detail below:

- Each cake consists of a mixture of sodium carbonate monohydrate and decahydrate. The decahydrate provides a source of moisture for the caking process and the monohydrate acts as sink for moisture. The components are mixed together and a portion of each sample is reserved to measure the initial moisture content with an Ohaus MB45 moisture analyzer.

- The powder cells are filled using a special feeder to eliminate segregation. The sample is consolidated by weights that are placed on top of the piston.

- The temperature profile mimics the changes that occur from day to night within a metallic bin stored outside and exposed to direct sunlight. It is a ramp and hold, as shown in figure 2-5, varying from 25°C to 50°C and back in a 24 hour cycle. The cakes are held at each temperature for approximately 7.5 hours and the temperature is increased or decreased at a rate of 2° per minute.

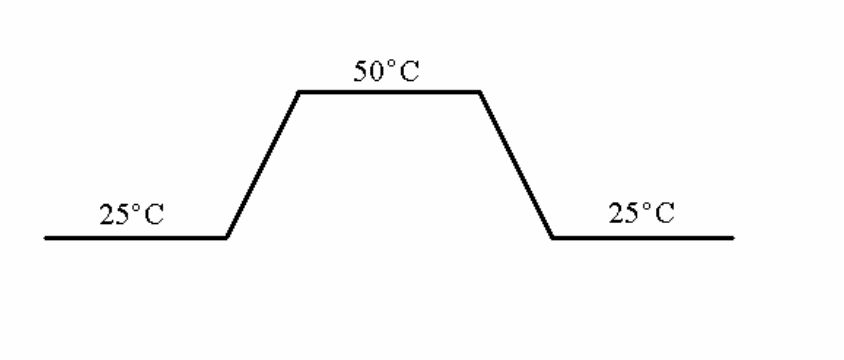

Figure 2-5. Temperature profile used for preparing the cakes

- After the temperature cycle is complete, the cakes are carefully moved from the consolidation bench and placed in the modified Indicizer® test cell. Finally, the strength is measured using the Johanson Indicizer®.

Schulze Shear Tester

The Schulze shear cell is a powder tester which is often used to measure the characteristics of powder flow. A schematic of this cell is shown in Figure 2-6. The powder is contained in an annular base which has an adjustable annular velocity. A top lid with short vanes sticking into the powder is prevented from rotating by tension bars which are connected to load cells. When the base rotates, the powder will shear somewhere between the bottom of the base and the vanes of the top lid. The load cells measure the force that is needed to keep the top lid in place. The measured force is equivalent to the shear force. The normal stress on the powder can be adjusted with weigths. The measurement procedure using the Schulze shear cell has been standarized by ASTM (ASTM, 2002).

A)

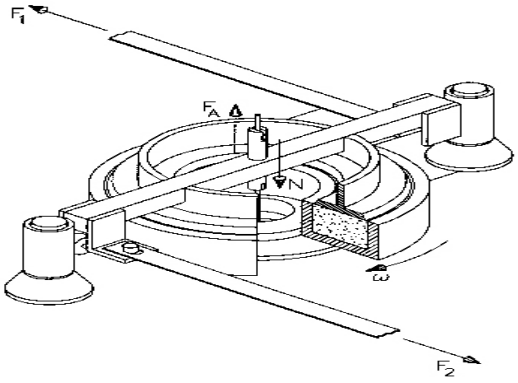

B)

Figure 2-6. Schulze shear tester: (A) image and (B) schematic.

The rationale for using the Schulze cell was to investigate the effects of relative humidity cycling on the strength of the material. A modified cell is used to enable the humidity cycling in the cell. This cell was designed for a previous study which investigated the effects of airflow on material flow properties. A schematic of the modified cell is shown in Figure 2-7. The modified tester can accommodate air flow through the cell. It has a permeable lid and the air is introduced from the bottom of the cell and leaves through the top lid. A porous membrane with a moderate pressure drop is used to ensure that the air is dispersed evenly on the bottom on the cell. The inlet air is conditioned with saturated salt solutions to control the relative humidity of the sample (Greenspan, 1977 and ASTM, 1996).

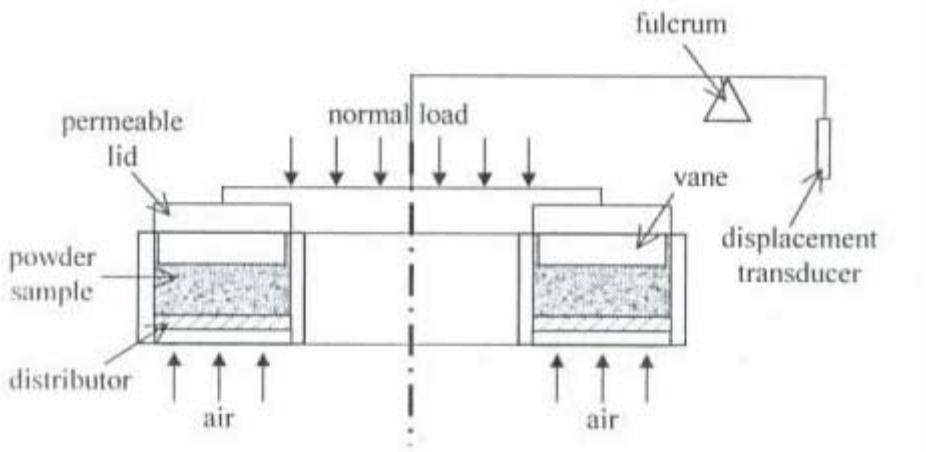

Figure 2-7. Schematic of the permeable Schulze cell.

The procedure for measuring the cake strength follows the ASTM Standard Shear Test Method for Bulk Solids Using the Schulze Ring Shear Tester (ASTM, 2002) with the following modifications.

- The sample is sheared to steady state and then held under a normal load for a period of 24 hours. Throughout this time, air is blown through the sample to equilibrate at a specified relative humidity. Humid air is passed through the sample for 12 hours to ensure that the system is in equilibrium. The moisture is adsorbed onto the surface of the particles and liquid bridges are formed between adjacent particles. Subsequently, dry air is passed through the sample such that the bridges solidify to form the cake. After drying the sample the air flow is stopped and the sample is sheared to determine the increase in failure stress.

- A new powder sample must be used for each point on the yield locus due to the formation of cakes in the cell. The points on the yield locus are measured for each relative humidity to create a family of loci. The loci are used to construct Mohr circles that determine the unconfined yield strength, f_c and the major principal stress, σ_1. Figure 2-1 is a schematic of data collected from the Schulze cell.

The Schulze cell is also used to measure the effects of temperature cycling on the strength of the material. A flexible heater is attached to the inner and outer circumference of the test cell. The temperature of the cell is controlled to the temperature profile as shown in Figure 2-5. Prior to exposure to the temperature profile the yield locus of the material is measured according to the ASTM procedure. After the temperature cycle the

yield locus of the caked sample is measured. Each point of this yield locus requires a new sample. The data from the Schulze cell experiments are compared to the results from the Johanson Indicizer®.

Unconfined Yield Strength Results

Effect of Moisture Content and Consolidation Pressure

The initial moisture content of the powder is important because it gives insight into the material's tendency to cake and the extent of caking. Materials with excess water have the ability to cake depending on the material properties and storage conditions. It has been observed that powders with higher moisture contents tend to exhibit a stronger propensity for caking than ones with lower moisture contents.

Sodium carbonate decahydrate with a water content of 61.2 % is used to vary the moisture content of the samples. The water is crystalline water contained in the structure of the material. At 32˚C, the material begins to decompose and loses water. Therefore adjusting the percentage decahydrate in a mixture effectively varies the moisture content of the sample. The unconfined yield strength results, from the Indicizer®, as a function of percentage sodium carbonate decahydrate in the mixture can be seen in Figure 2-8. The results indicate that the unconfined yield strength of the cakes increases as the percentage decahydrate increases. Other researchers have also observed that the cake strength increases with an increase in moisture content (Pietsch, 1969).

It can also be seen that only a small percentage of decahydrate is needed to yield strong cakes. If a material is very hygroscopic, such as sodium carbonate monohydrate, the minimum moisture content to induce a caking event is very low. Therefore the storage conditions of these materials are a vital factor in controlling the unwanted caking. At higher percentages of decahydrate (beyond 4%) the cakes are too strong to be

measured with the Johanson Indicizer®. The measurement limit of the Indicizer® is stated to be 2000 kPa (Johanson, 1992).

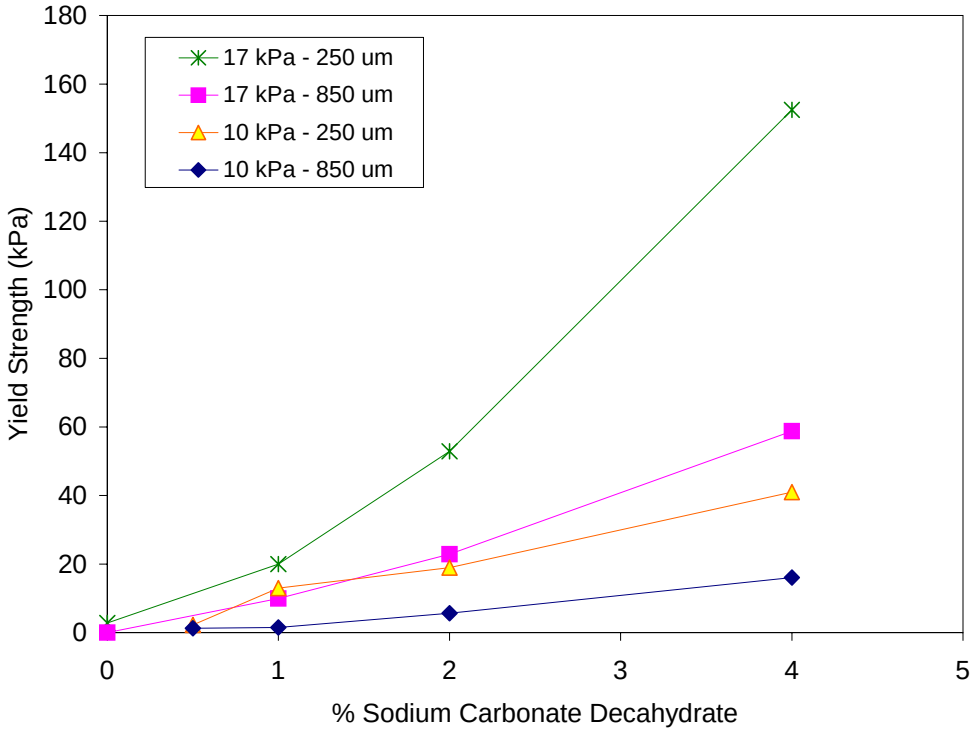

Figure 2-8. Unconfined yield strength of sodium carbonate monohydrate as a function of moisture content in the form of percent sodium carbonate decahydrate in the mixture.

It is believed that the consolidation stress has an effect on the bulk cohesive strength of the material. Not all materials exhibit this property but in the case of sodium carbonate, the strength increases with an increase in consolidation load. This is intuitive since larger consolidation loads will result in a denser material and larger interparticle contact areas. Figure 2-8 indicates a nearly linear dependence of consolidation pressure on the yield strength of the cakes. In Figure 2-9 the unconfined yield strength of carbonate as a function of the consolidation stress is plotted. It can be seen that the strength of sodium carbonate increases as the stress on the material increases.

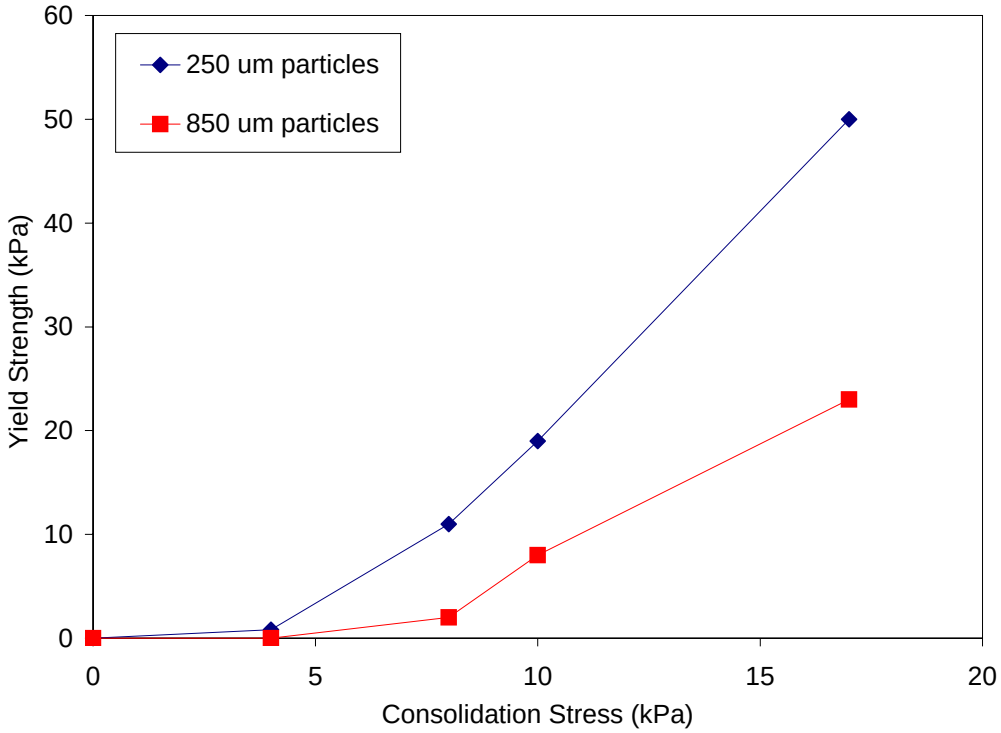

Figure 2-9. The yield strength as a function of consolidation pressure. The mean particle size of this material is 250 μm and the moisture content is 2% decahydrate.

Effect of Particle Size

The effect of particle size on the strength of powders has been widely researched. Rumpf was the first to theorize that the particle size influences the strength of a powder. His theory states that the particle size is inversely proportional to the tensile strength of the powder assuming that the porosity and the strength of the interparticle bonds are known. The details of Rumpf's theory are given in a later chapter. The yield strength measured by the Johanson Indicizer® is plotted as a function of the mean particle size d_{50} of the sodium carbonate. It can be seen in Figure 2-10 that the yield strength increases as the particle size decreases. As the particle size decreases the surface area and number of contact points increase such that there are a larger numbers of contact for the water to

migrate and a larger number of solid bridges formed. This hypothesis is verified by Figure 2-10 as the strength increases with a decrease in particle size.

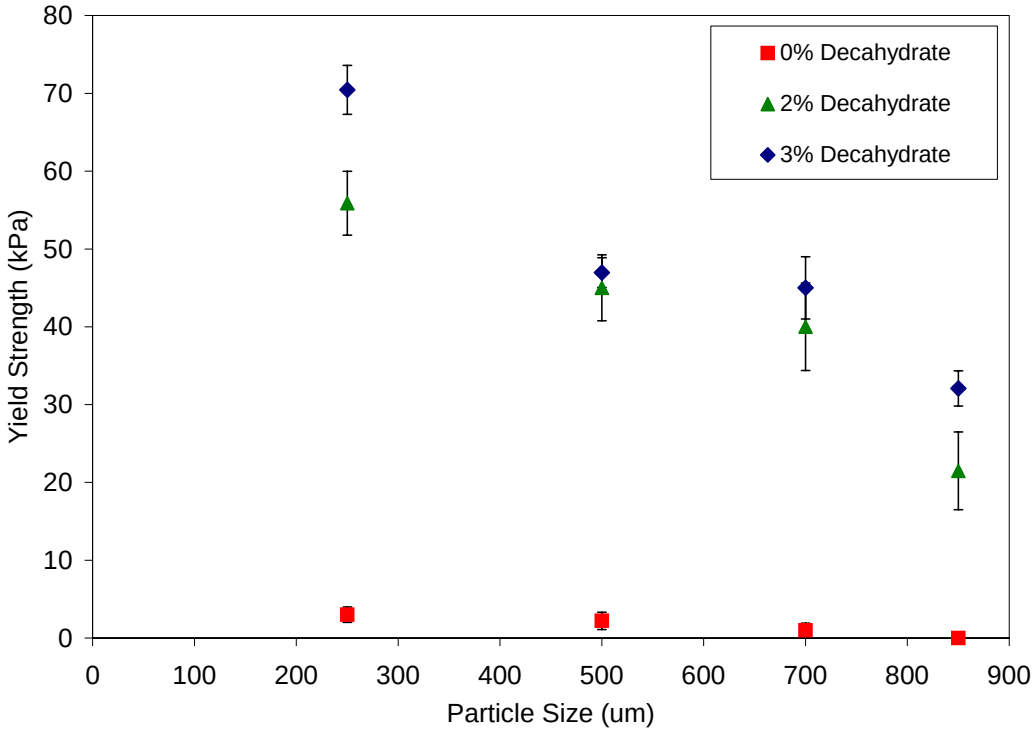

Figure 2-10. The yield strength as a function of the mean particle size. The consolidation pressure is 15 kPa.

Effect of the Number of Temperature Cycles

It is well known that caking is a time induced phenomenon (Teunou *et al.*, 2000, Purutyan *et al*., 2005). Thus the time of storage is also an important factor when considering the strength of caking. The unconfined yield strength measurements were made with both the Johanson Indicizer and the Schulze shear cell. The yield locus, measured with the Schulze cell, of a sample that has been exposed to air flow for a period of 24 hours is displayed in Figure 2-11. The time consolidation effects can be seen as the yield locus increases with time. The unconfined yield strength of the material is a

function of the shear stress as given in equation 2-3. Thus an increase in the shear stress results in an increase in the unconfined yield strength.

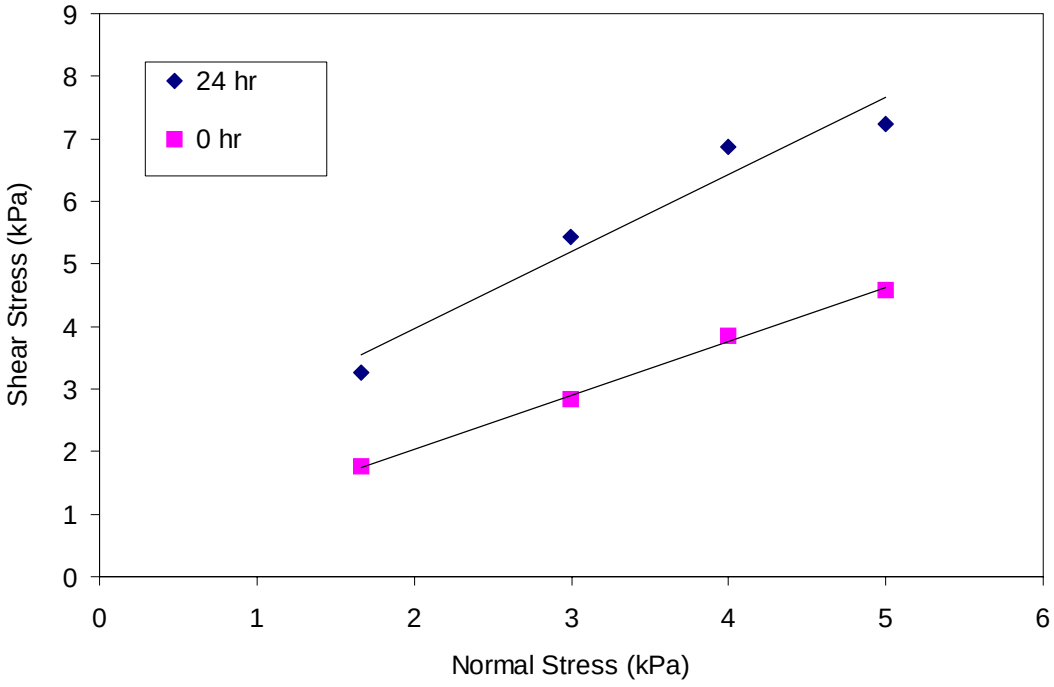

Figure 2-11. Yield locus of sodium carbonate for air at 75% RH for 24 hr. and 0 hr with a normal load of 16kPa.

It has been observed that the caking strength may increase as the number of temperature cycles increases (Johanson *et al.*,1996, Cleaver *et al.*, 2004). In other words, the longer a material experiences the day-to-night temperature changes, the greater tendency for increased caking. The yield strength of sodium carbonate is investigated as a function of the number of temperature cycles that the material experiences. The temperature cycles for this set of experiments are 4 hours long. It can be seen in Figure 2-12 that the unconfined yield strength as measured with the Johanson Indicizer® increases as the number of temperature cycles increases. It is possible that the duration of temperature cycle is not sufficient for the material to reach an equilibrium state. Thus

subsequent cycles initiate the release or uptake of moisture causing an increase in the strength until equilibrium. It is shown in Figure 2-12, that for the 2% decahydrate mixture, that the yield after 2 and 4 cycles are approximately equal. The same trend is not seen with the 4% decahydrate mixture. This could be due to the fact that the initial moisture content of 4% mixture is higher thus requiring more time for equilibration. It may also be attributed to the migration of dissolved material from a non-contact area to the contact zone during the recrystallization process.

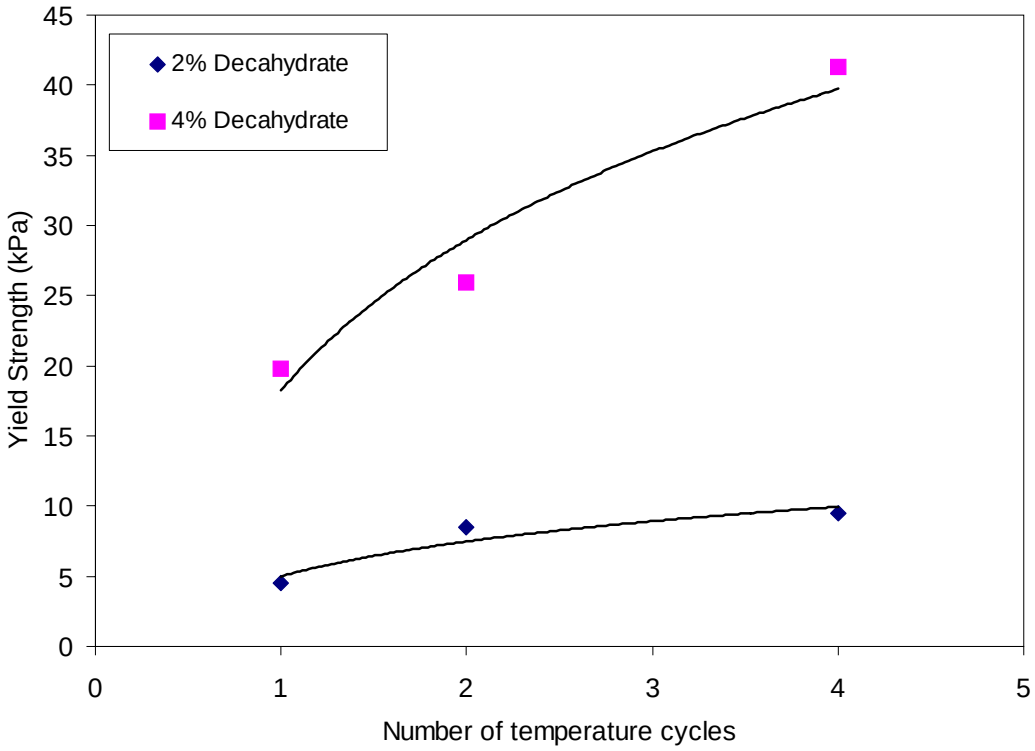

Figure 2-12. The yield strength as a function of the number of temperature cycles. The mean particle size is 250μm and the consolidation pressure is 15 kPa.

Effect of Relative Humidity

The effect of relative humidity has only recently received attention in the research of caking (Teunou *et al.*, 1999a, Leaper *et al.*, 2003). It is believed that changes in relative humidity could induce a caking event. The effects of relative humidity on the

cake strength of sodium carbonate are investigated using the Schulze shear cell. It can be seen in Figure 2-13 that the slope of the yield locus increases with an increase in relative humidity. This indicates that moisture is adsorbed by the particles at higher relative humidities. The moisture sorption causes the increase in shear stress which in turn increases the unconfined yield strength.

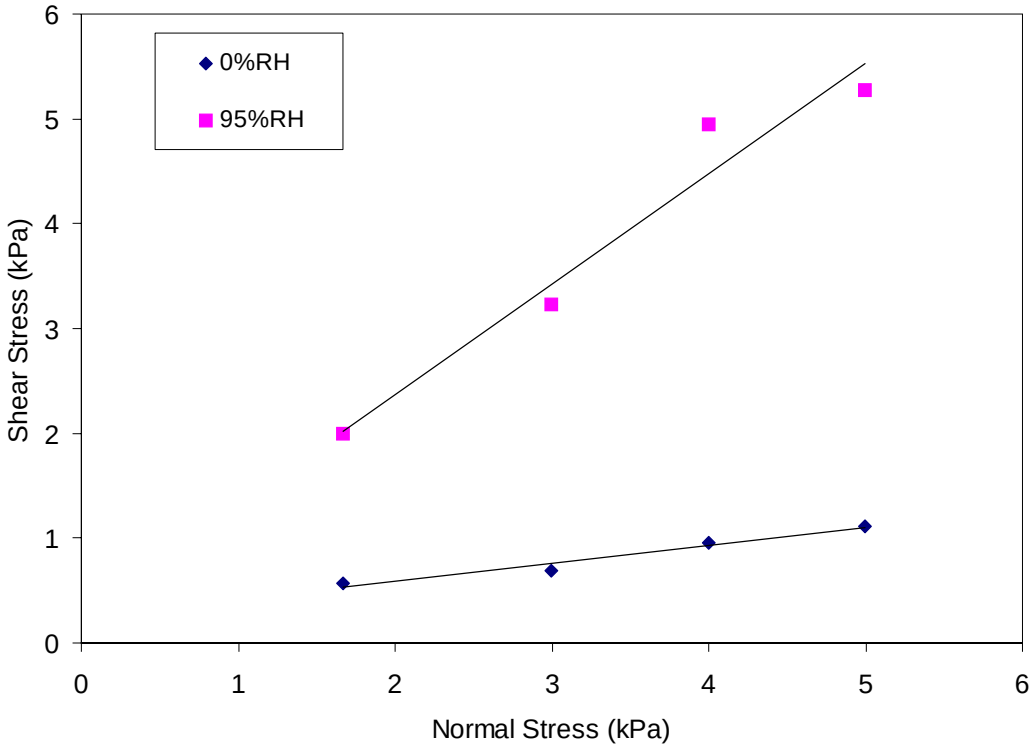

Figure 2-13. Yield locus of sodium carbonate for air as a function of relative humidity with a normal load of 4kPa.

It can be seen in Figure 2-14 that the unconfined yield strength increases with the relative humidity. The strength data seem to follow the same trend as the isotherm with the moisture pickup, thus verifying that the adsorbed moisture affects the cake strength. However, a change in relative humidity does not seem to produce a cake of the same strength as those created by a temperature change.

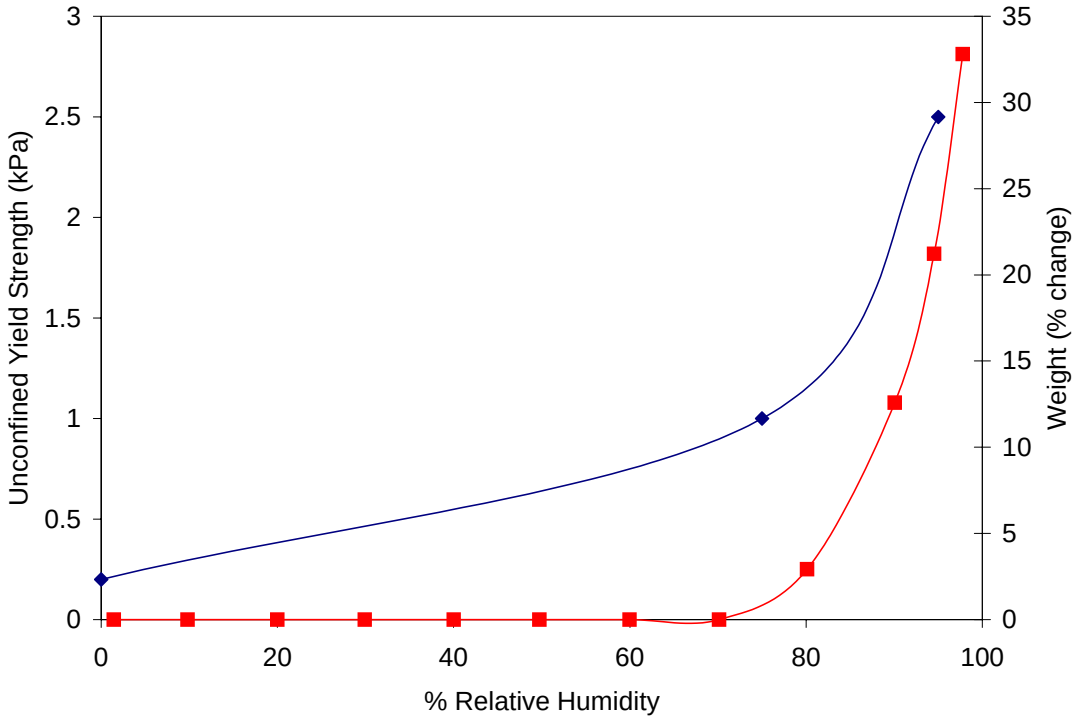

Figure 2-14. Unconfined yield strength as a function of relative humidity compared to the isotherm of sodium carbonate.

CHAPTER 3
ADSORPTION ISOTHERMS AND KINETICS

Perry (1997) defines adsorption as the accumulation or depletion of solute molecules at an interface. In the case of moisture migration caking, this entails the transfer and equilibrium distribution of moisture between the gas phase (the humid environment) and the particles. In this chapter the adsorption isotherms of sodium carbonate and salt are examined using dynamic vapor sorption techniques. It is shown that the isotherms are a good predictor to the onset of caking. The kinetic sorption curves are also measured to obtain the rates of adsorption and vaporization of water.

Adsorption Isotherms

During the processing and storage of bulk materials, the material is exposed to humid air in the environment. The humid air contains water vapor which can have a significant affect on the physical and chemical properties of the material. Water vapor from the environment can be absorbed into the structure of many materials and it may also be adsorbed onto the surface of these materials. In the case of amorphous solids, including pharmaceutical excipients and food products, absorbed water vapor is known to lower the glass transition temperature of the material thus promoting a caking event (Zhang *et al.*, 2000). In many crystalline materials, the water vapor is adsorbed on the surface causing dissolution thus also initiating a caking event. For food products, water vapor has a critical effect on the dehydration process and storage stability (Iglesias *et al.*, 1976).

At a given temperature and relative humidity, solids exhibit a maximum capacity to adsorb moisture and this is characterized by the sorption isotherms. Water vapor sorption isotherms are used to describe the interactions between a material and the humid air surrounding it. The isotherms are typically expressed as the water content (a loss or gain) as a function of the relative humidity (RH) or water activity at a given temperature. The adsorption of water vapor may be either physical or chemical and the vapor may adsorb in multiple layers. Brunauer *et al.* (Perry, 1997) described five types of physical adsorption as shown in Figure 3-1. Type I isotherm represent monomolecular adsorption of a gas and applies to porous materials with small pores. This is the well-known Langmuir isotherm. Type II and III isotherms represent materials with a wider range of pore sizes where gas is adsorbed in either a monolayer or multilayer. The sigmoid isotherm of Type II is typically obtained from soluble products which show an asymptotic trend as the water activity goes to one (Mathlouthi *et al.*, 2003). The Type III isotherm is known as the Flory-Huggins isotherm. This isotherm represents the adsorption of a solvent gas above the glass transition temperature. Type IV isotherms describe adsorption which causes the formation of two surface layers. Type V adsorption behavior is found in the adsorption of water vapor on activated carbon.

Some crystalline materials will exhibit sorption profiles other than those described by Brunauer *et al*. The adsorption/desorption isotherm of hydrated material sometimes appears as a stair like curve. The hydrates are formed at specific relative humidities. The material equilibrates at a low RH and when the RH increases the material becomes saturated increasing the moisture content of the material. This sequence appears as a staircase in the sorption isotherms. Anhydrous materials only adsorb trace amounts of

water at low RH. At a characteristic RH, the adsorption corresponds to saturation equilibrium. A vertical line on the sorption isotherm represents the saturation equilibrium.

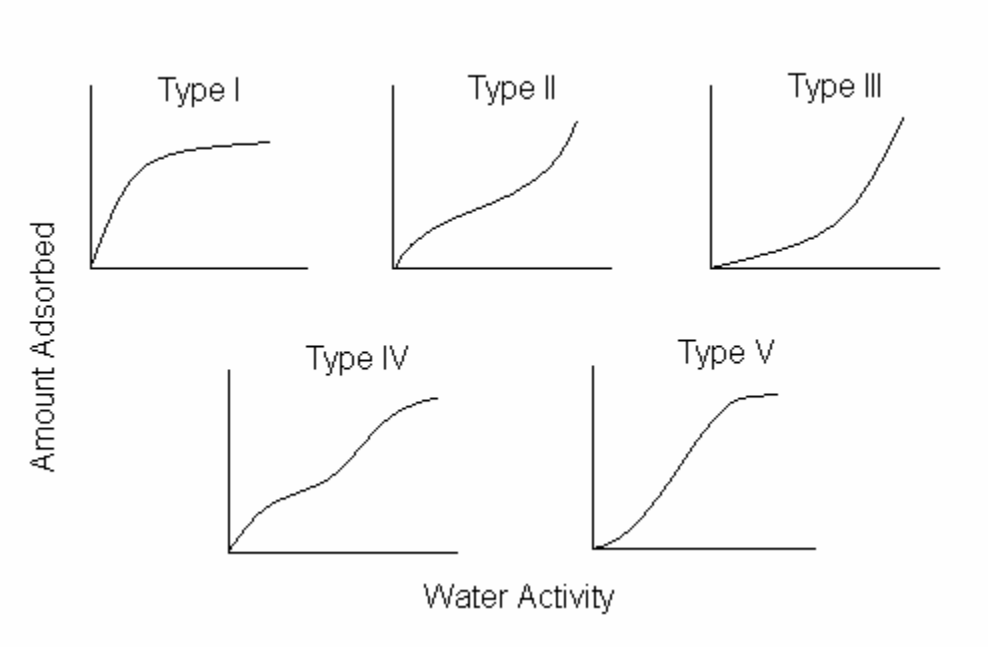

Figure 3-1. The five types of adsorption isotherms in the classification of Brunauer *et al.* (1940).

From the sorption isotherm fundamental material properties and important information about its handling can be derived. Properties such as hydrate formation, deliquescence, and hygroscopicity can be determined from the sorption isotherms. Sorption isotherms are also useful for a qualitative prediction of caking. The data obtained from the isotherm are used to determine the temperature and relative humidity conditions at the onset of caking. This is illustrated in the isotherms by a sudden increase in the moisture content at a critical relative humidity. Sorption isotherms are also a valuable tool for understanding the moisture relationship of a new product during the formulation stages (Foster *et al.*, 2004).

Mechanisms and Kinetics of Adsorption

The adsorption of a solute from a fluid phase is described by mass transport processes such as: interparticle mass transfer, intraparticle mass transfer and interphase mass transfer. These common transport mechanisms are illustrated in Figure 3-2. Interparticle mass transport is the diffusion of the solute (moisture in the case of caking) in the fluid phase through the particle bed. This type of transport is described by heat and mass transfer equations on a continuum scale. Interparticle mass transport is a subject of chapter 4. Intraparticle mass transfer, which includes pore and solid diffusion, describes the transport of the solute through the particle. Interphase mass transport is the transfer of a solute at the fluid-particle interface. Figure 3-3 is an illustration of interphase mass transport showing the sorption of moisture by a sorbent particle.

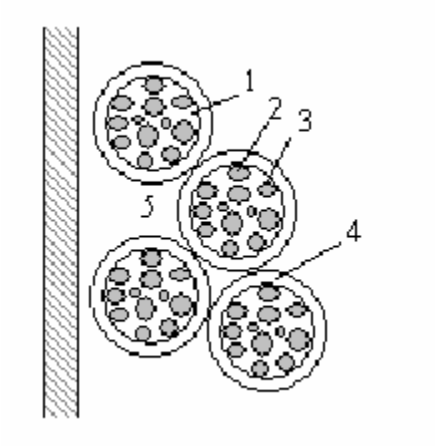

Figure 3-2. Mechanisms of mass transfer for absorbent particles (Perry, 1997): 1, pore diffusion; 2, solid diffusion; 3, reaction kinetics at boundary phase; 4, interphase mass transfer; 5, interparticle mixing.

In this research it is assumed that the particles are nonporous. This assumption is validated by measurements of the specific surface area by gas adsorption. The measured values for the specific surface area correspond the ideal values at a specific particle size.

For a packed bed system, the transport of moisture from the bulk of the fluid phase to the surface of the particle is described as interphase transport and the mass transfer rate is given by:

$$\frac{dq}{dt} = kA_{sp}(c_b - q) \qquad (3\text{-}1)$$

where k is the mass transfer coefficient, A_{sp} is the specific surface area, c_b is the moisture concentration in the bulk of the fluid, and q is the solids moisture content. To simplify the calculations of equation 3-1 it is assumed that the uptake rate is linearly proportional to the driving force, the so called linear driving force model. The moisture concentration in the bulk is equal to the equilibrium solids moisture content. Thus the particles in the system are in equilibrium with the fluid phase concentration of the bulk.

$$\frac{dq}{dt} = k_g A_{sp}(q_e - q) \qquad (3\text{-}2)$$

In equation 3-2 q_e is the equilibrium solids moisture content and k_g is the Glueckauf factor. The equilibrium concentration is determined from the isotherm of the material. The linear driving force model suggests that the concentration gradient is linearly proportional to the average moisture content of the system.

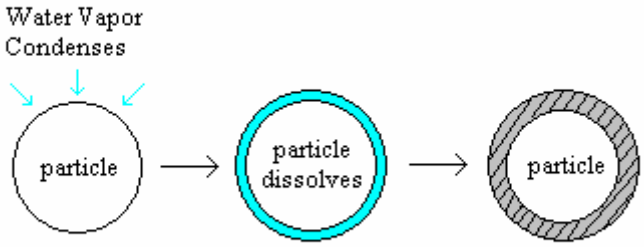

Figure 3-3. Sorption of moisture by a water soluble particle.

Measurement Techniques for Sorption Isotherms

There are two common methods for determining the sorption isotherms of powders or granular materials: static vapor sorption and dynamic vapor sorption.

Static Vapor Sorption

The method of static vapor sorption is a very time consuming and laborious process for measuring isotherms. A constant environment (temperature and relative humidity) must be maintained throughout the duration of the experiment. Several techniques are employed to produce a known constant humidity. The use of saturated salt solutions is the most common (Greenspan, 1977, ASTM, 1996). Known constant humidities are created by salts whose affinity for water regulates the water vapor pressure surrounding the material. Most often the salt solution and the sample are contained in dessicators for the period of time in which the sample is allowed to equilibrate at the specified humidity. The equilibration time is typically several weeks. The weight of the samples before and after equilibration are recorded and used to determine the moisture content of the sample at a particular relative humidity. Karl Fischer titration may also be used to determine the moisture content of the sample. Depending on the properties of the powder sample, this method can be time consuming.

Dynamic Vapor Sorption

An alternative, faster approach to static vapor sorption is dynamic vapor sorption. This method is more time efficient because a smaller sample size is used which decreases the equilibration time. The humid air is also either passed over or through the sample allowing equilibration to occur much faster. Dynamic vapor sorption is the chosen method of measurement for the sorption isotherms and sorption kinetics in this research. The equipment used is the VTI Symmetrical Gravimetric Analyzer (SGA 100).

Symmetrical Gravimetric Analyzer

The isotherm and kinetic measurements are made with the VTI Corporation Symmetrical Gravimetric Analyzer (SGA-100). The SGA-100 is a continuous gas flow adsorption instrument designed to study water vapor sorption isotherms. All measurements are taken at ambient pressure and the temperature range is from 0° to 80°C. A schematic of the instrument is shown in Figure 3-4.

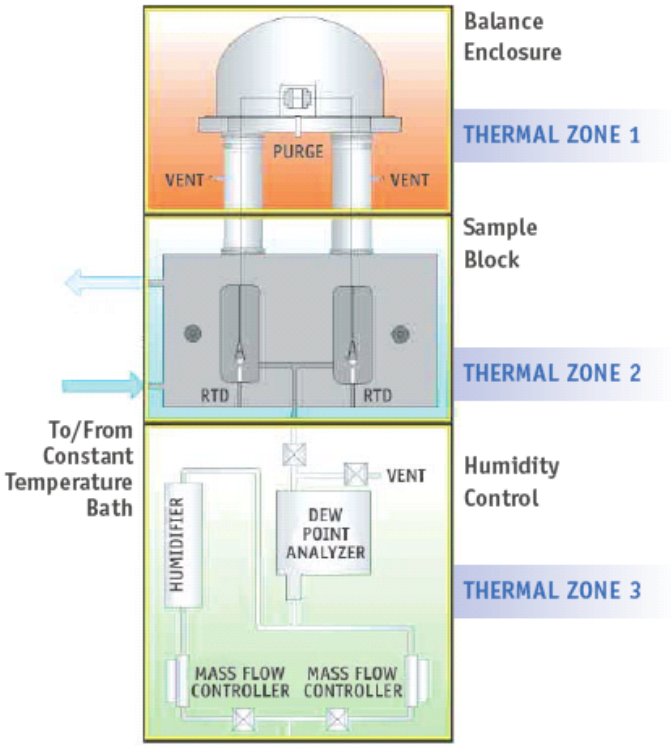

Figure 3-4. VTI Symmetrical Gravimetric Analyzer schematic (VTI website).

The instrument is designed with three separate thermal zones such that maximum temperature stability is achieved. Located in zone 1 is the Kahn microbalance. The microbalance has a sensitivity of 0.0001 μg. The temperature in this zone is maintained 15°C higher than the experimental temperature to avoid condensation. Higher temperatures along with a continuous purge stream of nitrogen in the balance chamber

ensure that there is no vapor condensation on the microbalance which could invalidate the results. Isolating the microbalance also eliminates the weight fluctuations caused by temperature gradients in the environment. Suspended from the microbalance are two thin metal wires, into zone 2, for the sample holder and reference sample holder.

The core of the instrument, an aluminum block containing the sample chamber, is located in zone 2. There are two rectangular cutouts (chambers); one houses the sample and the other houses a reference sample. Glass sample holders are suspended on the thin wires from the microbalance. Both sides are subjected to the same temperature and relative humidity conditions. The temperature in this zone can range from 0° to 80°C. It is controlled by circulating water from a constant temperature bath through the hollow wall aluminum block. The air temperature is measured with an RTD located at the bottom of each chamber.

The third zone is for the humidity control. It contains the chilled mirror dew point analyzer and a parallel plate humidifier which are maintained at 40°C. The system is fed with a constant supply of nitrogen. The nitrogen enters the parallel plate humidifier and is completely saturated (100 % RH) with respect to the experimental temperature. The saturated stream is mixed with a dry stream of nitrogen to obtain the desired relative humidity. The mixed stream passes through the dew point analyzer to be measured before entering the sample chamber. The dew point analyzer continuously measures the relative humidity stream to maintain control of the wet and dry mass flows.

The VTI Sorption Analyzer is a fully automated system that requires minimal user input. The operator must specify the operating conditions such as experimental temperature, relative humidity steps and the equilibrium criterion. The user input screen

is displayed in Figure 3-5. The experiment can be set for a drying step before the measurement of the isotherm. The relative humidity steps are customized by the user or chosen by the computer program if the initial and final step are specified. The data are recorded at intervals specified by the user. This is a time or percentage weight change condition. After the experimental parameters are set the material is loaded in the sample holder and the experiment begins.

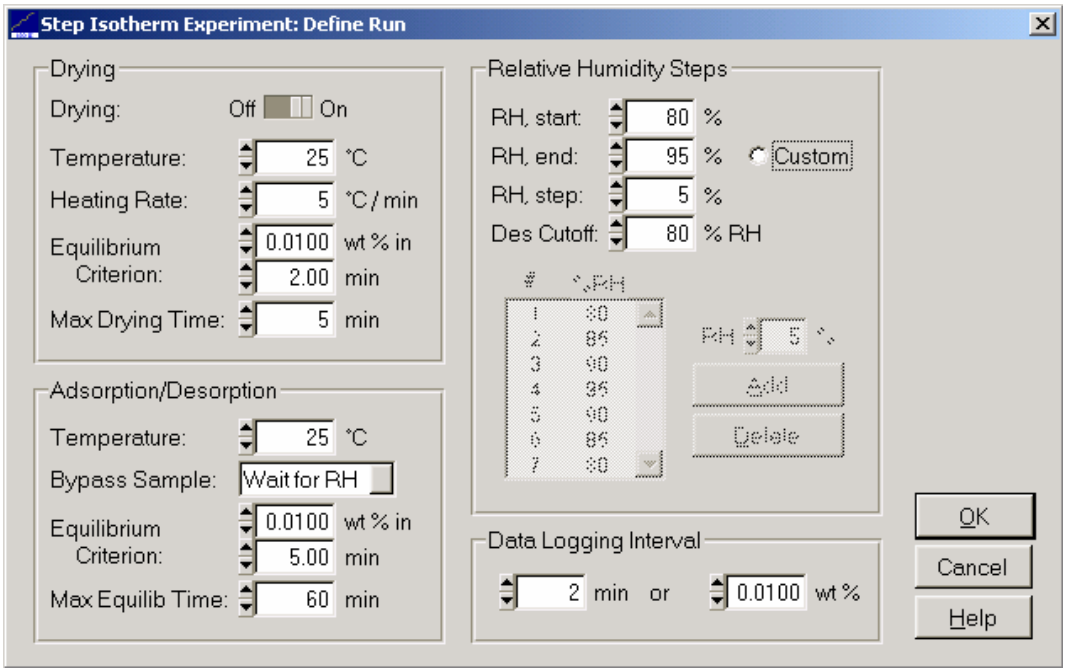

Figure 3-5. User input screen for the VTI Sorption Analyzer.

Experimental Parameters

The sorption isotherms are measured at three temperatures: 25°, 35° and 50°C. Measuring in this range provides an indication of how temperature affects the sorption process. The kinetic sorption curves are also measured to obtain the rates of adsorption and desorption of water. The data from the isotherms can be used to determine if water sorption at a specified relative humidity is sufficient for caking.

Only the sorption isotherms of single component systems are measured. However, the combined effect of individual adsorption isotherms in a mixture on the diffusion of moisture through the bulk and onto the particle surface is important. Consider a system containing two different particles with different isotherms. One particle can be a moisture sink for the water and the other particle can be a moisture source. Therefore, a caking event can occur due to differences in isotherms. The differences in isotherms not only affect the diffusion of moisture on the particle surface but also the kinetics of evaporation and crystallization of the bridges within the cake.

The standard procedure for measuring adsorption isotherms suggests drying the material introducing humidity (ASTM, 1996). However, the following isotherms are measured without a prior drying step. The drying step is only necessary to ensure that the starting point is known. Thus the moisture content of the material is taken prior to the isotherm measurements using an Ohaus MB45 moisture analyzer. The moisture contents are consistent within a range of less than 1%.

Sorption Isotherms for Sodium Carbonate

Sodium carbonate is one of the materials used in this study. This material is widely used in the glass industry as well as in the formulation of powder detergents. Sodium carbonate has a strong propensity to cake if not stored in a controlled environment. It is a colorless odorless material with three stable hydrate forms, monohydate (SCM), heptahydrate (SCH), and decahydrate (SCD). The phase diagram for sodium carbonate is shown in Figure 3-6 (OCI Chemical website). Heptahydrate is a semi-stable form and likely exist only in solution. It is made up of 57.4% water and is only stable in the temperature range of 32˚C to 36˚C. Sodium carbonate monohydrate granules contain 14.6% water. It loses water on heating (to 100 ˚C), and the solubility increases with

increasing temperature. Sodium carbonate decahydrate contains 61.2% water and the crystals readily effloresce in dry air and form lower hydrates. This is evident from the moisture sorption isotherm, Figure 3-7.

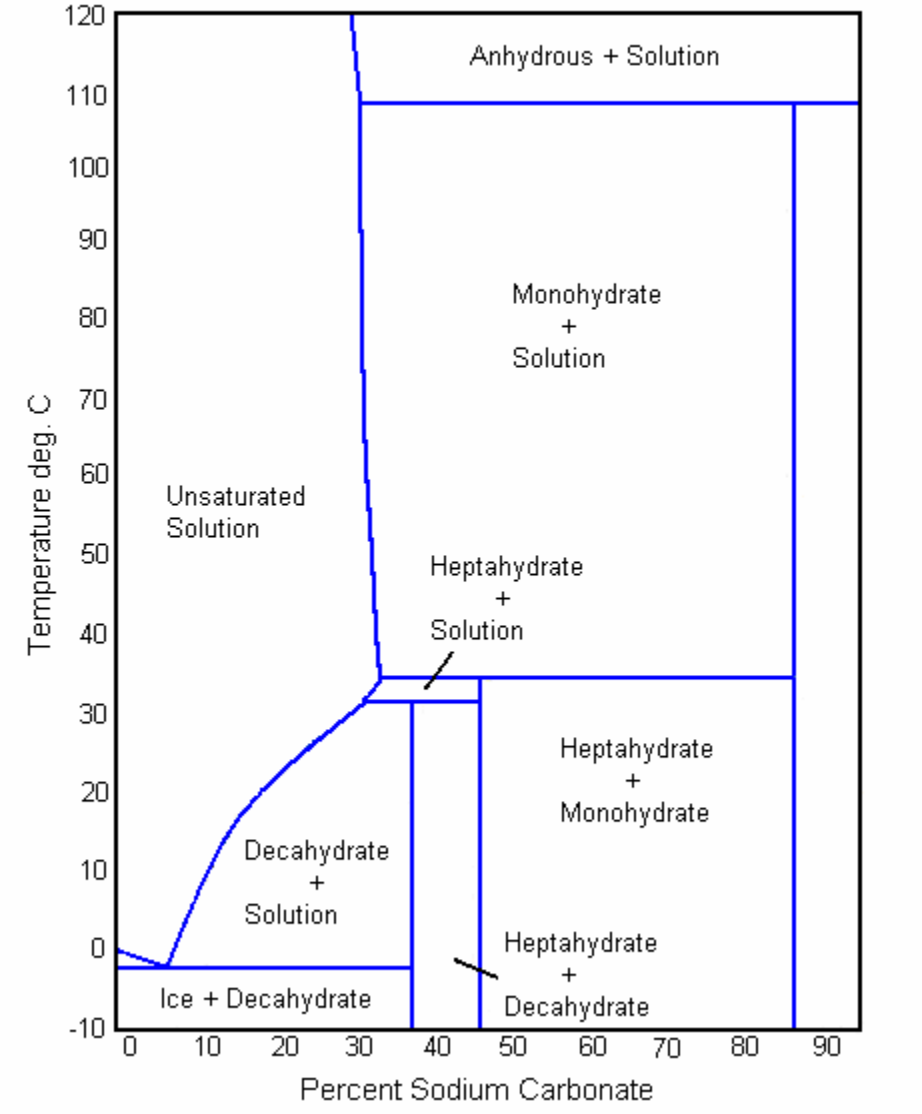

Figure 3-6. Phase diagram of sodium carbonate.

In Figure 3-7, the expected equilibrium moisture adsorption for both decahydrate and monohydrate is shown. The decahydrate appears to lose (47% moisture) at relative humidities lower than 70%. This corresponds to an average molar moisture content

equivalent to 7 moles of crystalline water. However, decahydrate shows a great propensity to deliquesce at relative humidities greater than 70% gaining almost 1.5 times its initial weight in moisture at 98% RH. Comparing this behavior to the monohydrate, shows a very different behavior. The monohydrate does not lose or gain moisture at relative humidities lower than 70% RH. This transition humidity, where deliquescence begins, is similar for the decahydrate. However, the monohydrate does not deliquesce as rapidly as the decahydrate. The deliquescent relative humidity is in the range on 70-80 %.

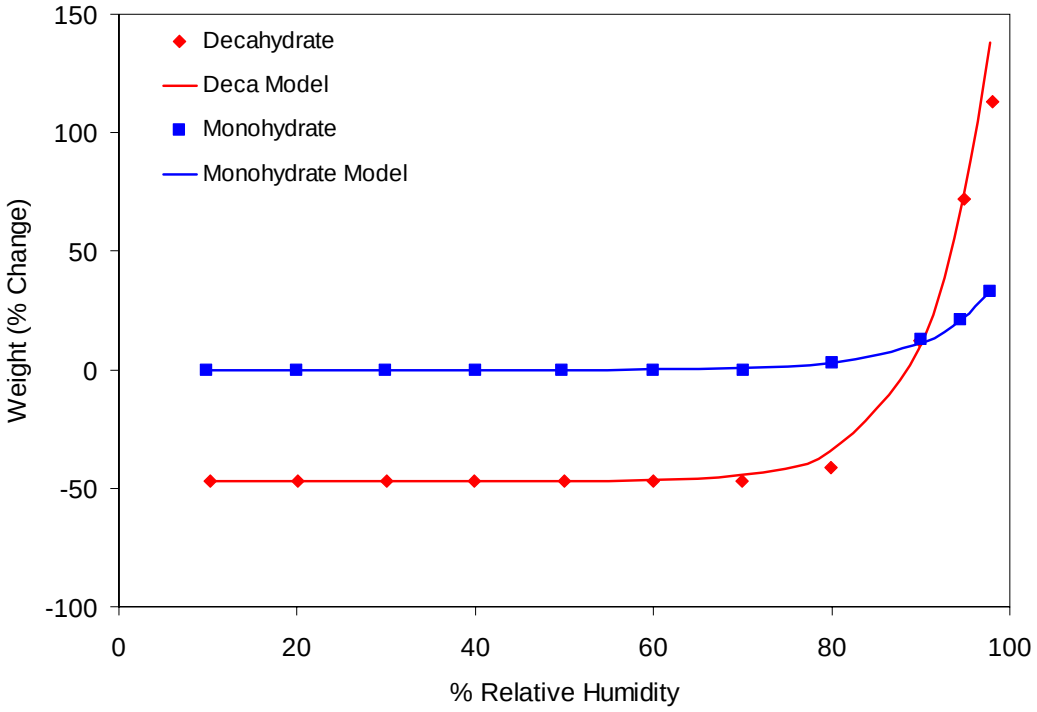

Figure 3-7. Adsorption isotherm of sodium carbonate at 25°C. The points indicate the experimental data and the lines are the adsorption isotherm model predictions.

The isotherms of sodium carbonate suggest that a mixture of decahydrate and monohydrate would exhibit different behaviors in terms of moisture pick-up at different relative humidities. For example, assume a mixture of decahydrate and monohydrate is in an environment where the humidity was less than 86 % RH but greater than 70% RH.

From the isotherms, it is sufficient to assume that decahydrate would lose its moisture and that moisture would be picked up by monohydrate. At relative humidities greater than 88% both decahydrate and monohydrate deliquesce. The degree of deliquescence at 90 % RH is the same for both the monohydrate and decahydrate. However, at relative humidities greater than 90% RH the degree of deliquescence of decahydrate surpasses that observed with monohydrate suggesting that a mixture of these two hydrates might cause the monohydrate to lose moisture and be picked up by the decahydrate. The pickup of moisture by the monohydrate and the loss of moisture by the decahydrate causes the caking. The additional moisture slightly dissolves the surface of the monohydrate particles. Bridges are formed between particles and a cake is created. Increasing the amount of decahydrate in the mixture will therefore increase the strength of the cake. Thus the use of several hydrates is ideal for controlling the initial water content of the samples.

In Figure 3-7, for the monohydrate, a 0 % weight change corresponds to 100% monohydrate. An increase in weight of 87% and 130% correspond to the formation of a heptahydrate and decahydrate, respectively. The endpoint of the monohydrate curve suggests that the material likely converts to a mixture of heptahydrate and monohydrate. At 25˚C, the monohydrate picks up moisture yet not enough to fully transform to the decahydrate or heptahydrate form. For the decahydrate, a decrease in weight of 56% would correspond to a decahydrate transformed into monohydrate. At a 0% weight change, the decahydrate is transformed to its original state. The endpoint of the decahydrate curve suggests that the material deliquesces with a total moisture gain of 130%.

The sorption of water vapor by sorption carbonate is not sufficiently described by the adsorption models proposed by Brunaeuer in Figure 3-1. It can be seen in Figure 3-7 that the isotherms of sodium carbonate at 25˚C are best described by the adsorption model proposed by Miniowitsch (1958).

$$q = Ae^{\frac{RH/100}{B}} + q_o \qquad (3\text{-}3)$$

In equation 3-3, A and B are constants, q_o is the initial weight lose and q is the moisture content. The constants A and B vary slightly with each fit and q_o is zero for monohydrate and -47 for decahydrate. For the decahydrate A=7.97e-7 and B=0.0669. For the monohydrate A=6.38e-7 and B=0.0723.

The desorption curves for sodium carbonate are shown in Figure 3-8.

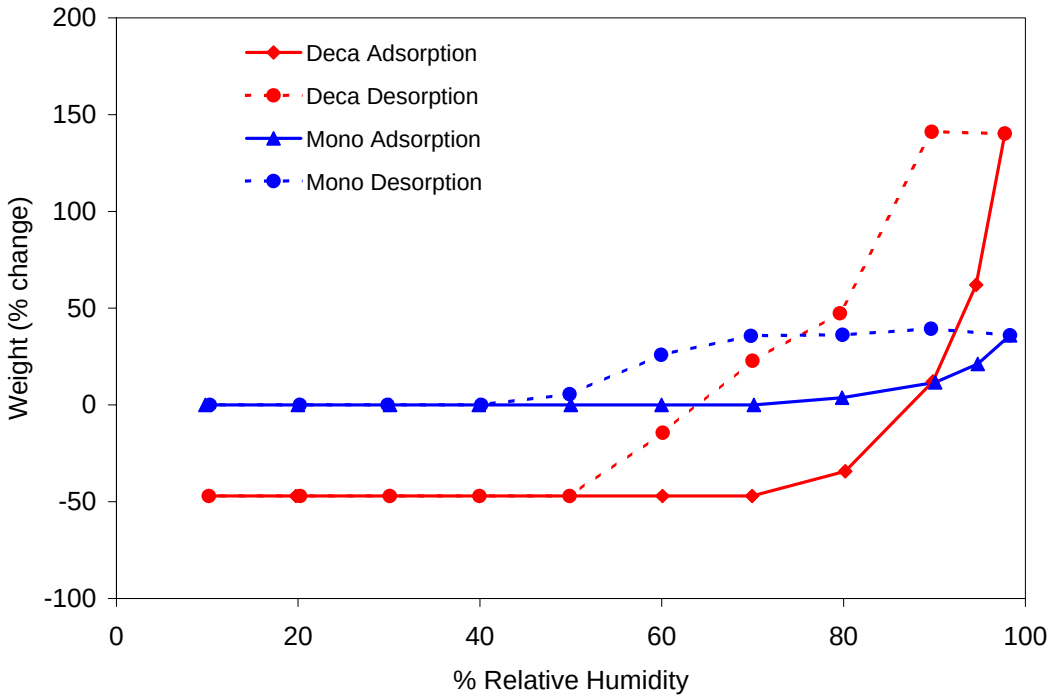

Figure 3-8. Sorption isotherm of sodium carbonate at 25°C.

It can be seen that adsorption and desorption of both the monohydrate and the decahydrate do not follow the same curve. There is a hystersis between the adsorption and desorption which implies that the sorption of sodium carbonate is not isotropic. Thus the desorption must be described by an equation different from that of the adsorption.

Effect of Temperature

The effect of temperature on the moisture sorption of sodium carbonate monohydrate and decahydrate is also investigated. It can be seen in Figures 3-9 and 3-10 that increasing the temperature increases the total moisture uptake.

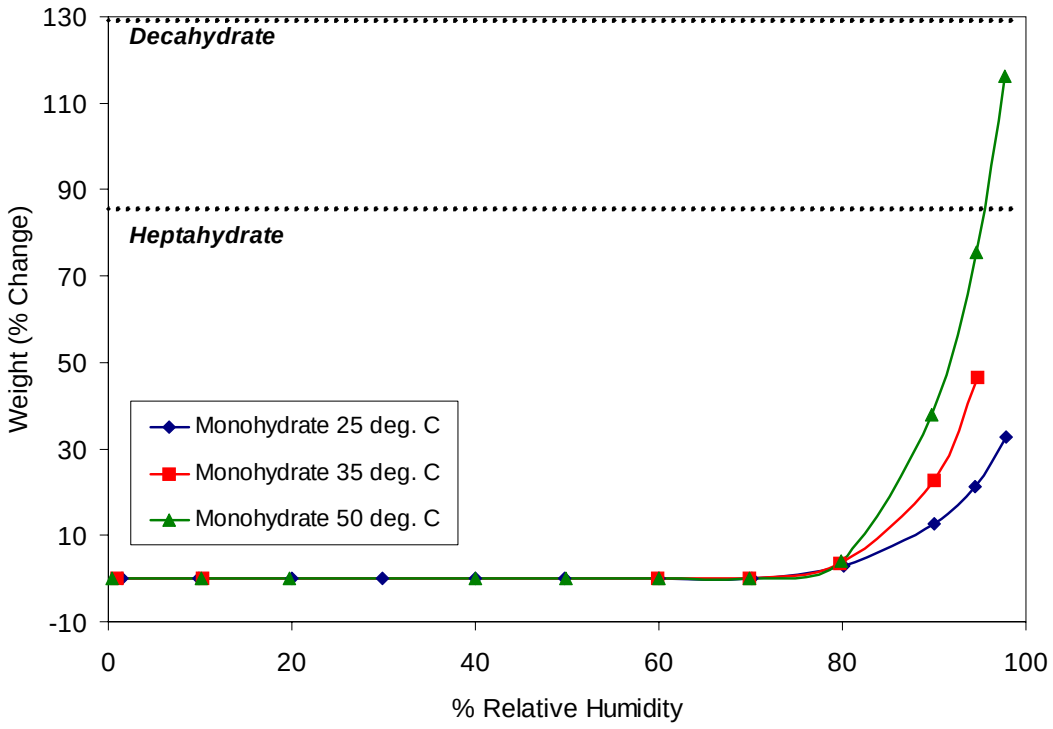

Figure 3-9. Sorption isotherm of sodium carbonate monohydrate at various temperatures. The dashed lines correspond to the point where the monohydrate converts to a heptahydrate or decahydrate.

The total moisture uptake of monohydrate at 35˚C is such that heptahydrate is formed. This result is verified by the phase diagram which suggests that the heptahydrate is stable in the temperature range of 32 -35 ˚C. At 50˚C the material shows significant

deliquescence with a gain in weight corresponding to a mixture of the decahydrate and heptahydrate forms. The same trends are observed with the decahydrate as seen in Figure 3-10. However deliquescence is substantially increased. At 35˚C and relative humidity values greater than 80% the material appears to form an unsaturated solution. Likewise, at 50˚C and relative humidity values above 85%, the result is an unsaturated solution.

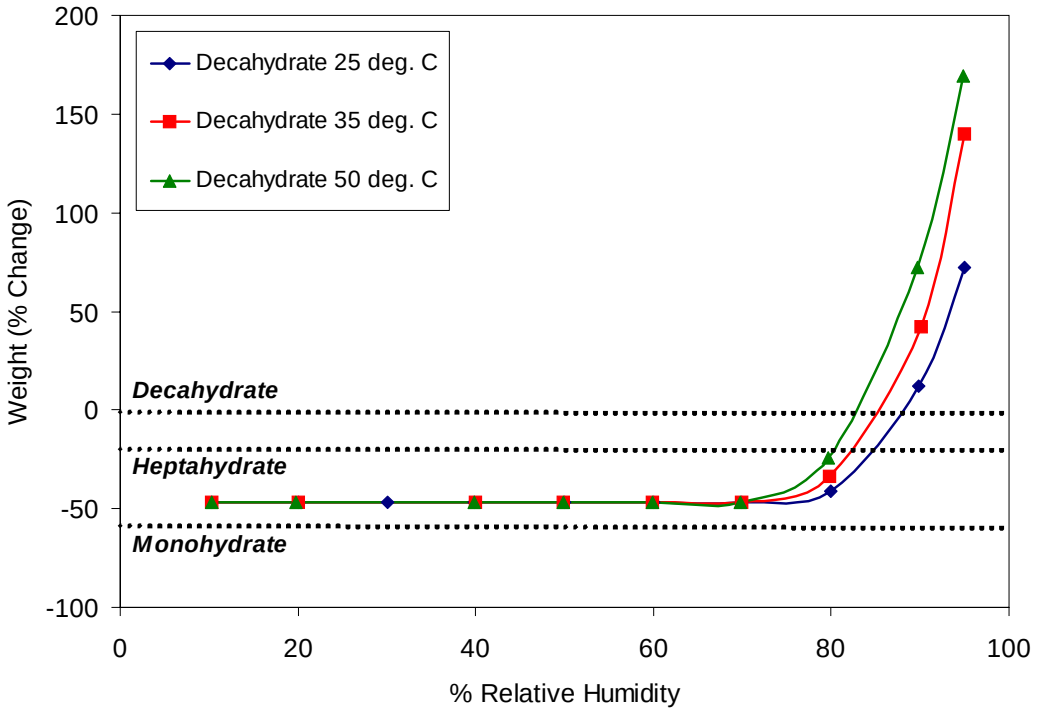

Figure 3-10. Sorption isotherm of sodium carbonate decahydrate at various temperatures. The dashed lines correspond to the point where the decahydrate converts to a monohydrate, heptahydrate or decahydrate.

The increase in moisture uptake is only observed beyond the deliquescence relative humidity. The deliquescence range remains unchanged within the temperatures investigated. This result is contrary to what various isotherm models would predict as a response to a temperature increase (Iglesias *et al*., 1976). At higher temperatures on the phase diagram the boundary between the unsaturated solution and the monohydrate plus solution has a negative slope. This suggests that as temperature increases the percentage

of sodium carbonate decreases. Thus as the temperature of the sample increases the moisture uptake increases.

Kinetics of Adsorption

The linear driving force model assumes that the order of the reaction of moisture adsorption/desorption is one. The kinetics (moisture content as a function of time) of sodium carbonate are investigated to validate the use of this model. The curves for the moisture content versus time for sodium carbonate decahydrate are shown in Figure 3-11.

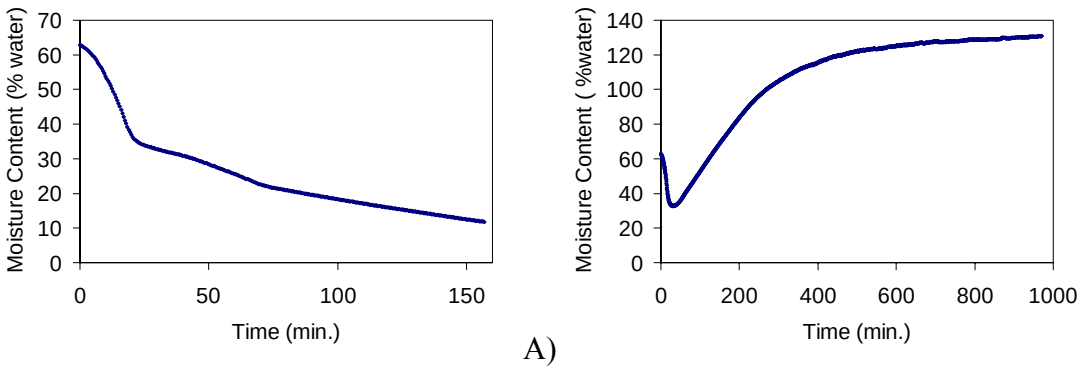

Figure 3-11. The moisture uptake of sodium carbonate decahydrate as a function of time. A)10%RH – represents the kinetics below the deliquescene relative humidity and B) 90%RH – represents the kinetics above the deliquescence relative humidity.

These two curves represent the typical kinetics of decahydrate above and below the deliquescence relative humidity. It can be seen that the kinetics at lower relative humidities are significantly faster than the kinetics at higher relative humidities, illustrated by the length of time required to reach an equilibrium state. This suggests that desorption of water occurs much faster than adsorption.

At higher relative humidities there is initially a loss of moisture corresponding to 5-7 moles of water. After desorption the material begins to adsorb moisture. This transient may be attributed to an artifact of the tester. Before the material is introduced into the sample chamber, the sorption analyzer operates at a default equilibrium condition of 0%

RH and 25˚C. It is possible to set the initial temperature of the chamber to the experimental temperature prior to the test by changing the setpoint of the temperature bath. However, it is not possible to change the default relative humidity. When the material is introduced into the sample chamber, the system must come to steady state at the specified experimental parameters. This process is not instantaneous. Hence there is an initial desorption of water which is caused by a low relative humidity in the sample chamber. The transient lasts for approximately 30 minutes. Thus the first 30 minutes of the curve are disregarded for determination of the order of the reaction.

To determine the order of the reaction the integral method of rate analysis is used. The reaction order is known (or suggested) from equation 3-2. If the reaction is first order, integration of equation 3-2 gives

$$-\ln\left(\frac{q-c_e}{q_o-c_e}\right)=k_g t \qquad (3\text{-}4)$$

The slope of the plot of $-\ln(q-c_e/q_o-c_e)$ as a function of time t is linear with a slope k_g. In Figure 3-11 the concentration data is approximated by the linear driving force model. The slope, intercept and correlation coefficient are given in Table 3-1. The slopes vary with the relative humidity implying that a single rate law may not describe the sorption of water. The rate of moisture sorption changes with a change in relative humidity.

The correlation coefficient for the curves of decahydrate at the specified relative humidities is in the range of 0.8453 – 0.9958. A coefficient of 1 would signify a perfect correlation. This result suggests that the linear driving force model is not perfect. However the kinetics of sodium carbonate may be approximated by this model with a reasonable certainty.

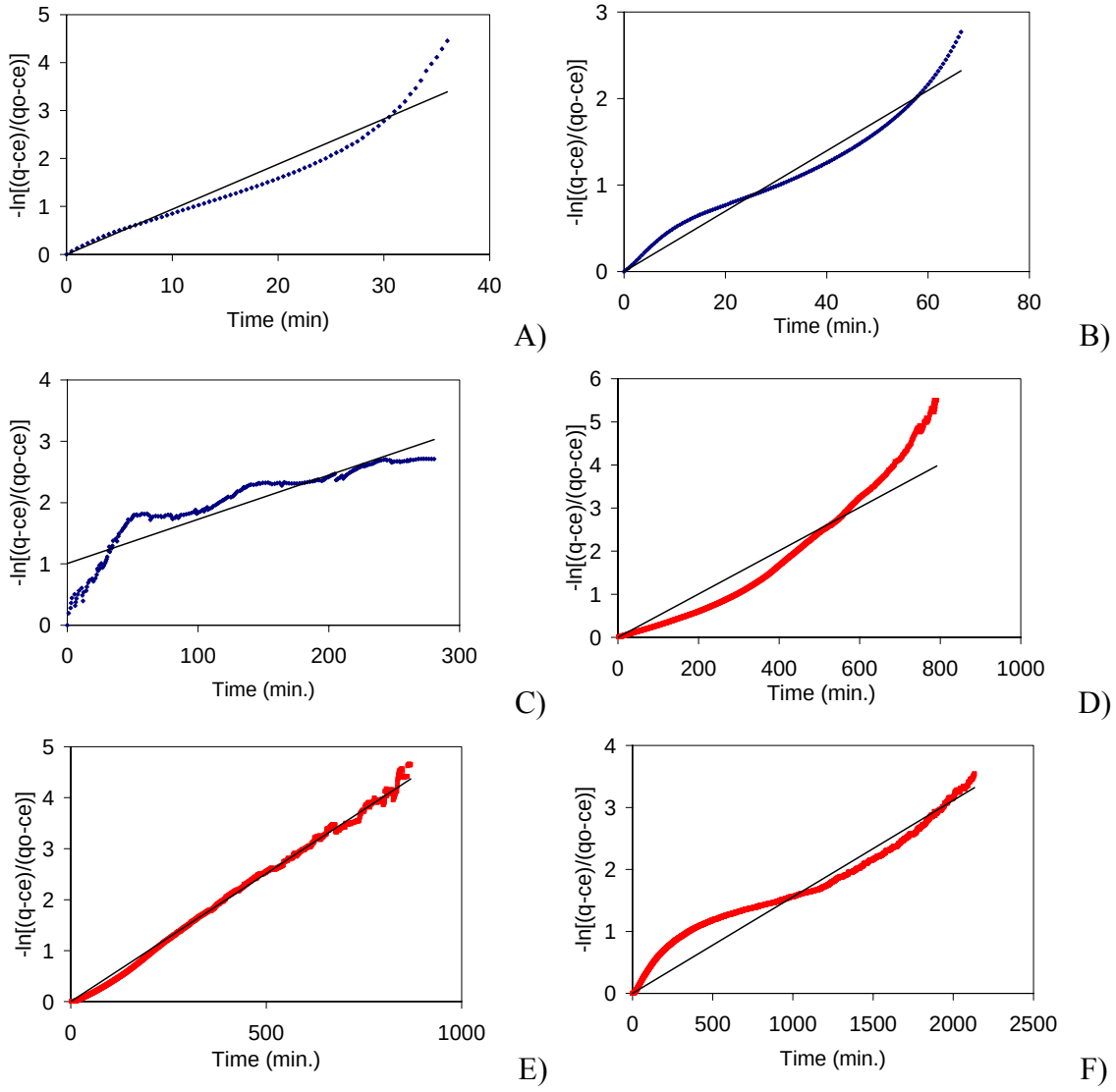

Figure 3-12. The kinetics of sodium carbonate decahydrate at 50˚C. A)10%RH, B)70%RH, C)80%RH, D)85%RH, E)90%RH, and F)95%RH

Table 3-1. Kinetics constants for sodium carbonate decahydrate

Relative Humidity (%)	Slope	Intercept	Correlation Coefficient (R^2)
10	0.1065	0	0.979
40	0.1049	0	0.9524
70	0.0946	0	0.9142
80	0.0072	1.0059	0.8453
85	0.005	0	0.9056
90	0.005	0	0.9958
95	0.0016	0	0.9077

The rate constants are plotted as a function of relative humidity in Figure 3-13. It can be seen that the rate if desorption is significantly greater than the rates of adsorption.

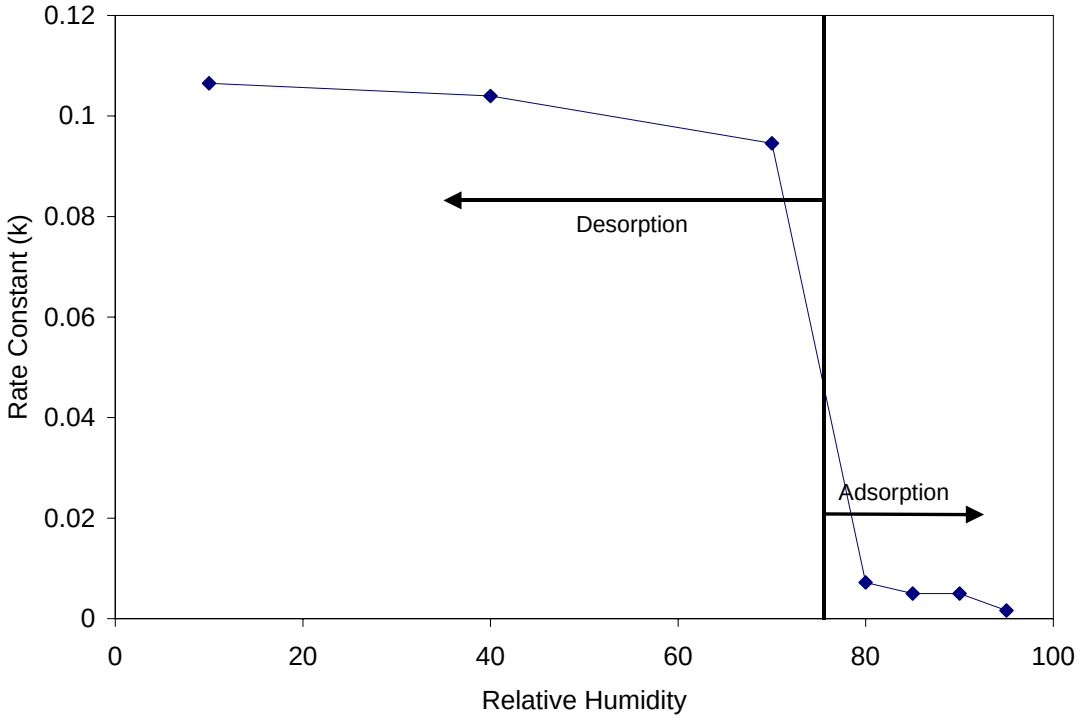

Figure 3-13. The kinetic rate constant for sodium carbonate decahydrate adsorption and desorption.

Sorption Isotherms for Sodium Chloride

Sodium chloride is also used in this study. This is a very complex material due to its deliquescence at high relative humidities. However there is an abundance of literature about this material due to its importance in all aspects of life. The sorption and kinetics of sodium chloride are well described in literature. Sodium chloride is highly soluble in water but only contains small amount of moisture after dehydration. It varies in color from colorless, when pure, to white, gray or brownish, typical of rock salt. The crystal structure can be modified with a change in temperature. At 20˚C, the critical relative humidity is 75%. Above this RH, the salt deliquesces. This is illustrated by the isotherm

in Figure 3-14. The isotherm for sodium chloride is plotted as function of temperature. It can be seen that the material adsorbs an undetectable amount of water at lower relative humidities. Beyond the deliquescence point there is a significant amount of sorption. This result is consistent with literature data (Greenspan, 1977).

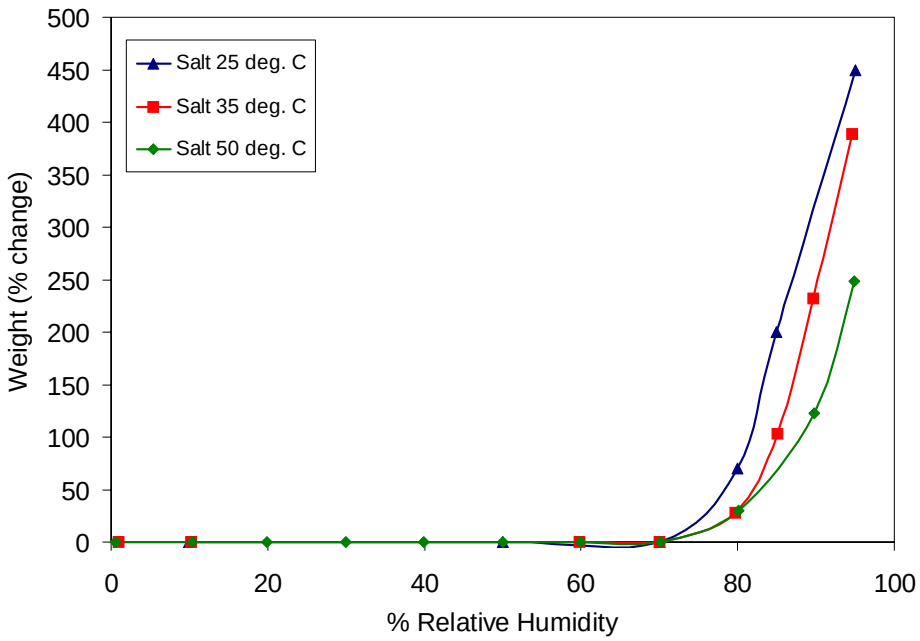

Figure 3-14. Sorption isotherm of sodium chloride at various temperatures.

CHAPTER 4
MOISTURE MIGRATION MODELING

This chapter explains the modeling of moisture migration through a particle bed. Moisture migration is described by the heat and mass transfer of the system along with the isotherms of the material. In the literature, it is assumed that free convection in the system can be neglected. However, it is shown that free convection plays a significant role in the heat and moisture transport of the system. It is also shown that the areas of caking within the bulk can be predicted given the proper model for the heat and mass transfer of the system.

Background

It has been shown in chapters 2 and 3 that heat and moisture play a significant role in the caking process. Thus, in order to better understand caking, it is essential that the heat and mass transport (moisture migration) is thoroughly explained. An important factor in describing moisture migration caking is the transport of moisture through the air and onto the surface of the particles. Other researchers have investigated specific parts of the process but few have attempted to describe the entire process of moisture migration. However, all attempts at describing moisture migration have included simplifying assumptions which render the models inaccurate.

Tardos *et al*. (1996a) studied diffusion of atmospheric moisture into a particulate material inside a container. The authors developed a model to describe the amount of moisture that penetrates from a stagnant layer of humid air above a particle bed. The goal of the study was to use the model to calculate the depth of moisture penetration as a

function of time. It was assumed that moisture migrates through the bulk by diffusion only and is driven by concentration gradients between the fluid phase and the particles. In the model, material is exposed to a step change in moisture content due to an increased amount of moisture in the air above the particle bed. The equations that describe the system are

$$\frac{\partial c}{\partial t} = D\frac{\partial^2 c}{\partial z^2} - \frac{(1-\varepsilon)}{\varepsilon}\frac{\rho}{\rho_a}\frac{\partial q}{\partial t} \tag{4-1}$$

$$\frac{\partial q}{\partial t} = k_g(q_e - q) \tag{4-2}$$

where q_e is the equilibrium moisture content given by the sorption isotherm, c is the vapor phase concentration, q is the solid moisture content, D is the diffusion coefficient, ε is the bed porosity, ρ and ρ_a are solid and air densities and z and t are distance and time. It is assumed that the rate of adsorption is proportional to the concentration difference such that k_g is constant. K_g is the called the Glueckhauf factor or linear driving force coefficient. The Glueckhauf factor is a function of the particle radius R and the diffusivity D_e.

$$k_g = 15\frac{D_e}{R^2} \tag{4-3}$$

Equation 4-1 is based on one-dimensional diffusion in the z direction. The initial conditions are chosen such that there is a uniform concentration of vapor in the powder bed and the moisture content of the solid is in equilibrium with the vapor phase. Experiments were preformed to verify the model and it was found that the model did not accurately predict the data for all times. At shorter times the model under predicts the measured data. This simple model is only an approximate prediction of the data. It fails to

address the effects of temperature and free convection on the moisture migration through the particle bed.

The results from the moisture migration modeling were applied to caking of fine crystalline powders in a second paper by Tardos (1996b). The purpose of this study was to examine the caking behavior of fine, bulk powders while exposed to humid atmospheres. The depth of penetration of moisture into the powder bed was calculated by solving equations 4-1 through 4-3. The caking ratio defined by Tardos is the height of the portion of the upper surface of the powder at a critical moisture content divided by the total powder depth. The critical solids moisture content is the value at which caking of the powder begins. Hence, the tendency of a powder to cake can be determined from this simple model given that the material properties of the powder relevant to caking are known.

Tardos also suggests that hydrate formation causes swelling in the powder bed. This compression is associated with caking. Due to the adsorption of moisture, various hydrates are formed which cause a swelling of the powder. This increase in bulk volume is on the order of 10% or more and occurs at relative humidities of hydrate formation. Tardos finds a relationship between the increase in bulk volume and the caking propensity of the powder using dilatometer testing of sodium carbonate. These findings suggest that the powder swelling is primarily responsible for the caking of the powder.

Rastikian and Capart (1998) later developed a model for caking of sugars in a silo during storage. The purpose of the study was to create a model to predict the moisture content profiles, air humidity and temperature inside a laboratory silo. The model includes not only the mass transport but also the heat transport which Tardos fails to

address. The system is described by the following two equations for heat and mass transport as well as the kinetic equation for the drying of sugar.

Mass balance equation:

$$\frac{\partial c}{\partial t} = D_e\left(\frac{1}{r}\frac{\partial c}{\partial r} + \frac{\partial^2 c}{\partial r^2} + \frac{\partial^2 c}{\partial z^2}\right) - \frac{F_a}{\rho_a}\frac{\partial c}{\partial z} + k_f\left(c_e - c\right) \qquad (4\text{-}4)$$

In equation 4-4 c is the concentration of the air, c_e is the equilibrium concentration at the particle surface, D_e is the effective mass diffusivity of the water vapor, F_a is the flow-rate of the inlet air, ρ_a is the density of the air, and r and z are the radial and axial coordinates.

Heat balance equation:

$$\frac{\partial T}{\partial t} = \frac{\lambda_s}{\rho c_{ps}}\left(\frac{1}{r}\frac{\partial T}{\partial r} + \frac{\partial^2 T}{\partial r^2} + \frac{\partial^2 T}{\partial z^2}\right) - \frac{F_a c_{pa}}{\rho c_{ps}}\frac{\partial T}{\partial z} - \frac{\rho_a}{\rho c_{ps}} k_f\left(c_e - c\right)H_v \qquad (4\text{-}5)$$

In equation 4-5 T is the temperature of the air, λ_s is the thermal conductivity of the solid, ρ is the density of the solid, c_{ps} is the specific heat of the solid, c_{pa} is the specific heat of the air and H_v is the enthalpy of water vaporization.

A laboratory silo was constructed in which humid air is blown through the bed of sugar. The temperature along the height of the silo and the relative humidity of the air above the particle bed are measured. These experimental data are compared to the proposed model. It was found that the model approximates the temperature profile within the silo reasonably well. However, Rastikian *et al*. assumed that the mass and heat transfer by diffusion in the radial direction can be neglected. Also, the system is based on forced convection through the particle bed. If material inside a silo is stored in an uncontrolled environment, it is more realistic to expect free convection in the system. Dehydration during storage and mass transfer likely occur through free convection.

Leaper *et al*. (2002) developed a model of moisture migration through a bulk bag as a function of humidity cycling. The model is based on the work of Rastikian *et al*. and Tardos. The purpose of this study was to predict the temperature profile and moisture content profile of the material within the bulk bag. It was assumed that moisture migrates by diffusion only due to moisture concentration gradients caused by fluctuating local relative humidity. The authors developed a procedure to calculate the profiles as follows:

- Determine the temperature profile using a simplified one-dimensional finite difference model which does not account for convective heat transfer.

$$\dot{Q} = \lambda_s A_{sp} T_i^{j-1} - T_{i-1}^{j-1} \quad \text{and} \quad T_i^j = \frac{\dot{Q}t}{m_{solid} c_{ps}} + T_i^{j-1} \tag{4-5}$$

  where T_i^j is the temperature at node position i and timestep j. $\dot{Q}$ is the heat flowrate through and specific transfer area A_{sp}, m_{solid} and c_{ps} are the mass and heat capacity, respectively.

- After the temperature profile is determined the RH profile can be calculated for a specific temperature.

$$H = \frac{RH}{100} \cdot H_w \tag{4-6}$$

  where H_w is the saturated humidity and RH is the relative humidity. The saturated humidity is simply the maximum concentration of water vapor possible at a specific temperature. This variable can be obtained from the partial vapor pressure of water.

$$H_w = \frac{p_{H_2O}}{p_T - p_{H_2O}} \frac{mw_{water}}{mw_{air}} \tag{4-7}$$

  where p_{H2O} is the partial pressure of water vapor, p_T is the total pressure and mw_{water} and mw_{air} are the molecular weights of water and air, respectively. The solids moisture content q of the sample is calculated using equations 4-6 and 4-7.

$$q_{tot} = m_{air} \frac{RH}{100} H_w + \frac{m_{solid} q}{100} \tag{4-8}$$

  where q_{tot} is the total moisture content, m_{air} is the mass of air and m_{solid} is the mass of solid.

- As the temperature changes, the RH profile at each node is adjusted to reflect moisture migration due to diffusion.

$$H_i^j = DA_{sp}H_i^{j-1} - H_{i-1}^{j-1} + H_{i-1}^j \quad (4\text{-}9)$$

where D is the diffusion coefficient for the moisture migration.

- Finally, the new equilibrium RH_{eq} and solids moisture content q_{eq} can be calculated. Thus equation 4-8 is adjusted to include the equilibrium values.

$$q_{tot} = m_{air}\frac{RH_{eq}}{100}H_w + \frac{m_{solid}q_{eq}}{100} \quad (4\text{-}10)$$

The sorption isotherms are used to derive an empirical relationship between the equilibrium solids moisture content q_{eq} and relative humidity RH_{eq}.

To verify the model, the solids moisture content was measured after exposing the material to a temperature cycle. The authors conclude that they can create a profile of the solid moisture content in the bulk and as a result they can predict cake formation.

All of the current models are useful as a first approximation of moisture migration caking. However, they reduce the fundamental transport equations, i.e. the moisture migration, to a simplified case that disregards pertinent details of the caking process.

Moisture Migration Model

The driving force of moisture migration caking is a concentration gradient within the bulk. This gradient causes transport of moisture through the interstitial voids of the bulk solid. Bulk materials are typically stored in an environment where temperature and relative humidity are not controlled. Thus, changes in the temperature from day to night can induce a thermal gradient through the material which affects the local relative humidity surrounding the particles. The changes in relative humidity caused by temperature fluctuations initiate the moisture migration through the bulk. With the additional moisture in the air, particles will adsorb moisture until an equilibrium state is

obtained. The equilibrium condition is determined from the sorption isotherms of the material. The isotherm represents the equilibrium relationship between the bulk solid moisture content and the relative humidity of air surrounding the particles as described in the previous chapter.

The process of moisture migration can be described by fundamental transport equations of heat, mass, and energy. It is assumed that the air surrounding the material is stagnant; therefore the only velocity gradient is that due to free convection. The partial differential equations will be solved using finite element techniques.

The location of the moisture is determined using finite element methods modeling. This result can be used to locate the formation of solid bridges within a bulk material. The following steps are required to achieve this result:

- Determine if convection plays a role in the caking process by comparing the temperature profiles from the models with and without a convective term. Analyze the Peclet number in the cell to determine if convection is a dominant mode of transportation for the moisture.
- Calculate the diffusion through the cell from the temperature profile.
- Determine where the moisture migrates in space and time i.e. the solids moisture content over time.

Finite Element Modeling

The moisture migration process is modeled using finite element methods utilizing the COMSOL Multiphysics software. This method is used to solve partial differential equations (PDEs) which describe and predict the moisture migration in caking. The behavior of moisture is modeled on a continuum scale. The flow of air, the heat transfer through bulk solids, and the moisture content of the solid within the cell are described. This is used to predict the amount of material or the thickness of the layer of material involved in a caking event and also the strength of the cake.

The general approach to solving PDEs using the finite element method includes discretization, developing the element equations, characterizing the geometry, applying boundary conditions and obtaining a solution. The discretization involves dividing the solution domain into simple shape regions or elements either in one, two, or three dimensions as shown in Figure 4-1. The points of intersection of the lines are called nodes.

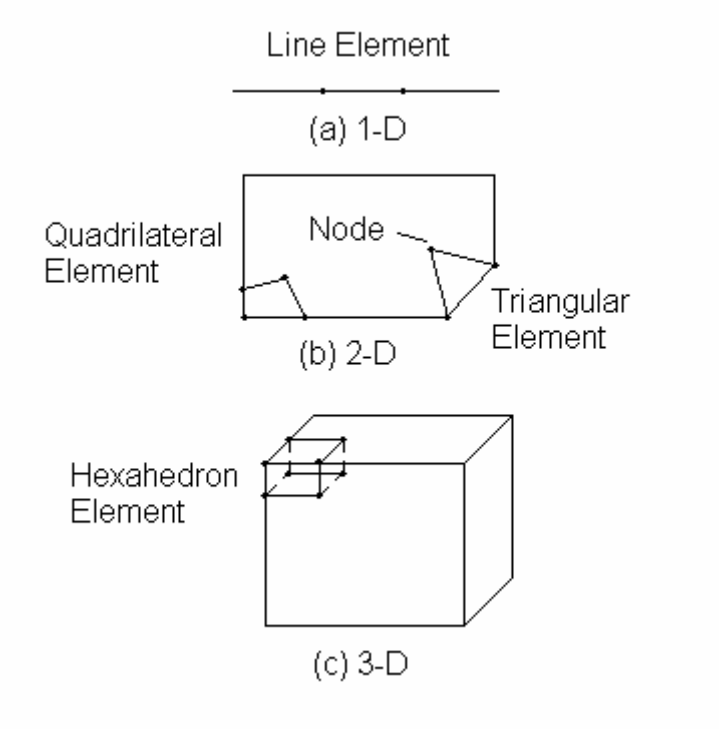

Figure 4-1. Examples of the elements used in FEM (A) one-dimensional (B) two-dimensional and (C) three-dimensional.

Approximate solutions for the PDE's are developed for each of these elements. The equations for the individual elements must be linked together to characterize the entire system. The total solution is obtained by combining the individual solutions. Continuity of the solution must be ensured at the boundaries of each element. The value of unknown parameters is generated continuously across the entire solution domain. After the boundary conditions are applied, the solution is obtained using a variety of numerical

techniques. COMSOL Multiphysics is the software used to solve the partial differential equations.

About COMSOL Multiphysics

COMSOL Multiphysics is an interactive environment for modeling and solving scientific and engineering problems based on partial differential equations (PDEs). The power of this program lies in its ability to couple several different physical phenomena into one system and solve the PDEs simultaneously. The finite element method (FEM) is used to solve the PDEs in two dimensions. FEM is a discretization of an original problem using finite elements to describe the possible forms of an approximate solution. The geometry of interest is meshed into units of a simple shape. In 2D, the shape of the mesh elements is a triangle. After the mesh is created, approximations of the possible solutions are introduced described by a function with a finite number of parameters, degrees of freedom (DOF).

Model Geometry

The geometry used in the COMSOL solver is modeled after the cells used to make the cakes as shown in chapter 2, Figure 2-4. A schematic of the geometry is shown in Figure 4-2. The width of the cell is 0.026 meters and the height is 0.02 meters. The bottom plate, labeled subdomain B, is made of aluminum and is the location of the heat source. The walls, labeled subdomain C, are made of phenolic which is a insulating material. The powder is contained in the center of the cell, labeled subdomain A. The cell is assumed to be axisymmetric for the simplification of the model and reduced computational time. There are 7272 triangular elements in the mesh as shown in Figure 4-3. The size of the mesh elements along the boundary are smaller than those in the domain.

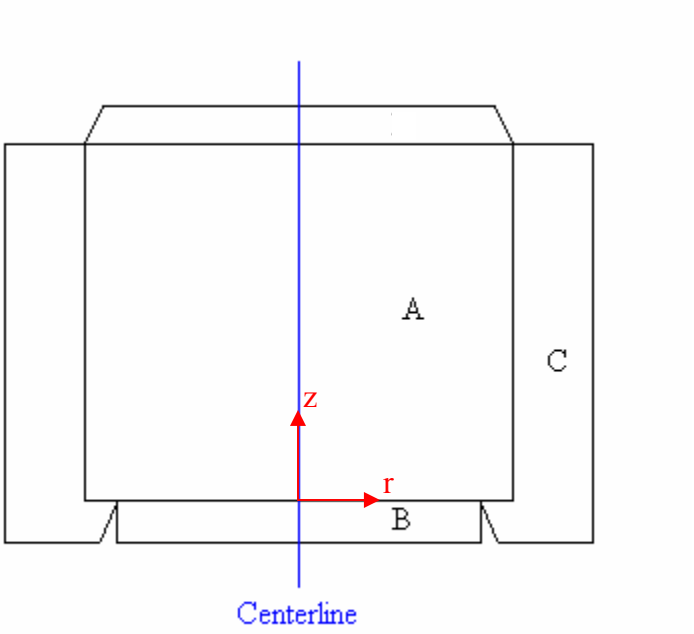

Figure 4-2. Schematic of the geometry used in the COMSOL solver. The lettered areas label the domains.

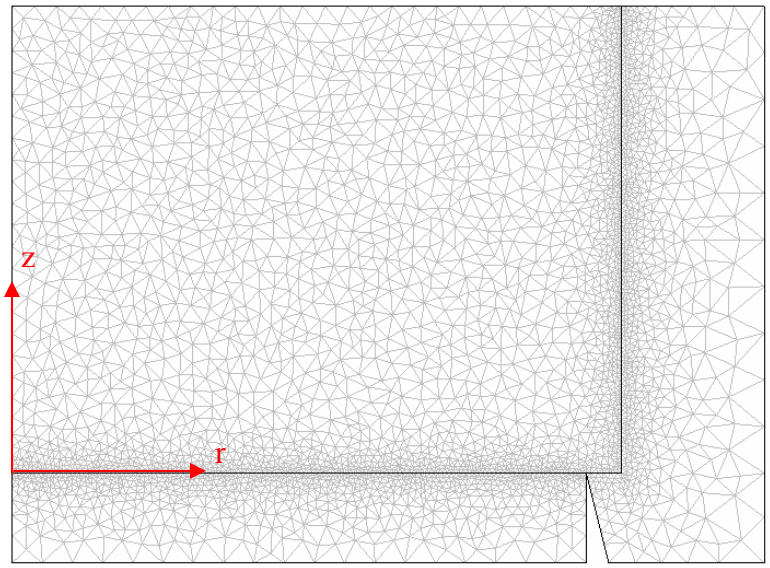

Figure 4-3. Caking cell geometry with mesh elements.

Partial Differential Equations

The process of moisture migration through a porous media from the atmosphere is governed by transient differential equations of heat (convection-conduction), mass

transfer (convection-diffusion), adsorption/desorption, and continuity and momentum (Brinkman's equation). To construct a mathematical model of the moisture migration, the following assumptions are considered:

- Powder grains are isothermal and in equilibrium with surrounding gas. This can be justified by the fact that grains are small and flow rate of gas is low.
- Heat generated or absorbed by adsorption/desorption is neglected.
- There is no mass (moisture) transfer from grain to grain through diffusion or capillary bridges.

The partial differential equations used to describe the moisture migration are given in detail below.

Convection-conduction

The convection-conduction equation is used to described the temperature distribution within the system.

$$\sigma_{ts}\rho C_p \frac{\partial T}{\partial t} + \nabla \cdot \left(-k\nabla T + \sum_i h_i \vec{N}_{D,i}\right) = Q - \rho C_p \vec{u} \cdot \nabla T \qquad (4\text{-}11)$$

where σ_{ts} is a time scaling coefficient, ρ is the density, C_p is the heat capacity, k is the thermal conductivity, T is the temperature, Q is the heat source, u is the velocity, and $h_i N_{D,i}$ is a species diffusion term. The temperatures of the fluid and particles are assumed to be in equilibrium. This can be justified by the fact that, for small particles, heat diffuses by conduction almost instantly. Equation 4-11 is applied to every subdomain. However, convection is not include in subdomains B and C. The velocity is determined from the Brinkman equation. The time scaling coefficient is one for all subdomains. The appropriate constants for each subdomain are specified.

Convection-diffusion

The convection-diffusion equation describes the mass transport in the system.

$$\sigma_{ts} \frac{\partial c}{\partial t} + \nabla \cdot \left(-D\nabla c\right) = R - \vec{u} \cdot \nabla c \qquad (4\text{-}12)$$

where D is the diffusion coefficient, R is the reaction rate term and c is the concentration. Since mass transfer only occurs in the bulk, this equation is only applied to subdomain A. The reaction rate term is a source or sink term for the water vapor on the fluid phase which is described by the change in solids moisture content with time. The time scaling coefficient is one.

Brinkman Equation

It is believed that free convection plays a role in the moisture migration through the system. Caking is known to be a time induced event. Thus if free convection aids the moisture migration process, the cakes may develop in a shorter period of time. This would indicate that free convection can play a major role in inducing cohesive storage time effects. The Brinkman equation coupled with the continuity equation is used to describe free convection in the system. The pressure distribution is calculated and consequently the velocity distribution (free convection) within the system and at its boundary. The Brinkman equation is a derivative of Darcy's law. Darcy's law describes flow through a porous medium. However, the Brinkman equation accounts for the viscous forces (Brinkman, 1947).

$$\rho\frac{\partial\vec{u}}{\partial t}+\frac{\eta\vec{u}}{\kappa}=\nabla\cdot\left[-p\vec{l}+\eta\left(\nabla\vec{u}+\left(\nabla\vec{u}\right)^{T}\right)\right]+\vec{F} \qquad (4\text{-}13)$$

where u is the velocity, η is the dynamic viscosity, κ is the permeability, p is the pressure, l is an identity matrix and F is a volume force ($-\rho g$). The equation for the permeability and the density as a function of temperature are given in Appendix B.

Solids moisture content

The solids moisture content is described by the linear driving force model. The equation used by COMSOL is given by:

$$\frac{\partial q}{\partial t} + \nabla \cdot \Gamma = F \qquad (4\text{-}14)$$

where F is a source term and Γ is a flux vector. The source term F is given in equation 4-2. However the rate constant k_g is determined from the kinetic data in chapter 3. The dissolution of the material and the evaporation of the moisture vapor is described in this model. Both adsorption and desorption must be considered because there is a hystersis in the sorption curve; the adsorption and desorption are not equal. The equilibrium conditions are not the same. The equations for the isotherm curves used in the model are given in chapter 3. The relative humidity is calculated from the saturation concentration as given in Table 4-1 and Appendix B.

Model Parameters

The experimental temperature and solid moisture content within the Johanson Indicizer® caking test are used as the initial and boundary conditions for the finite element modeling. The boundaries are identified in Figures 4-2 and 4-4. The boundary conditions, initial conditions and constants are listed in Tables 4-1 through 4-3.

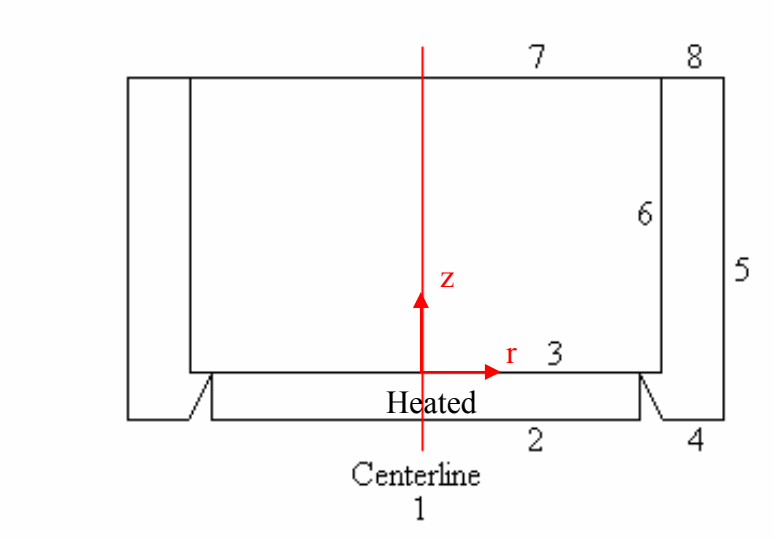

Figure 4-4. Boundary conditions.

Table 4-1. Parameters for COMSOL simulations.

Initial Pressure, *p_init*	101325 Pa	Gas Constant (fluid), *R_fluid*	R_fluid
Initial Temperature, *T_init*	298.15 K	Linear driving constant (isotherm), *k_ads*	0.0013
Porosity (ε)	0.5	Linear driving constant (isotherm), *k_des*	0.0013
Particle Diameter, *P_diam*	0.001 m	Antoine's coefficient, *a_a*	16.75667
Viscosity (air), v	1.8e-5 Pa s	Antoine's coefficient, *b_b*	4087.342
Permeability, κ	*permea*	Antoine's coefficient, *c_c*	-36.0551
Diffusivity, D	4.2e-6 m^2/s	Constants (isotherm), *A1*	0.47
Heat Capacity (solid), C_p	1500 J/kg K	Constants (isotherm), *A2*	0.47
Heat Capacity (fluid), C_f	1005 J/kg K	Constants (isotherm), *B1*	13.5
Conductivity (solid), k	0.2 W/m K	Constants (isotherm), *B2*	13.5
Density (solid), *dens_s*	2250 kg/m^3	Temperature Fluctuation, *T_fluct*	±15 K
Density (bulk), ρ	1600.24 kg/m^3	Initial Concentration, *c_init*	0.01
Molecular Weight (water), *mol_w*	18	Initial Saturated Concentration (moles), *c_sat_mol_init*	*c_sat_mol_init*
Molecular Weight (air), *mol_a*	29	Initial Saturated Concentration, *c_sat_init*	*c_sat_init*
Gravity, g	9.81 m/s^2	Initial Relative Humidity (bulk), *RH_init*	RH_init
Gas Constant, *R_gas*	8.314	Initial Solids moisture content, *u_init*	*u_init*

The temperature profile imposed on boundary 2 is given in Figure 4-5. The temperature profile is a sine wave and is maintained over a 24 hour time period. The maximum temperature is 55˚C and the minimum temperature is 25˚C.

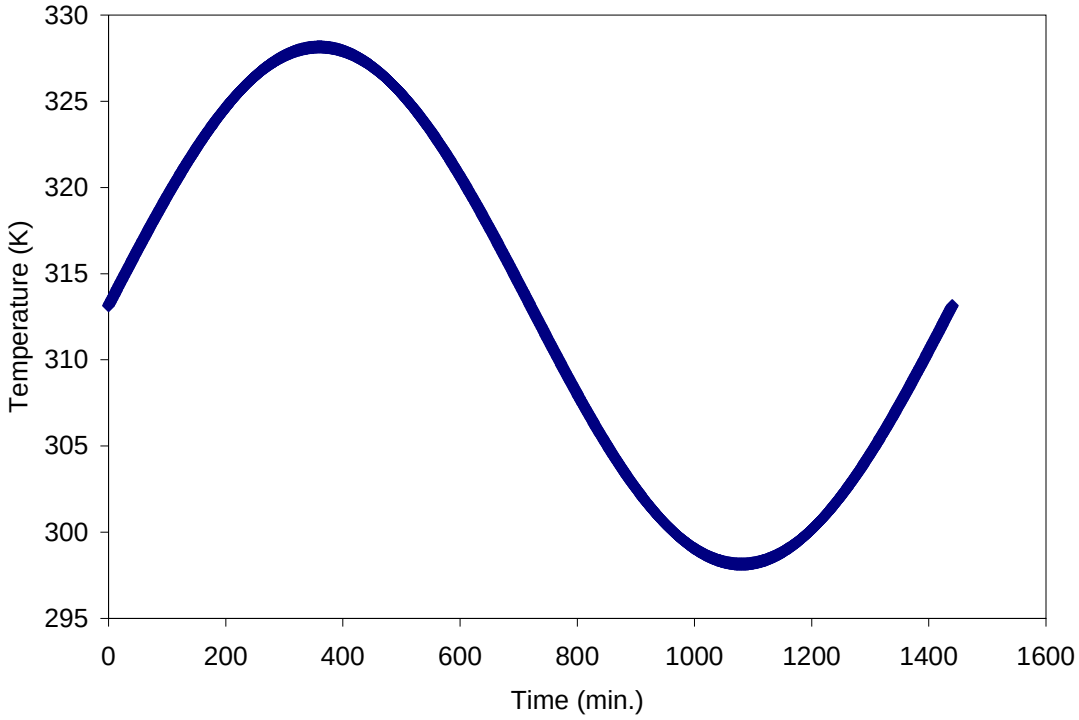

Figure 4-5. Temperature profile imposed at the base of the cell in the finite element simulations.

The initial temperature of the powder is 25˚C and the initial temperature of the heat source is 40˚C. The temperature surrounding the cell is maintained at 20˚C. There is flux at the outer boundaries (5,8,7). Heat is conducted through the material and across the inner boundaries (3,6).

Table 4-2. Boundary conditions for COMSOL simulations.

	Convection-conduction	*Convection-diffusion*	*Brinkman Equation*	*General PDE*
1	Axial symmetry	Axial symmetry	Axial symmetry	Axial symmetry
2	T_B	-	-	-
3	-	Insulated	No Slip	Neumann
4	T_B	-	-	-
5	$hA(T-T_\infty)$	-	-	-
6	-	Insulated	No Slip	Neumann
7	$hA(T-T_\infty)$	Insulated	No Slip	Neumann
8	$hA(T-T_\infty)$	-	-	-

Table 4-3. Subdomain conditions for COMSOL simulations.

	Convection-conduction	*Convection-diffusion*	*Brinkman Equation*	*General PDE*
A	Yes	Yes	Yes	Yes
B	Yes	-	-	-
C	Yes	-	-	-

The variables listed in Tables 4-1 and 4-3 are described in Appendix B.

The Role of Convection in Moisture Migration

Temperature Profiles

The current models for moisture migration available in literature assume that free convection does not contribute to the heat transport in the system. Finite element simulations are executed with and without convection to determine the significance of convection. Temperature profiles along the centerline and near the insulated boundary (6) are shown in Figures 4-6 and 4-7. The temperature profiles in these figures include convection.

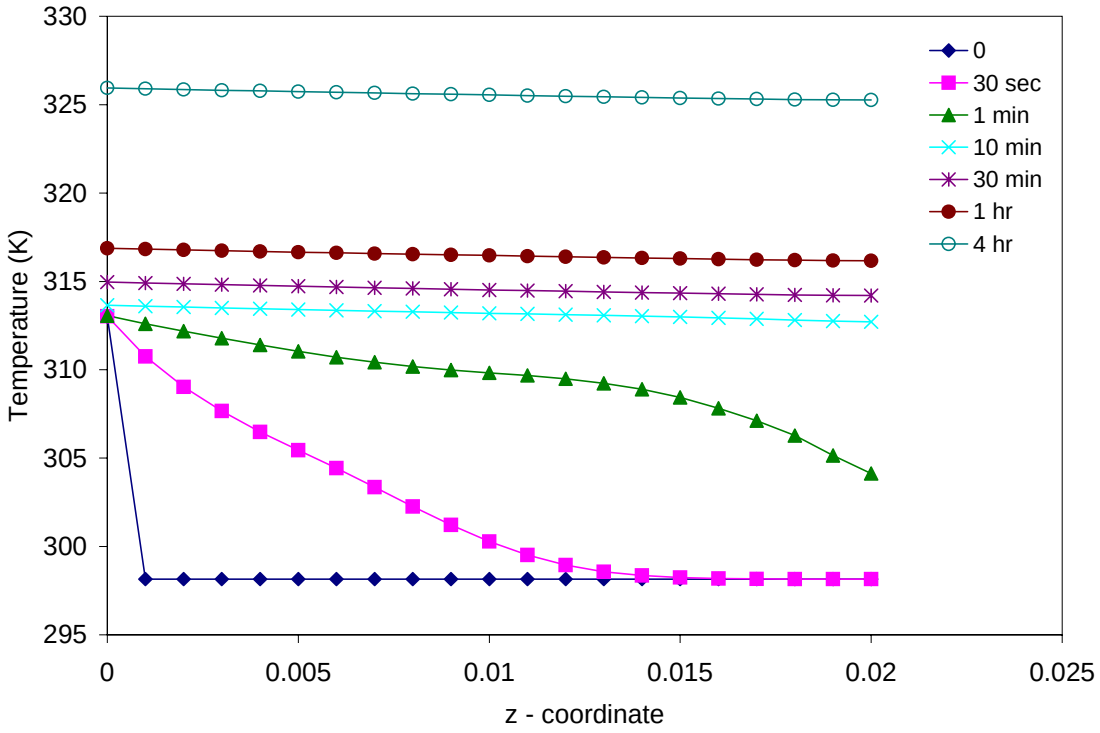

Figure 4-6. Temperature profile along the centerline of the cell with convection included.

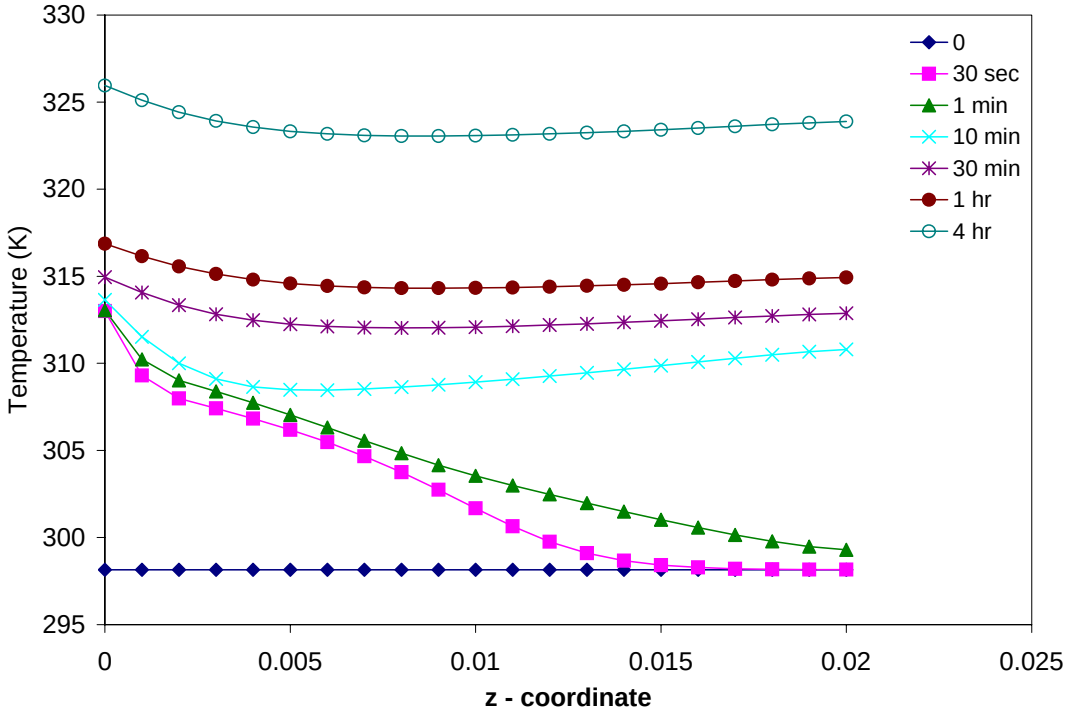

Figure 4-7. Temperature profile near the insulated boundary of the cell with convection.

It can be seen in Figure 4-6 that the temperature along the centerline increases until the setpoint temperature is achieved. The setpoint temperature is obtained after only five minutes. An oscillation of the temperature is seen after one minute. This is attributed to the free convection plumes that initially develop within in the cell. These plumes are shown in Figure 4-8. The plumes appear from zero to two minutes and then disappear. It can be seen in Figure 4-7 that the temperature profile near the insulated boundary reaches the setpoint temperature after thirty minutes. The oscillations in this figure are also attributed to the formation of plumes. Temperature profiles for the case of no free convection are shown in Figures 4-9 and 4-10. It can be seen that the setpoint temperature is obtained after four hours. Comparing this result to the free convection included case suggests that the free convection does play a significant role in the heat transport of the system. If free convection is included, the cakes will develop in a shorter period of time.

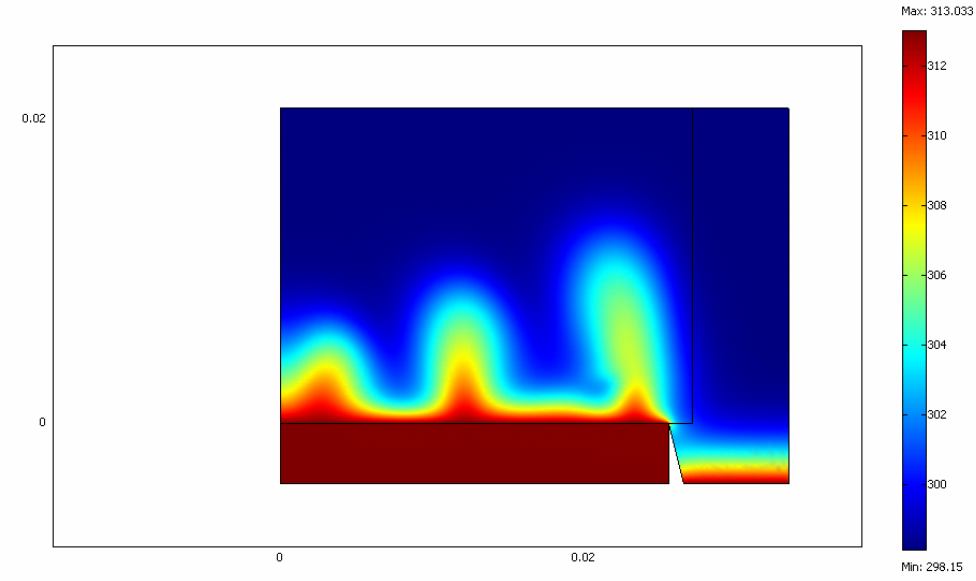

Figure 4-8. The temperature profile within the cell illustrating the convective plumes that develop.

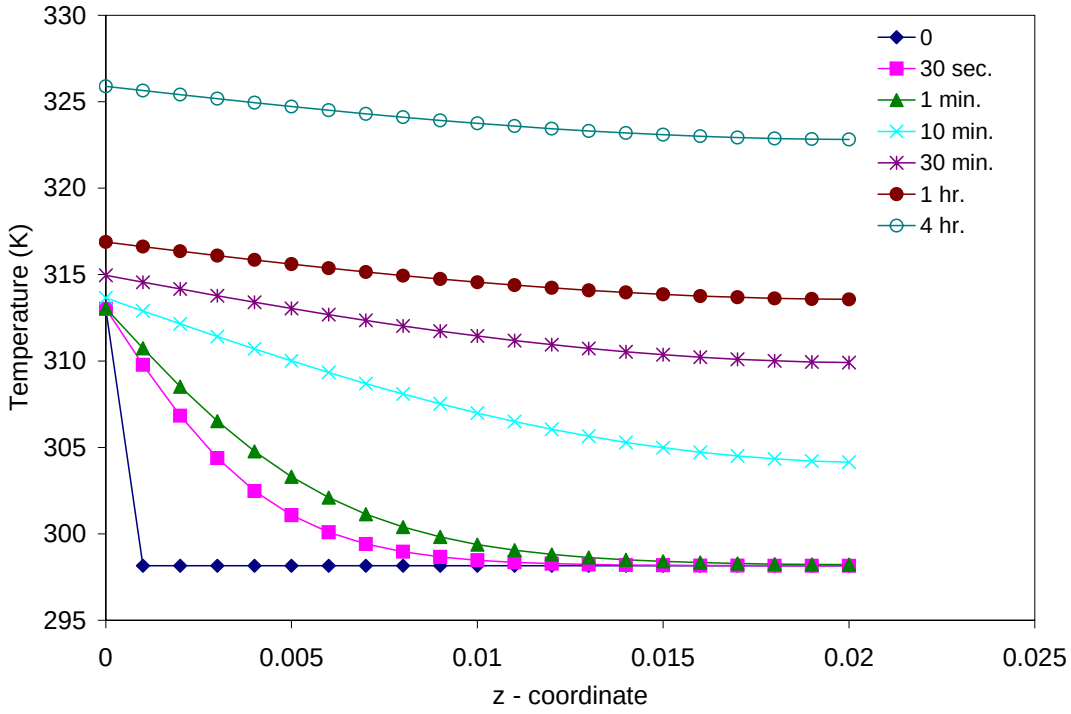

Figure 4-9. Temperature profile along the centerline of the cell without convection.

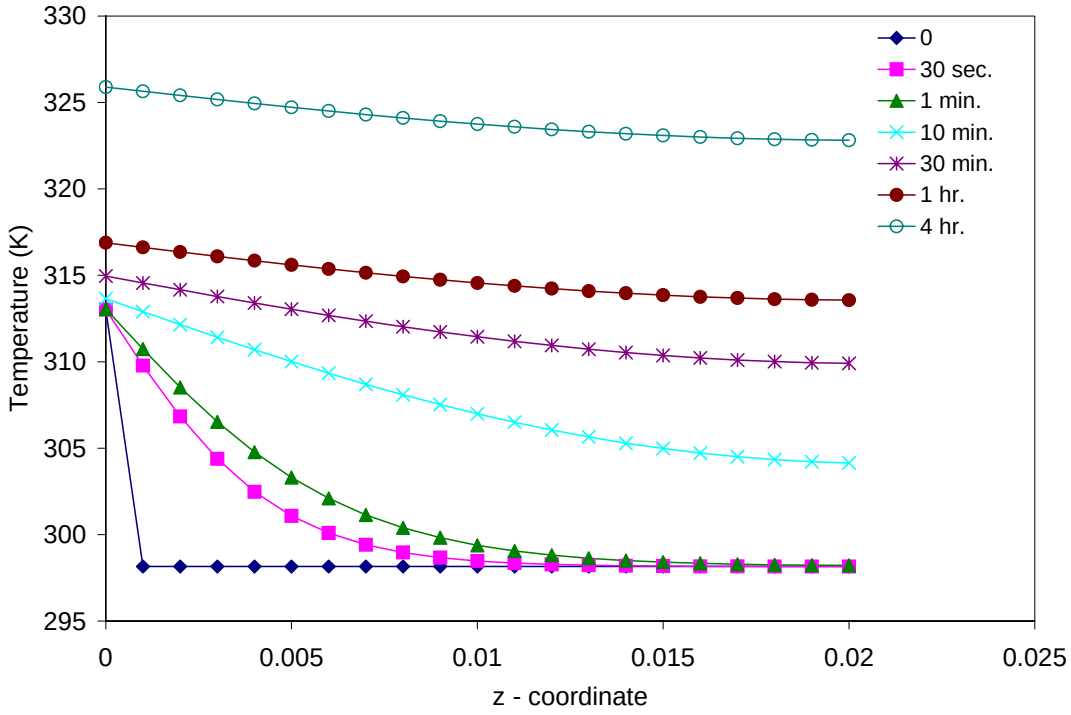

Figure 4-10. Temperature profile near the insulated boundary of the cell without convection.

The temperature in the center of the cell is plotted in Figure 4-11. The difference between the convection and non-convective profiles are shown. With the free convection in the system, the response to a change in temperature occurs faster than conduction only.

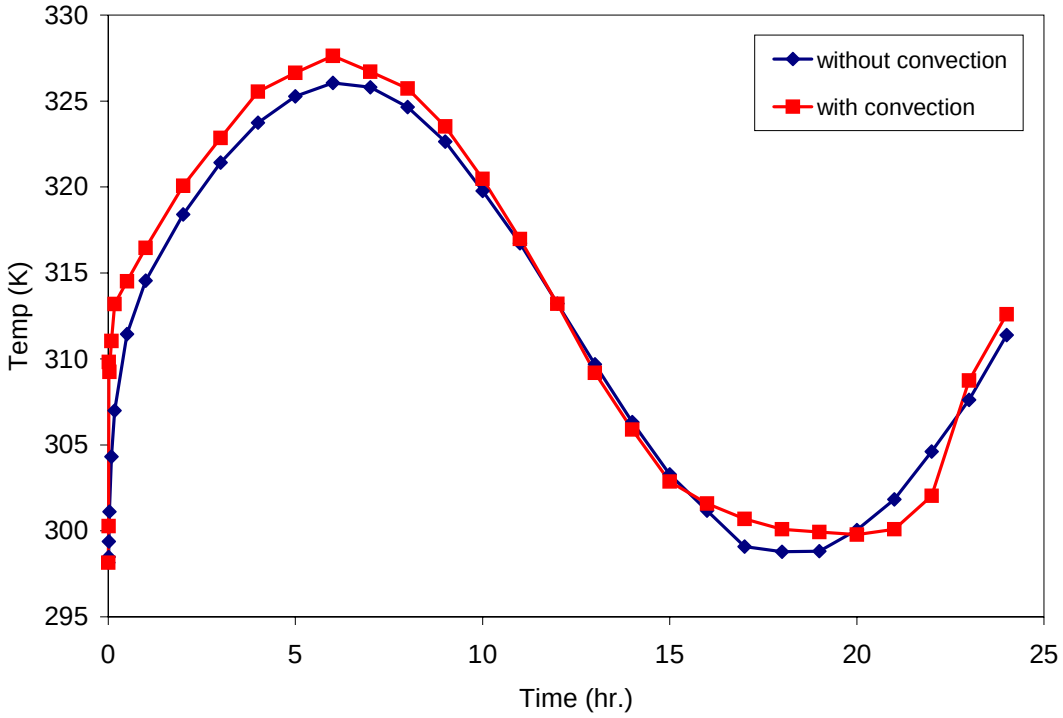

Figure 4-11. Temperature profile at the center of the cell, with and without convection.

The variation of material temperature as a function of time is most critical in the region where shear takes place i.e. near the cell wall (insulated boundary). In this region bonds between particles are being broken and the force required to break these bonds determine the cohesive properties measured with this test cell. Temperature profiles in this region also indicate that free convection speeds the caking process and results in higher cell temperatures during heat-up (see Figure 4-12).

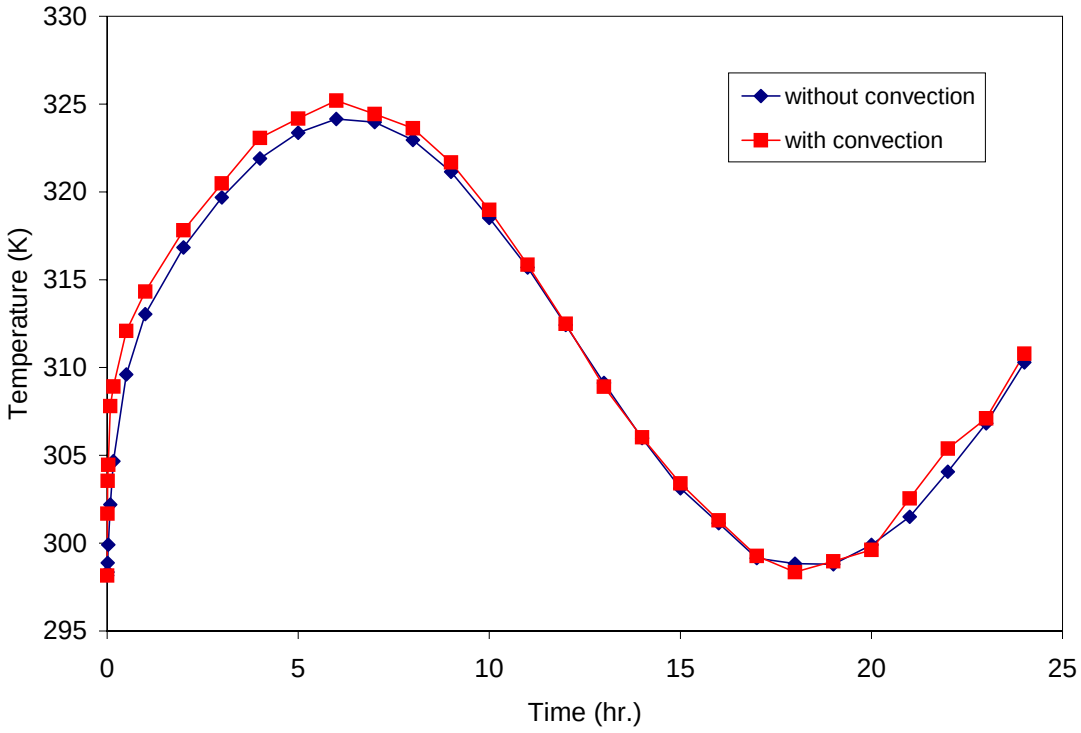

Figure 4-12. Temperature profile at the cell wall, with and without convection.

An analysis of the cell Peclet number is also used to determine if convection contributes significantly to the moisture migration through the cell in caking. The Peclet number is the product of the Reynolds number and Prandtl number. The physical interpretation is the ratio between the heat transfer by convection to the heat transfer by conduction.

$$Pe' = \frac{\rho C_p v_o (T - T_o)/l_o}{k(T - T_o)/l_o^2} \qquad (4\text{-}11)$$

The Peclet number gives an idea of the dominant mode of heat transfer through the cell. A high Peclet number means that the heat transfer from convection can not be neglected and the heat transfer from conduction is not substantial. If the number is low, then heat transfer from convection can be assumed negligible. When convection is added

to the model, the cell Peclet number is in the range of 1 to 5. This suggests that convection is the dominant mode of heat transport.

Solids Moisture Content

The solids moisture content of the material is important because a change in this quantity determines the extent of caking in the system. Adsorption of moisture and increase in the solids moisture content specifies the amount of dissolved materials available for the creation of solid bridges. The desorption of moisture, a decrease in the solid moisture content, specifies the amount of crystallized solid material in the bridge.

Thus far, it has been determined that the convective system dominates the moisture migration process. Therefore, the results shown include free convection in the system. The solids moisture content within the cell is given in Figure 4-13. The moisture content is plotted as a function of the position along the height of the cell at various times. It can be seen that the material in the lower half of the cell does not undergo a change in moisture content. Near the top of the cell the moisture content changes in time and increases and decreases with the temperature. The moisture content follows the same trend as the temperature profile with time shown in Figure 4-14. This figure shows a cyclic moisture profile in the shear region of the test cell. The frequency of the moisture cycle follows the temperature profile but lags the temperature profile. An increase in the moisture content followed by a subsequent reduction is the mechanism behind solid bridge formation suggests that the cake will develop in the region near the wall and will be most pronounced at the top surface of the test cell. The regions of greatest caking potential are areas with significant adsorption and desorption as a function of time.

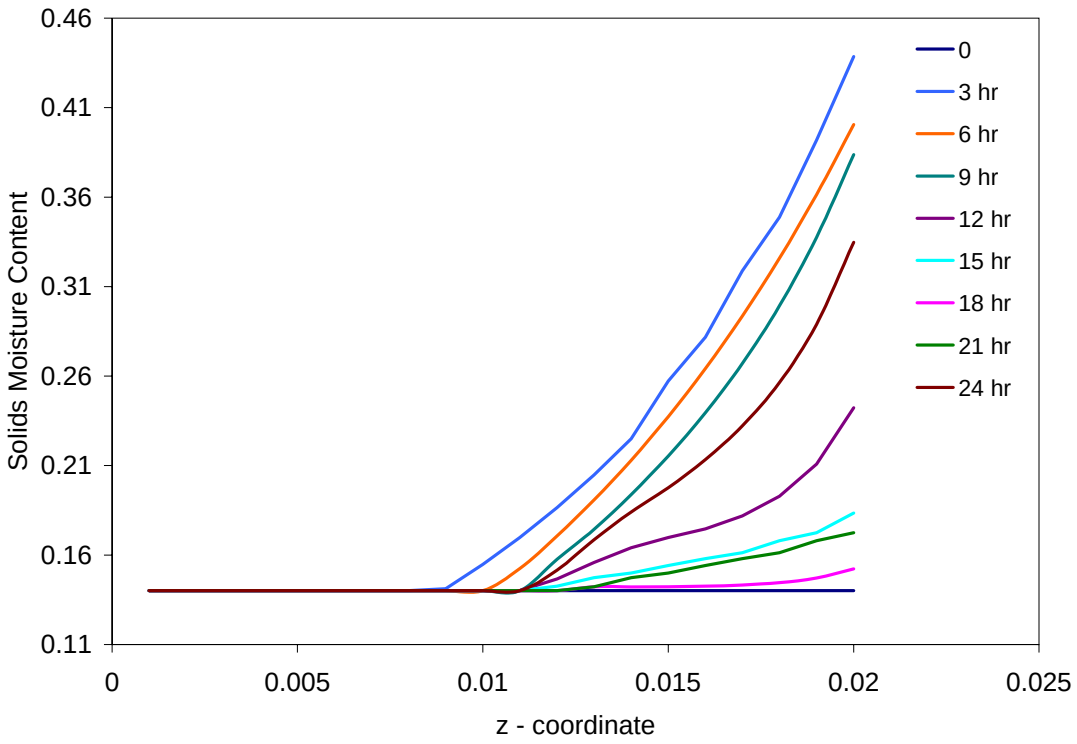

Figure 4-13. Solids moisture content profile at the centerline of the cell with convection.

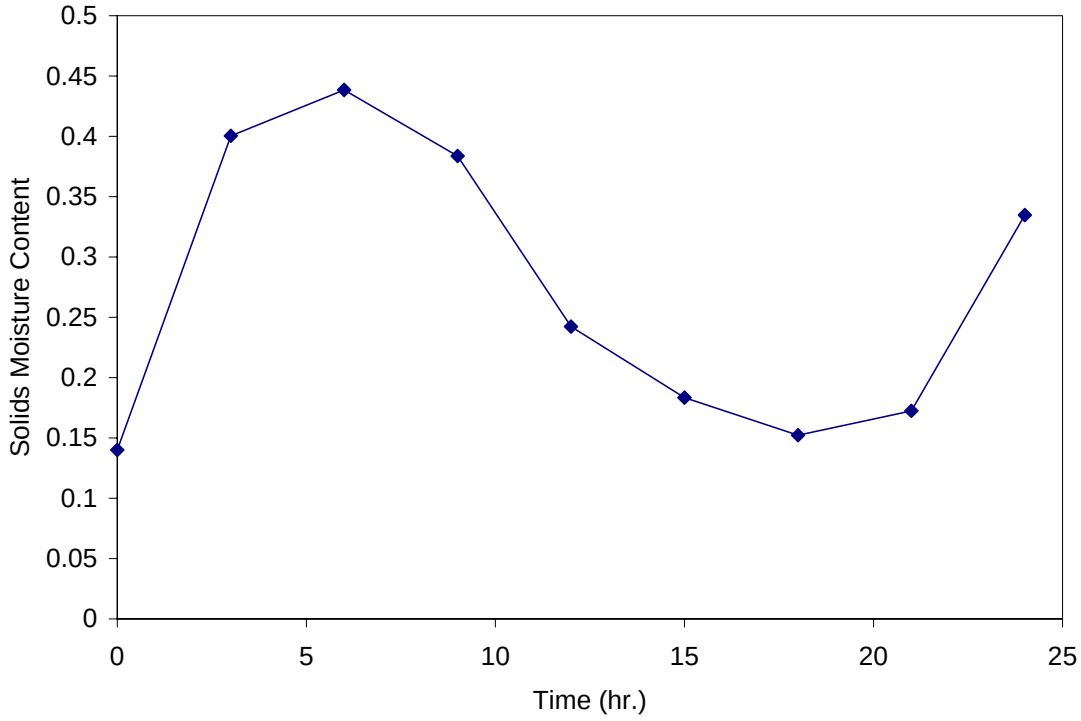

Figure 4-14. Solids moisture content as a function of time at the center of the cell.

This re-crystallization effect can best be seen by superimposing the temperature profile computed within the shear region on the phase diagram for the sodium carbonate system. Figure 4-15 shows the operating curve for the test cell. Material within the cell initially starts at a solids concentration of 14%. The change in temperature and moisture content causes material within the cell to cross a phase boundary. Increasing the temperature causes the sodium carbonate to dissolve forming a solution of monohydrate. Subsequently cooling the material causes the carbonate to cross the phase boundary and form solids bonds between particles.

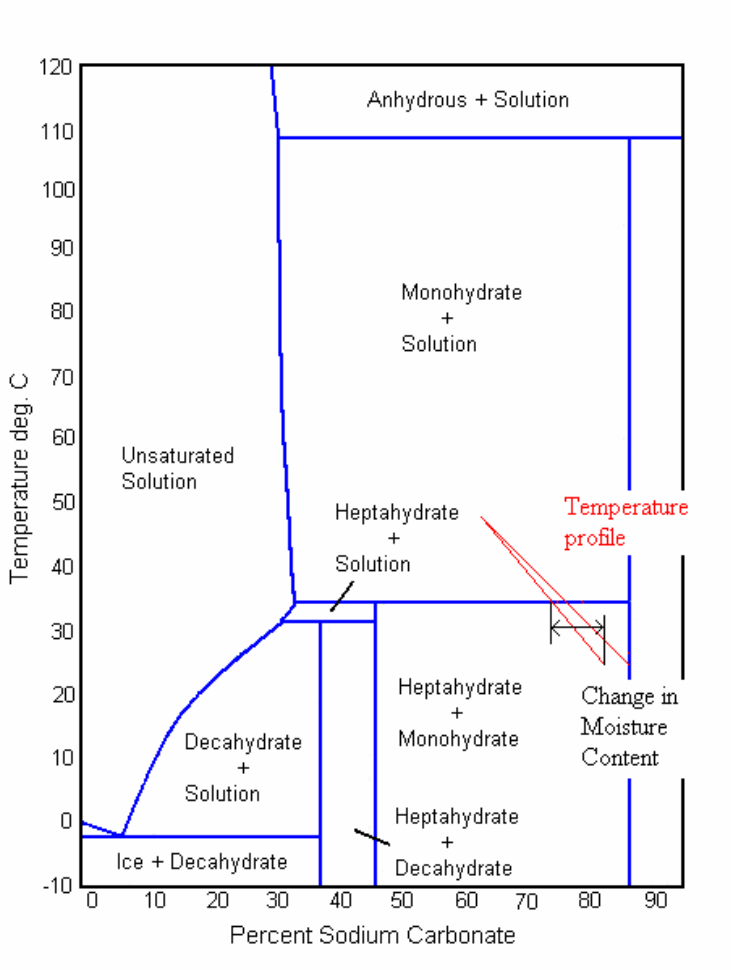

Figure 4-15. Phase diagram of sodium carbonate with temperature profile imposed.

It is possible to approximate the cake strength if the change in solids moisture content is known. The solids moisture content affects the unconfined yield strength by influencing the radius of the crystallized bridge *b* formed between particles. A detailed description of cake strength predictions and the factors that influence the strength is given in the following chapter. Nonetheless, the approximate strength of the cake can be determined from the variation in solids moisture content with time. The area of interest is the moisture content near the insulated boundary since the shear plane in the Johanson Indicizer® is located in this region. The shear region is indicated by the hatched area in Figure 4-16. The change in solids moisture content in this region dictates the strength of the cake. The moisture content distribution near the insulated boundary is shown in Figure 4-16. It can be seen that the moisture content varies along the height of the cell. However, it does not change significantly within the radius of the shear plane. Because of this insignificance, the unconfined yield strength is assumed to be constant in this region. For larger variations in the moisture content within the shear plane, the averaged unconfined yield strength must be considered.

Using the equations in chapter 5, it is determined from the moisture content profile within the shear plane that the unconfined yield strength increases by 18% at a consolidation stress of 10 kPa over the length of the caking event. Given the same conditions, the yield strength data from chapter 2 indicates that the strength increases by 40%. Although the unconfined yield strength approximation from the moisture migration analysis and the experimental data are not exact, these values have the same order of magnitude. This comparison establishes a basis for estimating the unconfined yield

strength as a function of the solids moisture content calculated from an finite element moisture migration analysis.

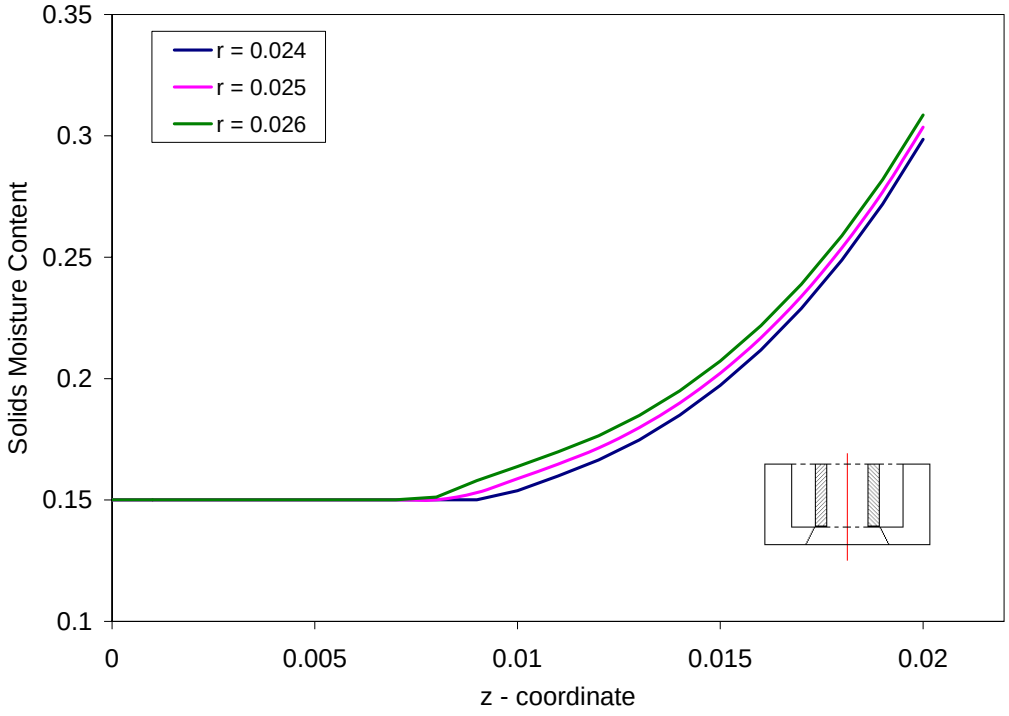

Figure 4-16. Equilibrium solids moisture content as various positions along the radius.

CHAPTER 5
EVALUATING THE CAKE STRENGTH OF GRANULAR MATERIAL

In this chapter a model for evaluating the cake strength of granular material is developed. Although there are models available in literature for estimating cake strength, it is shown that these models are often times inadequate predictors. All of the current models suggest that the strength is influenced by a single variable. However, it is well known that several factors affect the strength of cakes. Therefore a new model is developed which includes the dependency on the particle size, moisture content, consolidation stress, and other material properties.

Background

A useful tool for understanding the caking of granular materials is a model predicting cake strength. This is not only useful for understanding the effects of the influential properties of caking but it can also be used as a predictive measure for future events. Rumpf (1958) was the first to propose a theory for the tensile strength of agglomerates and many of the present models are based on his work. He developed expressions for the strength of agglomerates with various types of interparticle bonds. One mechanism for agglomeration is the formation of liquid bridges. Rumpf suggests that the tensile strength of an agglomerate is proportional to the inverse of the particle diameter squared.

$$\sigma_t = \frac{k_o(1-\varepsilon)}{\pi d_p^2} H \qquad (5\text{-}1)$$

In equation 5-1 σ is the tensile strength of the agglomerate, ε is the porosity of the cake, d_p is the particle diameter, k_o is the coordination number (number of contacts per particle), and H is the strength of the interparticle bond. The flaw of this equation is based on the unrealistic assumption that the bridges fail simultaneously and that all the particles are of equal size. Rumpf also proposed a theory for agglomeration due to the formation of solid crystalline bridges. This equation is based on moisture content of the material and the concentration of material in the bridge.

$$\sigma_t \approx y_k q \frac{\rho}{\rho_k}(1-\varepsilon)\sigma_k \qquad (5\text{-}2)$$

In equation 5-2 y_k is the concentration of the dissolved species k, q is the moisture content of the particles before caking, ρ is the density of the particle, ρ_k is the density of k in the crystal bridge, and σ_k is the strength of a crystal bridge. It is assumed that by random packing the mean volume fraction of particles is equal to the mean cross sectional fraction of these particles. Thus, the dependence of the strength on particle size is lost and the tensile strength is proportional to the volume fraction of crystalline material in the bridge times the strength of the bridge. This assumption differs from Rumpf's previous theory that states that the strength of an agglomerate is inversely proportional to the diameter of the particle. Similar to the first equation, it is assumed that all bridges fail simultaneously. Neglecting these critical parameters renders an inadequate predictive model for the cake strength of granular materials.

Other researchers have used Rumpf's model to verify experimental data for various materials. Pietsch (1969a) applies Rumpf's model to investigate the influence of drying rate on the tensile strength of pellets bound by salt bridges. He measured the agglomerate strength using a vertical tensile tester. The details of this tester are described in chapter 2.

Pietsch altered Rumpf's equation to include a mean tensile strength as given in the equation 5-3.

$$\sigma_t = \frac{M_s \rho}{M_p \rho_s}(1-\varepsilon)\overline{\sigma}_k \qquad (5\text{-}3)$$

where M_s and M_p are the mass of the salt in the dry agglomerate and the mass of the agglomerate, respectively, ρ_s and ρ are the densities of the salt and solid particles, and σ_t is the average tensile strength of the bridges. Since the strength of the bridges varies with changing crystal structure, an average tensile strength is used. He assumes that a crust, consisting of solid bridges, is formed around the cake during the drying process due to the crystallization of the salt solution. This crust changes the drying rate of the cake, effectively changing the strength of the cake. The crust is removed before measurements are taken for the strength of the material. Pietsch reports that the tensile strength of the core agglomerate is highly influenced by the drying rate.

Tanaka (1978) further developed Rumpf's model by incorporating the structure of the agglomerate. He included the effects of heat and mass transfer on the formation of the solid bridges. Tanaka used a model of contacting spheres with pendular water as shown in figure 5-1. The particles in the agglomerate are assumed to be monosized with a radius of R. A fictitious sphere of radius r approximates the curvature of the bridge. The volume of the bridge V and the narrowest width of the bridge b are derived as a function of R and θ. Hence V and b are related by the parameter θ according to the following equation.

$$b/R = 0.82\left(V/R^3\right)^{0.25} \qquad (5\text{-}4)$$

Equation 5-4 implies that the cake fails at the narrowest width of the bridge (neck). The volume V between two particles is a function of the total volume of a single particle V_t and the number of contact points per particle

$$V = 2V_t / k_o \tag{5-5}$$

In equation 5-5 k_o is the coordination number. This number is approximated by Rumpf (1958) as inversely proportional to the porosity ε ($k_o \approx \pi/\varepsilon$).

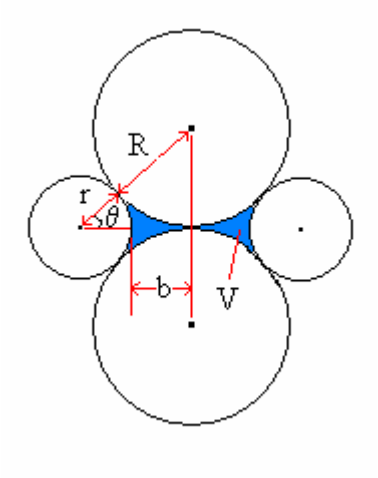

Figure 5-1. Model of contacting spheres with pendular water used to calculate the volume and width of the bridge.

Tanaka used the relationship between the volume and the width of the solid bridge combined with Rumpf's model to form the following equation for the tensile strength of powders.

$$\sigma_t = 0.17 \frac{(1-\varepsilon)}{\varepsilon} \left\{ \frac{8\varepsilon}{3(1-\varepsilon_c)} C_e (q/100) X^{1/(1-X)} \right\}^{1/2} \sigma_k \tag{5-6}$$

where σ_z is the tensile strength of the recrystallized solid bridge, C_e is the equilibrium concentration, q is the initial moisture content, ε_c is the porosity of the recrystallized bridge, and X is a lumped parameter which is function of the temperature and humidity. It is assumed that the solid bridges are formed from dissolved material due to heat and mass

transfer in the system. Equation 5-6 implies that the tensile strength is independent of particle size and rather a function of the moisture content and equilibrium concentration of the solid and the rate of mass transfer.

Thus far the equations for evaluating caking have been focused on the tensile strength of the material as a function of particle size and moisture content. However, of greater importance with regards to this research is how the unconfined yield strength is affected by these properties. It can be shown that the tensile strength σ_t is proportional to the unconfined yield strength f_c from the construction of Mohr circles and a yield locus in figure 5-2.

$$f_c = \sigma_t \frac{1+\sin\phi}{1-\sin\phi} \tag{5-7}$$

where ϕ is the internal angle of friction.

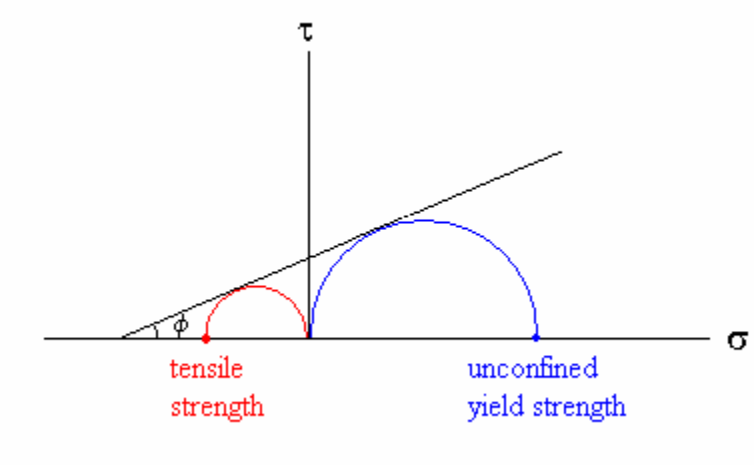

Figure 5-2. Mohr circles demonstrating the relationship between tensile strength and the unconfined yield strength.

Tomas *et al*. (1982) formulated a model to investigate the unconfined yield strength as a function of storage time using Rumpf's and Tanaka's model. The unconfined yield

strength is measured using the Jenike shear tester. The authors propose that the unconfined yield strength σ_c varies with the moisture content q of the material as follows:

$$d\sigma_c = \sigma_{Ds}(1-\varepsilon)Y_S[-dq(t)] \tag{5-8}$$

The kinetics of the materials is assumed to follow the linear driving force model of equation 5-9. This equation is integrated over the storage time to find the moisture content of the material at a particular time:

$$-\frac{dq}{dt} = -kA_{sp}(q - q_E) \tag{5-9}$$

Equation 5-10 relates the unconfined yield strength to the decrease in moisture content over time through the combination of equations 5-8 and 5-9.

$$\sigma_c = \sigma_{Ds}(1-\varepsilon)Y_S(q_O - q_E)[1-\exp(-kA_{sp}t)] \tag{5-10}$$

In equation 5-10 σ_c is the unconfined yield strength, σ_{Ds} is the compressive strength of the solid bridge, Y_S is the solubility, q_o and q_E are the initial and equilibrium moisture contents, k is the mass transfer coefficient of water, A_{sp} is the specific mass transfer area, and t is the time. This model gave only slight agreement with experimental results. However, the authors state that this model can be used to approximate the acceptable moisture content as a function of storage time to avoid situations of caking.

The above models for evaluating cake strength have focused on temperature induced caking. In other words a temperature perturbation is assumed to initiate a caking event. However, it is has been observed that a change in relative humidity can also trigger a caking event (Kun *et al.,* 1998). The effect of humidity cycling has been studied by Leaper *et al*. (2003). The authors make use of Tanaka's model to develop a relationship

between the cake strength and the number of humidity cycles. It is suggested that if the porosity and particle size remain constant the tensile strength can be given as

$$\sigma_t = K_h \sqrt{N} \tag{5-11}$$

where K_h is a parameter that incorporates the crystal bridge strength, particle size, porosity, and humidity swing and N is the number of humidity cycles. This model was compared to experimental results from a simple compression tester adapted to control the relative humidity of the sample. The authors found that the cake strength does indeed vary with the number of humidity cycles. The parameter K_h in equation 5-11 was calculated from experimental data to be 26 while the number of cycles N is raised to the power 0.546.

Most of the understanding of agglomerate breakage and all of the previous models are based on the work of Rumpf. More recently, the principles of fracture mechanics have been used to evaluate the strength of agglomerates as an alternative approach to Rumpf's theory. Kendall (1988) and Adams (1985) have proposed a fracture mechanics description of agglomerate breakage. It is believed that internal flaws or cracks within the material are responsible for the failure of the agglomerate. The authors describe agglomerate strength in terms of fracture mechanics parameters and the size of the crack which depend on the geometry and packing of the agglomerate.

Kendall (1988) states that the fracture mechanics approach to agglomerate strength is based on three levels of magnification: particle-particle contacts, an assembly of particles, and a block of material which behaves as an elastic solid. At the particle level the particles are held together, without binder, by an interfacial energy Γ. The interfacial

energy can be determined from the size of the contact zone. From fracture mechanics analysis, the diameter *d* of the contact zone is given by

$$d = \left(\frac{9\pi\Gamma {d_p}^2}{2E} \left(1 - \nu^2\right) \right)^{1/3} \tag{5-12}$$

where d_p is the diameter of the elastic particles, E is Young's modulus and ν is Poisson's ratio. The Young's modulus of an assembly of particles differs from that of two particles in contact. This is due to the elastic deformation of the assembly under stress. The effective Young's modulus E^* for an assembly of particles is given by

$$E^* = 17.1\left(1-\varepsilon\right)^4 \left(\frac{E^2\Gamma}{d_p} \right)^{1/3} \tag{5-13}$$

where ε is the porosity. The assembly of particles also has an effective cleavage energy ${R_c}^*$.

$${R_c}^* = 56\left(1-\varepsilon\right)^4 \left(\frac{\Gamma_c^5}{E^2 {d_p}^2} \right)^{1/3} \tag{5-14}$$

In equation 5-14 Γ_c is the fracture energy. The agglomerate is treated as a continuous medium and the fracture stress σ_f is given by

$$\sigma_f = 0.893 E^* {R_c}^* \left(\pi a\right)^{-1/2} \tag{5-15}$$

where *a* is the length of the crack. Equation 5-15 applies to clean, smooth elastic spheres and is verified with experimental data on alumina and titania agglomerates. The results prove that this model is a better predictor of agglomerate strength as a function of particle size when compared to the theory of Rumpf. However, Kendall's model fails to address the inherent plasticity of most materials during fracture.

Two different approaches, Rumpf's theory and fracture mechanics principles, for evaluating the strength of agglomerates have been discussed thus far and the dissimilarities between the models are apparent. One major difference between the models lies in Rumpf's derivation of his theory. He assumes that the particles are bound together by interparticle forces and the addition of such forces yields the ultimate strength of the agglomerate. Whereas the fracture mechanics view is that the agglomerate is an elastic body that satisfies the Griffith energy criterion of fracture. Other distinctions between to two theories include the functionality of particle size and porosity and the assumption of Rumpf that the bridges fail simultaneously.

In this research, the principles of fracture mechanics are applied to evaluate cake strength. The fracture stress σ_f of the material is assessed to determine the unconfined yield strength of the cake. The fracture stress is defined as the minimum amount of energy needed to fracture the bonds of the cake. An essential factor lacking in the fracture mechanics model as well as the models of Rumpf is the functionality of consolidation stress on the strength of the material. As shown in chapter 2, there is a strong relationship between the unconfined yield strength and the consolidation stress. Therefore, a new modified fracture mechanics model is proposed for evaluating cake strength which includes the structure of the bridge, particle size, moisture content and consolidation stress.

Modified Fracture Mechanics Model for Evaluating Cake Strength

The principles of fracture mechanics have been applied to the field of particle technology as an alternative approach to Rumpf's theory in determining the strength of agglomerates. A theory has been developed to explain the failure of solids caused by

flaws or imperfections in the structure of the solid and the elastic and plastic deformation of the material. The current models proposed by Kendall (1988) and Adams (1985) are based on Linear Elastic Fracture Mechanics (LEFM). This concept is applicable to materials with relatively low fracture resistance. Failure below their collapse strength is common therefore these materials can be analyzed on the basis of LEFM (Broek, 1988). The failure of very brittle materials can be described using LEFM, however most real materials exhibit plastic deformation during failure. For this condition, Elastic-Plastic Fracture Mechanics (EPFM) must be applied. The fracture parameters of many crystalline materials, which are prone to cake, are sufficiently described using LEFM. However the caking process alters the surface characteristics of these materials thus affecting the mechanics of fracture. This change is caused by the creation of 'soft' material in the contact zones due to the dissolution of the particle surface. The bridges formed throughout the process of caking may completely solidify to create a brittle structure. However, it is most probable to assume there is partial solidification of the bridges creating a structure which will deform during fracture. Therefore EPFM will give a better approximation to cake strength.

Before introducing EPFM it is useful to review LEFM. The fracture parameters in both areas are directly related and the principles of fracture mechanics were originally developed for linear elastic materials.

Linear-elastic Fracture Mechanics

LEFM is based on an energy balance in which the strain energy released at the crack tip provides the driving force to create new surfaces (Griffith, 1920). In order for fracture to occur, the rate at which energy is released in the solid must be equal to or greater than the cleavage resistance R_c. Thus the elastic energy release rate of the crack G

must be equal to the crack resistance R_c before crack propagation and fracture can occur. The Griffith criterion for fracture is given by:

$$\frac{\beta^2 \pi \sigma^2 a}{E} = R_c \quad \text{or} \qquad G = R_c \tag{5-16}$$

where β is a dimensionless factor based on the geometry of the solid, a is the crack length, and E is Young's modulus of elasticity. Applying Hooke's law $(\sigma = \varepsilon E)$, equation 5-16 can be written as follows:

$$\beta^2 \pi \sigma \varepsilon a = R_c \tag{5-17}$$

An alternative approach to the Griffith fracture criterion is investigating the stress field at the tip of the crack (Irwin, 1957). The stress intensity factor K defines the behavior of the crack under an applied load. This approach is simply the study of stress and strain fields near the tip of a crack in an elastic solid. Since the stresses are elastic, they must be proportional to the stress (or applied load) σ. Irwin proposed the following equation for the stress field near the tip of a crack.

$$K = \beta \sigma (\pi a)^{1/2} \tag{5-18}$$

In equation 5-18 β is a dimensionless geometry parameter, a is the crack length and σ is the applied load. The crack will grow when K reaches a critical value K_c.

$$K_c = \beta \sigma_f (\pi a)^{1/2} \tag{5-19}$$

At the time of fracture the stresses in the crack tip are equal to those in the elastic solid and K_c becomes the toughness of the material. K_c is a measure for the crack resistance of a material and is called the plane strain fracture toughness (Broek, 1977). It can be shown that the elastic energy release rate is equivalent to the stress intensity factor (Broek, 1988).

$$G = \frac{K^2}{E} \tag{5-20}$$

Elastic-plastic Fracture Mechanics

EPFM incorporates the plastic deformation at the crack tip during fracture that is neglected in LEFM. The fracture parameter used to describe the crack propagation is the J-integral. The J-integral defines the strain energy release rate for EPFM. Therefore J is equivalent to G for linear-elastic materials. Similarly, the symbol J_R is used to denote the fracture energy for non-linear elastic materials. For the case of plastic deformation the geometry factor is termed H and this quantity may vary from the linear elastic case. For LEFM the stress-strain curve is linear and it follows Hooke's law, however for EPFM the stress-strain curve is non-linear. The stress-strain curve is approximated by the Ramberg-Osgood equation (equation 5-21), where n is the strain hardening exponent and F is the plastic modulus.

$$\varepsilon = \frac{\sigma}{E} + \frac{\sigma^n}{F} \tag{5-21}$$

Using this approximation for the stress-strain relationship, the equation for the plastic fracture energy becomes:

$$J_R = \frac{H\sigma^{n+1}a}{F} \tag{5-22}$$

where H is the geometry factor, a is the crack size and J_R is the fracture energy for non-linear materials. If $n = 1 (F = E)$ equation 5-22 reduces to the equation 5-16 for linear elastic materials. The total fracture energy is the addition of the elastic and plastic fracture.

$$G + J_R = J_{Tot}$$

or (5-23)

$$\frac{\beta^2 \sigma^2 \pi a}{E} + \frac{H \sigma^{n+1} a}{F} = J_{Tot}$$

Fracture will occur when the stress σ exceeds a critical value that satisfies equation 5-23. For most real materials, the plastic term is much larger than the elastic term (Mullier *et al.*, 1987). Therefore the elastic term is negligible and the fracture stress σ_f can be approximated by

$$\sigma_f = \left(\frac{F J_R}{H a} \right)^{1/(n+1)} \quad (5\text{-}24)$$

It must be noted that the fracture stress σ_f is a tensile stress and must be changed to an unconfined yield strength f_c, by equation 5-7, for the purpose of this research.

The basis of the new model for evaluating cake strength is given by equation 5-24. The fracture stress is analogous to the tensile stress of the material. This parameter as defined by fracture mechanics is a bulk property. It must be considered that there may not exist a bridge between every adjacent particle. Thus the tensile stress is defined as the single bridge strength. The bulk tensile strength is determined by multipling the bulk tensile strength by the coordination number of the particles. The probability of a bridge existing is determined from X-ray tomography images. Using X-ray tomography a three dimensional figure is constructed of the caked sample. The figure is sliced along the x, y, and z planes. The bridges appear as the gray matter between particles, as illustrated in figure 5-3. Each slice is analyzed and the probability P_b of a bridge existing between particles is given by ratio of the number of contacts with a bridge to the total number of contacts.

Figure 5-3. X-ray tomography slice of caked sodium carbonate.

The existence of a bridge does not mandate that it will contribute to the unconfined yield strength. It is postulated that only the major forces within the shear zone influence the strength. Thus the probability of shearing across a major force P_f must also be considered. A value of P_f=1 would represent the breakage of all bridges in the shear zone.

Combining the probabilities of bridge existence and failure with equations 5-7 and 5-24 the unconfined yield strength f_c of a caked material can be written as

$$f_c = \sigma_{f,tot} \frac{1+\sin\phi}{1-\sin\phi} \tag{5-25}$$

where

$$\sigma_{f,tot} = \bar{\sigma}_f \frac{n_1 n_2}{2} P_b P_f \tag{5-26}$$

where $\overline{\sigma}_f$ is the average fracture stress of a bridge, P_b is the probability that a solid bridge will form between the particles, n_1 is the number of layers in the shear zone and n_2 is the total number of possible contacts in one layer of the shear zone. The average fracture stress is used in equation 5-26 because of the distribution particle sizes.

Model Parameters

The parameters of the model given in equation 5-25 are calculated in the proceeding sections.

Calculating the narrowest width of the bridge as a function of the bridge volume

Similar to Tanaka's derivation, a model of contacting spheres with pendular water is used for the geometrical calculations. Figure 5-1 shows the model of two contacting spheres with the same radius *R*. Circles of radius *r* represent the boundary of the pendular water with surrounding air. The volume of water at one contact point is *V*. The smallest radius of the bridge is b. The terms *b* and *V* are calculated in terms of *R* and θ as shown in equations 5-28 and 5-29.

$$r = \frac{R(1-\sin\theta)}{\sin\theta} \tag{5-27}$$

$$b = (R+r)\cos\theta - r = R\left[1 - \frac{(1-\cos\theta)}{\sin\theta}\right] \tag{5-28}$$

$$V = 2\left[\int_0^{\theta} \pi\{(R+r)\cos\theta - r\cos\alpha\}^2 r\cos\alpha d\alpha - \int_{\theta}^{\frac{\pi}{2}} \pi R^3 \cos^3\theta d\theta\right] \tag{5-29}$$

It is important to establish a link between the smallest radius of the bridge *b* and the volume of water at a contact *V*. The smallest radius of the bridge *b/R* is related to the volume V/R^3 by the parameter θ. This relationship is plotted on a logarithmic scale in figure 5-4 and is given by:

$$\frac{b}{R} = 0.69\left(\frac{V}{R^3}\right)^{0.24} \tag{5-30}$$

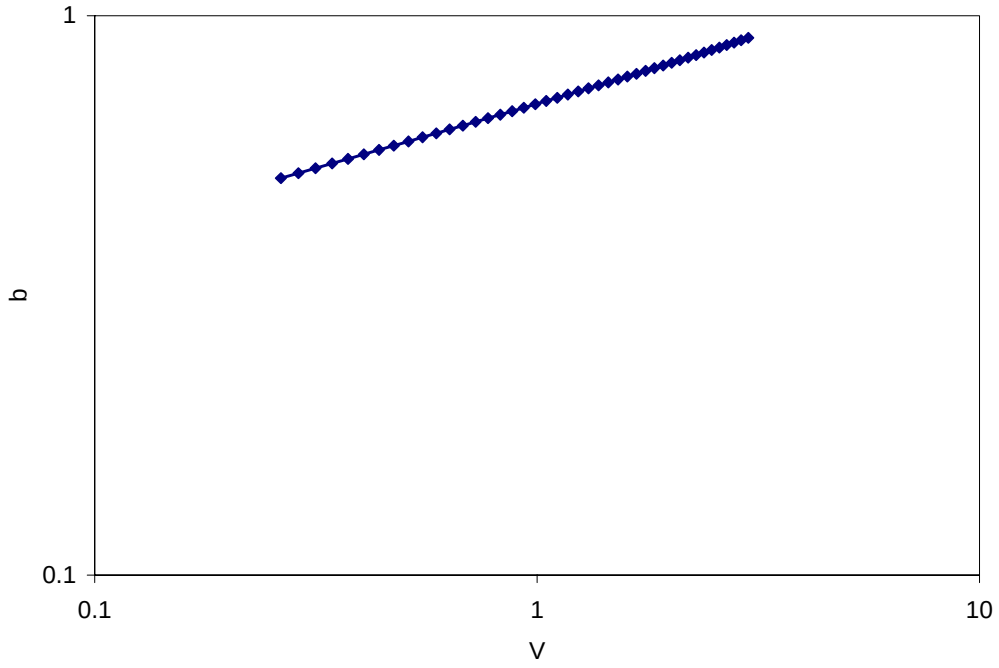

Figure 5-4. Logarithmic plot of the smallest radius of the bridge b vs. the volume of the bridge V.

The volume of water at a contact V is a function of the total volume on the surface of a single particle V_t and the coordination number k_o. If it is assumed that the coordination number k_o is inversely proportional to the porosity ε, then the volume of a contact is given by equation 5-5 (Rumpf, 1958). The initial total volume V_{to} can be expressed in terms of the moisture content of the material q.

$$V_{to} = qV_p\frac{\rho_c}{\rho_w} = \frac{8\pi}{3k_0}R^3 q\frac{\rho_w}{\rho_c} \tag{5-31}$$

where V_p is the volume of the particle ($4/3\pi R^3$), and ρ_w and ρ_c are the densities of the cake and water, respectively. Thus the initial total volume at a contact V_{to} is given in terms of the particle radius, moisture content, coordination number and densities.

The volume calculated in equation 5-31 is for a liquid bridge. For the case of caking, the heat and mass transport in the system must be considered. As a bridge forms there will be evaporation of water from the bridge and dissolution of the particle surface. Thus equation 5-30 becomes

$$\frac{b}{R} = 0.69\left(\frac{V_{sb}}{R^3}\right)^{0.24} \tag{5-32}$$

where V_{sb} is the volume of the solid bridge. The dissolution rate of the solid and vaporization rate of the water must now be included in the calculation of the volume of a solid bridge. The dissolution rate is given by

$$\frac{dw}{dt} = k_d\left(C_e - C\right) \tag{5-33}$$

where w is the weight of the dissolved solid, k_d is the mass transfer coefficient for dissolution, C_e is the equilibrium concentration, and C is the concentration of the dissolved solid. The vaporization rate of the water is given by

$$-\frac{dV}{dt} = k_v\left(H_w - H\right) \tag{5-34}$$

where k_v is the drying rate, H_w is the saturation humidity of the air and H is the absolute humidity. The concentration may be written as a function of the volume of water at a contact.

$$C = \frac{w}{V} \tag{5-35}$$

Differentiating equation 5-35 with respect to V gives

$$\frac{dw}{dV} = C + V\frac{dC}{dV} \tag{5-36}$$

From equations 5-33 and 5-34 the relationship between the weight of the dissolved solid and the volume of water at a contact is written as

$$\frac{dw}{dV} = \frac{k_d\left(C - C_e\right)}{k_v\left(H_w - H\right)} \tag{5-37}$$

Combining equations 5-36 and 5-37 gives the concentration of the dissolved solid as a function of the volume of water at a contact.

$$\frac{dC}{dV} = \frac{1}{V}\frac{k_d\left(C - C_e\right)}{k_v\left(H_w - H\right)} - \frac{C}{V} \tag{5-38}$$

Equation 5-38 is solved for the initial conditions of t=0, V=V_{to} and C=0.

$$V = V_{to}\left[\frac{XC_e - \left(X-1\right)C}{XC_e}\right]^{1/(X-1)} \tag{5-39}$$

where X=k_d/k_v(H_w-H) and assumed to be constant. If it is assumed that the solids stop dissolving when the equilibrium concentration is reached then C=C_e and V=V_e and equation 5-39 becomes

$$V_e = V_{to}X^{1/(1-X)} \tag{5-40}$$

and the volume of the crystal bridge is written as

$$\frac{V_{sb}}{R^3} = \frac{C_eV_e}{\rho_bR^3} = \frac{C_eV_{to}}{\rho_bR^3}X^{1/(1-X)} \tag{5-41}$$

The final form of the relationship between the smallest bridge radius and the volume of the bridge is given by substituting equations 5-32 and 5-31 into 5-41.

$$\frac{b}{R} = 0.69\left(\frac{8\varepsilon}{3}\frac{\rho_w\rho_p}{\rho_b}qC_eX^{1/(1-X)}\right)^{0.24} \tag{5-42}$$

Calculating the length of the crack

The length of the crack is an important parameter in determining the fracture stress of the material. It is a function of the particle radius *R* and the smallest radius of the bridge *b*. Thus the fracture stress dependence on particle size is established in this parameter. The crack size is defined as the void space between the bridges in an assembly of particles as shown in Figure 5-4. From the figure it can be seen that the length of the crack can be expressed as

$$a = 2R - b \tag{5-43}$$

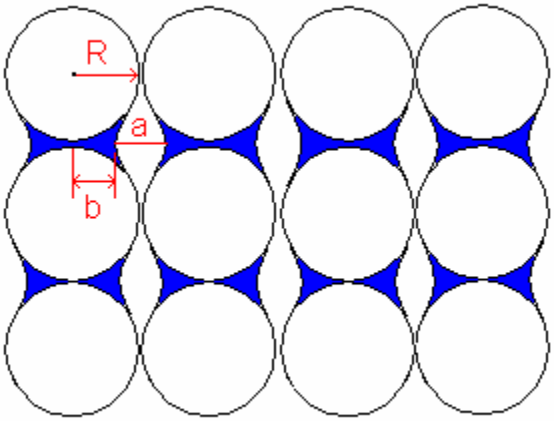

Figure 5-4. Schematic of an agglomerate showing the length of the crack *a*.

Stress-Strain parameters *F* and *n*

The stress-strain curve is assumed to be nonlinear due to the plastic deformation in the crack zone during fracture and can be estimated by the Ramberg-Osgood model, equation 5-21. The parameters of the curve are found by plotting the stress vs. strain on a log scale where the slope of the line is *n* and the intercept is *F*. The stress-strain curve for sodium carbonate is shown in figure 5-5. The stress-strain curve is measured using an MTS Alliance™ RT 30kN. A tablet is made with the dimensions of 23mm in diameter

and 90mm in height. The load applied to the tablet and the displacement of the cross beam is recorded as the tablet is compressed at a constant velocity.

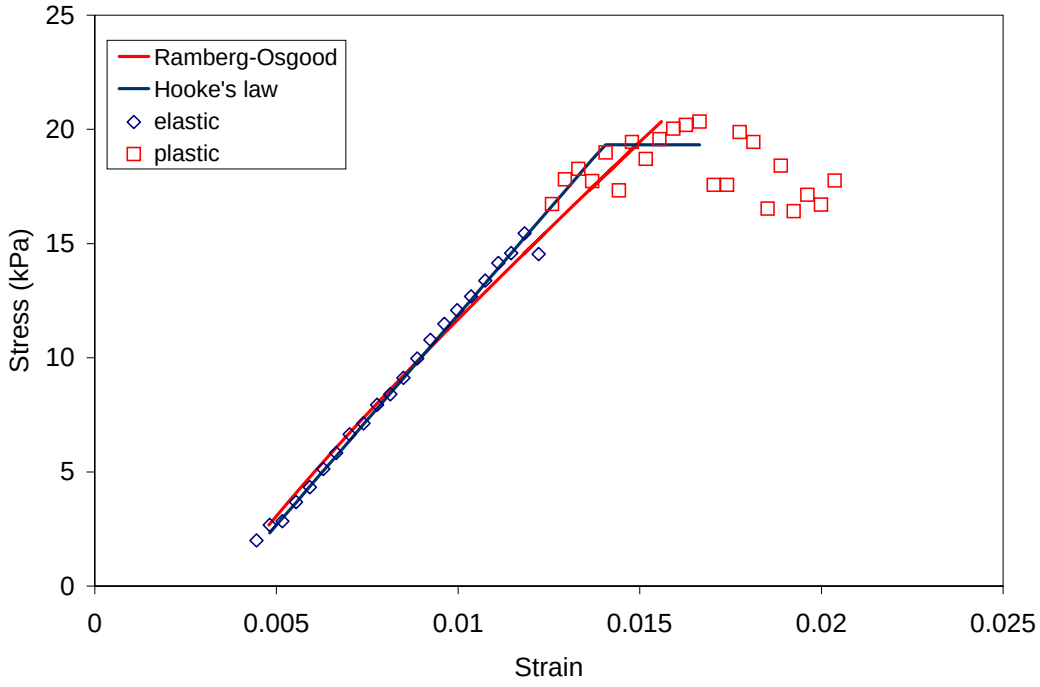

Figure 5-5. The stress-strain curve for a sodium carbonate tablet.

From figure 5-5, the plastic modulus F and strain hardening exponent n are found to be 4604 kPa and 0.834, respectively. It can be seen in figure 5-5 that the stress-strain curve for sodium carbonate is approximately linear. This implies that there is little plastic deformation during failure. The stress-strain data of sodium carbonate is fitted with Hooke's law and the Ramberg-Osgood model. Both models produce an adequate fit and therefore are equally applicable for determining fracture parameters.

The stress-strain curve for lactose in the form of infant formula (Nestle Good Start) is shown in figure 5-6. It can be seen the there is plastic deformation and the Ramberg-Osgood equation is a good predictor of the material response.

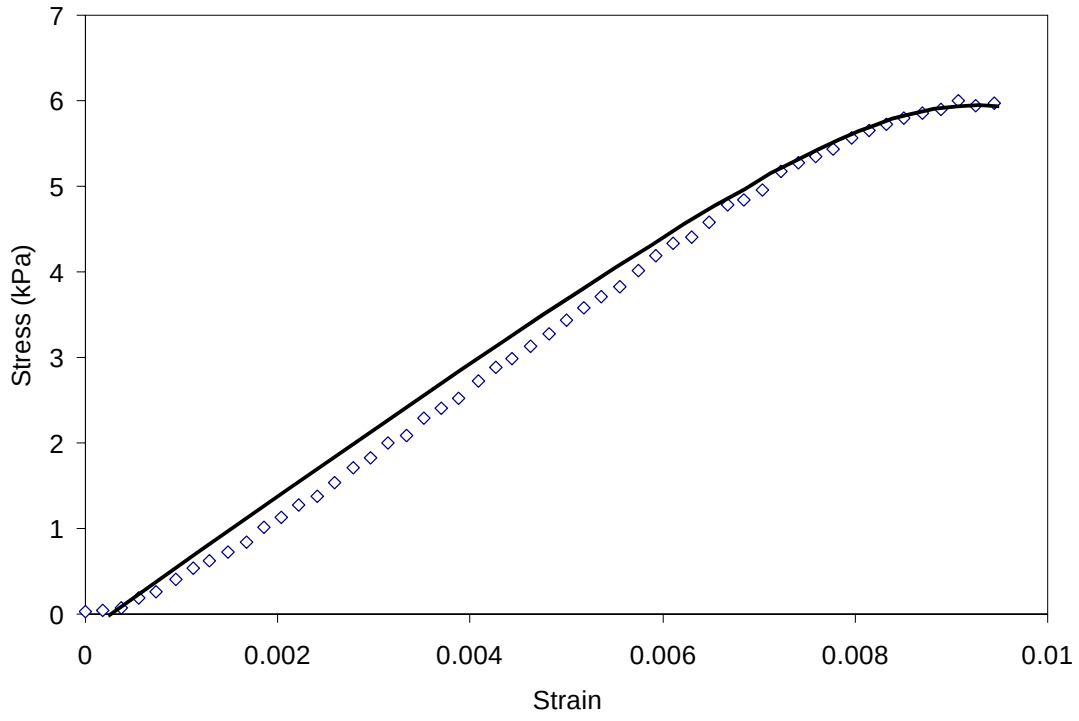

Figure 5-6. Stress-strain curve for lactose.

Geometry of the agglomerate - calculating *H*

The geometry factor H is dependent on the crack size, the width of the sample and the strain hardening exponent n. This factor has been calculated for various geometries and n-values for elastic fractures. It can be assumed that H is a function of the linear-elastic geometry factor β for small values of n and a (Broek, 1988).

$$H = \pi\beta^{n+1} \tag{5-44}$$

Comparison of the Model with Experimental Data

Effect of Particle Size

The effect of particle size on the strength of granular materials has been widely researched. As stated previously, Rumpf was the first to theorize that the particle size influences the strength of a powder. He stated that the particle size is inversely proportional to the tensile strength of the powder assuming that the porosity and the

strength of the interparticle bonds are known, equation 5-1. This equation implies that the strength increases as the particle size decreases. Because Rumpf's model is formulated for the tensile strength of a material it must be modified by equation 5-7 to compare with unconfined yield strength data. Qualitatively, the data for sodium carbonate correlate with this theory as shown in Figure 2-11. From this figure, it can be seen that the unconfined yield strength decreases as a function of an increase in the mean particle diameter of the sodium carbonate as measured by the Johanson Indicizer. However, when fitting Rumpf's model, there is not a good agreement with the data. It is shown in figure 5-7 that the model estimates the trend of the data but the magnitude is incorrect. Rumpf's model fails not only because of the incorrect functionality of particle size but also because of the assumption of simultaneous bridge failure.

The fracture mechanics model created by Kendall and Adams is also used to explain the dependency of particle size. This model is given in equation 5-15 but must also be modified by equation 5-7 for the comparison of the unconfined yield strength results. In equation 5-15 it is stated that the strength of the cake is inversely proportional to the square root of the particle diameter. Figure 5-7 shows approximations of the yield strength using the models of Rumpf and fracture mechanics. It can be seen that the fracture mechanics model gives an accurate estimation of the unconfined yield strength as a function of particle size. This correlation between experimental data and the models is verified by Kendall (1988). He found that the strength of titania powder varied with the particle diameter according to the theory of fracture mechanics.

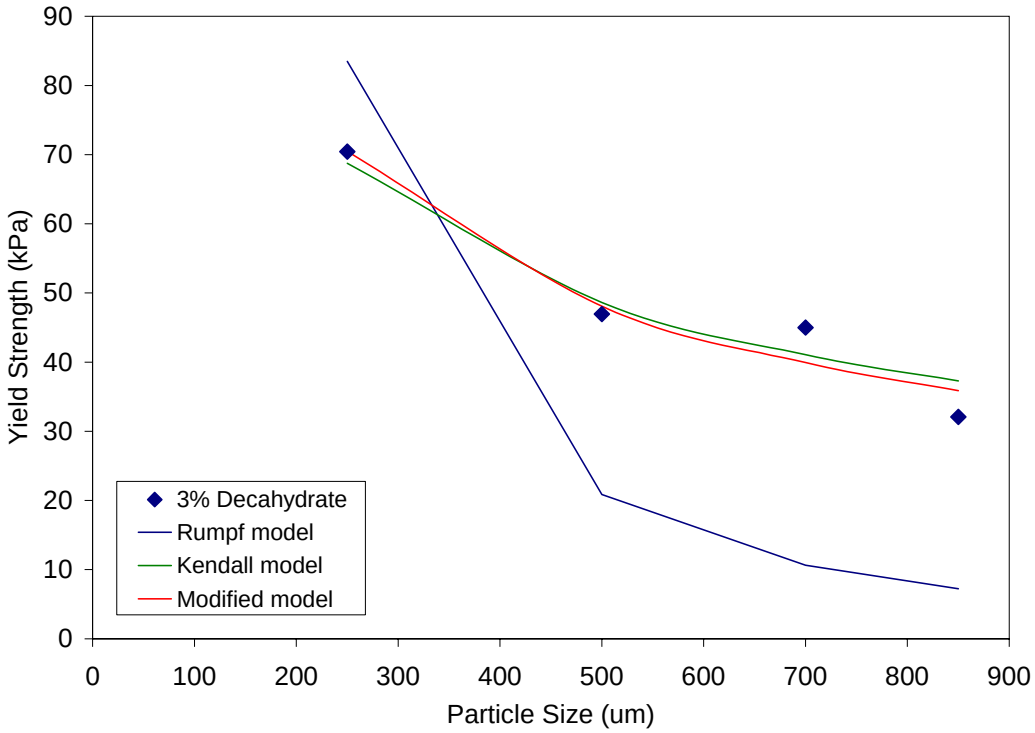

Figure 5-7. Yield strength of sodium carbonate as a function of particle size. The data is fitted with the models of Rumpf and Kendall.

The new model proposed in equation 5-25 is also fitted to the data as shown in figure 5-7. It can be seen that the model agreement with the data only slightly differs from the Kendall model. This can be attributed to the fact that the stress-strain curve for sodium carbonate shown in figure 5-5 shows that there is little plastic deformation during failure. Thus the LEFM model adequately predicts the cake strength. This implies that plastic deformation during failure is not significant to the cake strength of crystalline material. However, for most materials there is significant plastic deformation during failure. This is demonstrated by the stress-strain curve for lactose (Nestle Good Start Infant formula). In this case, the modified fracture mechanics model is a better predictor of the strength.

Effect of Moisture Content

In many of the models the moisture content is the determining factor of cake strength. This is first stated by Rumpf in his model for solid bridges as he assumes that the mean volume fraction is equal to the mean cross sectional fraction. Thus the strength dependence on particle size becomes a secondary affect to the primary influence of moisture content. The unconfined yield strength of sodium carbonate as a function of the moisture content is shown in figure 5-8. The data are fitted with the models of Rumpf and Tanaka. The latter suggests that the strength will plateau at a particular moisture content. This implies there is a critical moisture content after which the strength will not further increase.

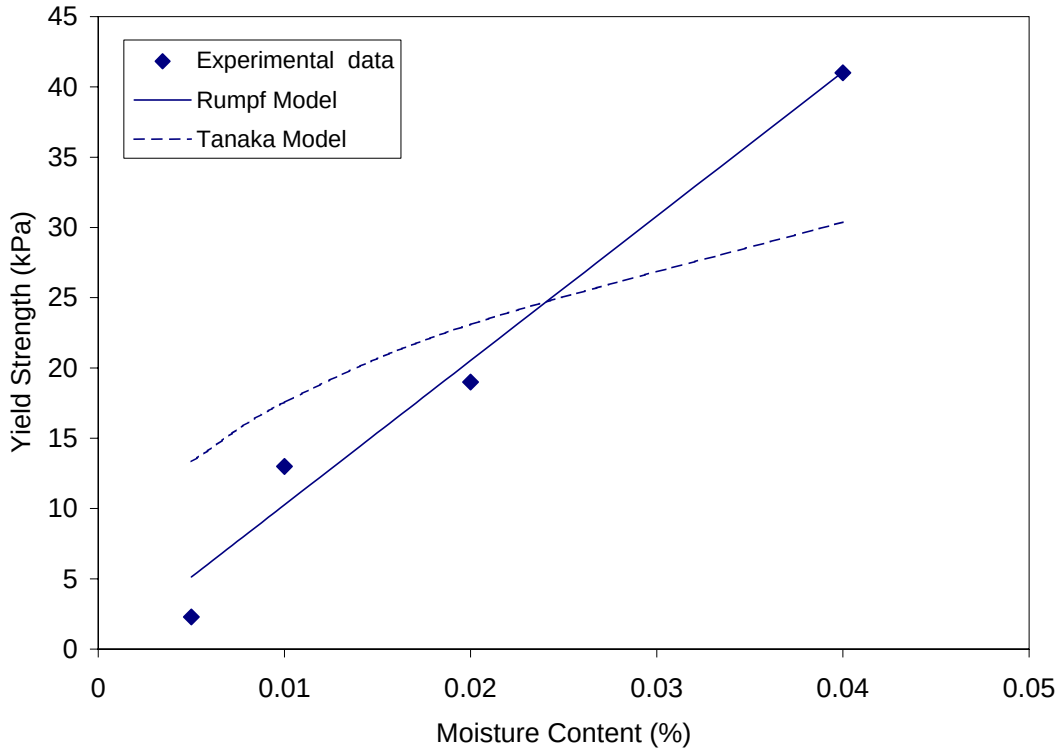

Figure 5-8. The yield strength of sodium carbonate as a function of moisture content. This data is fitted with the models of Rumpf and Tanaka.

It can be seen in figure 5-8 that Rumpf's model is a better predictor than Tanaka's model. This can be attributed to the varying significance of the moisture content in each model. In equation 5-5 Tanaka suggests that the strength is proportional to the square root of the moisture content. Rumpf's model suggests that the strength is directly proportional to the moisture content of the material.

Effect of Consolidation Stress

Although the current models are adequate predictors of cake strength as a function of particle size and moisture content, there exists no model which incorporates all the variables affecting caking. Also lacking in the current models is the effect of the consolidation stress on cake strength. It is shown in chapter 2, that the unconfined yield strength increases by a factor of three with an increase in the consolidation stress. This observation may be explained with the following theories: an increase in the contact area, an increase in the true contact area, and an increase in the number of contact forces due to an increase in the consolidation stress.

Both Rumpf's and Tanaka's models assume only point contacts between the particles. However, it has been shown by Hertz (Briscoe, 1987) that the size of the contact zone varies with the consolidation stress.

$$A = \left(\frac{3LR}{4E} \right)^{1/3} \tag{5-45}$$

where A is the radius of the contact area, L is the stress, R is the radius of the particle and E is Young's modulus. The change in contact area yields a displacement δ (or deformation) of the particle within the contact zone as illustrated in figure 5-9.

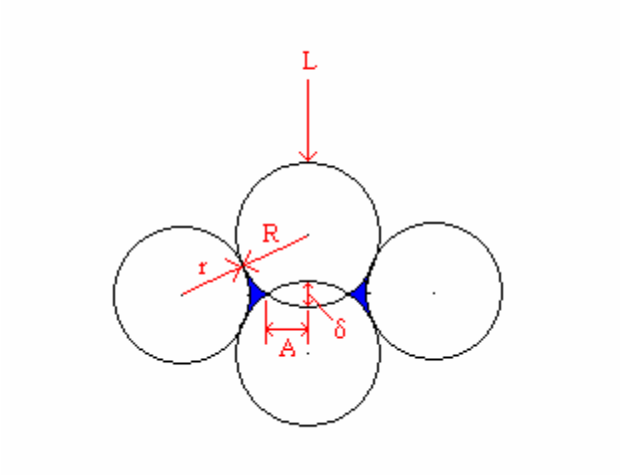

Figure 5-9. Illustration of Hertz contact model

The displacement δ is defined as the Hertz contact radius squared divided by the radius of the particle.

$$\delta = \frac{A^2}{R} = \left(\frac{3L^2}{4E^2R}\right)^{1/3} \tag{5-46}$$

According to the Hertz theory the contact area increases as the consolidation stress increases. Consequently the length of the crack a (Figure 5-4) may vary. The crack length is a function of the particle radius R and the smallest radius of the bridge b. While the particle radius remains constant with an increase in stress, the bridge radius may change due to a change in volume V. Thus varying the contact area has a direct effect on the relationship between the bridge radius b and the volume of the bridge V. The fracture stress of the material is dependent on the bridge radius b thus affecting the unconfined yield strength of the material. The curvature of the bridge which is approximated with equation 5-27 is modified to include the Hertz theory.

$$r = \frac{R(1-\sin\theta) - \frac{\delta}{2}}{\sin\theta} \tag{5-47}$$

Equation 5-47 is used in equations 5-28 and 5-29 to calculate the bridge radius and volume using Hertz's contact model. It can be seen in Figure 5-10 that the bridge radius changes only slightly with the inclusion of Hertzian contact. This suggests the applied consolidation stress does not significantly effect the yield strength with a Hertzian contact model.

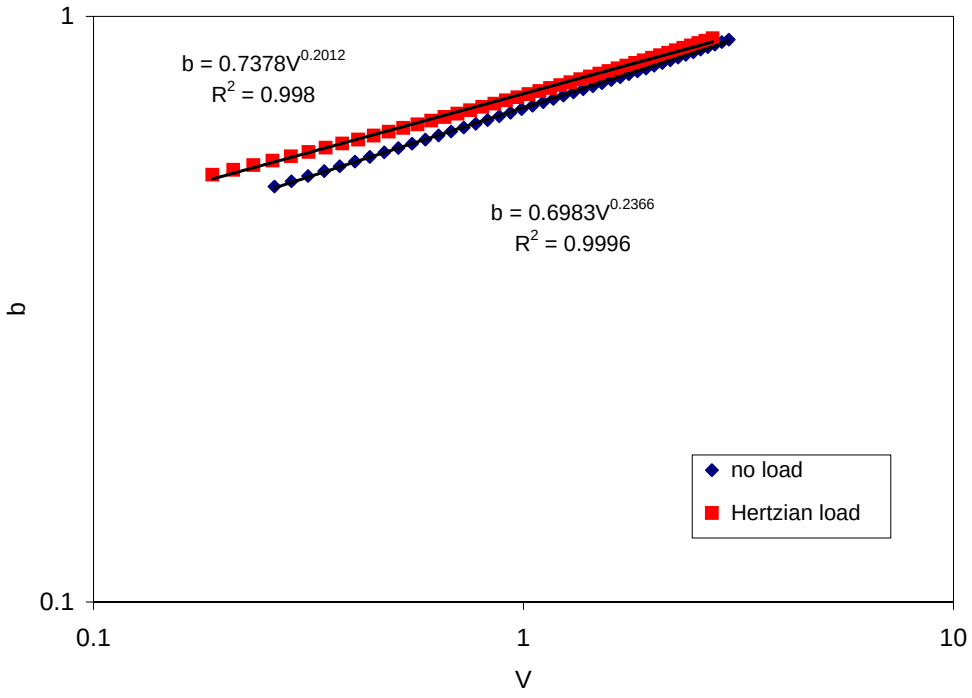

Figure 5-10. The volume of a bridge using the Hertzian contact model.

The Hertzian contact model applies to smooth elastic particles. However most materials are not perfectly smooth but have a rough particle surface. Because of the surface roughness, the true contact area is usually much smaller than the apparent contact area (Persson, 2000). It has been observed that changes in the true contact area have an effect on the mechanical properties of powders (York *et al.*, 1973). York *et al.* postulated that the changes occur due to melting at the asperities where the particles actually touch. Under a load, high pressures develop at the asperities, which subsequently lower the

melting point of the material. The Skotnicky thermodynamic equation is used to determine the change in the melting point. At the contact points the material can melt due to the high stress and solid bonds are formed when the material resolidifies. These new bonds cause an increase in the strength of the material. Consequently, a change in the true contact area due to compression of the material can have an effect on the cake strength. However, the applicability of this model is limited to dry materials.

During a caking event solid bridges are formed between the particles. The size of a bridge depends on the volume of water at the contact. If the water volume fills the space between the asperities, it is likely that the asperities will dissolve and become a part of a large bridge. This can be seen in the X-ray tomography picture in Figure 5-3. The solid bridges in the contact zone are of the same magnitude as the particle size which indicates that a surface area larger than the asperity size was wetted during caking.

In this work a model is proposed for the increase in cake strength as a function of consolidation stress based on the distribution of contact forces within the particle bed. It is believed that not all bridges in the cake contribute to its strength. Instead, it is the distribution of the major contact forces within the shear zone that dictate the strength. When a consolidation load is applied to a material the stress between the particles not only increase in magnitude but they are also redistributed, creating an increase in the number of major contact forces within the shear zone. The contact forces between the particles are illustrated by the force chains in Figure 5-11. This image is produced from Discrete Element Methods (DEM) modeling as example later in this section. If the major contact forces are redistributed when the consolidation stress on the material increases, then the spacing between the force chains will decrease.

Experimentally this concept is difficult to verify. Therefore Discrete Element Methods (DEM) modeling is used to validate this theory. DEM is a numerical technique which solves engineering problems that are modeled as a large system of distinct interacting bodies or particles that are subject to collective motion. This technique is used to investigate the effects of microscopic mechanical properties on the macroscopic response of the body. The stress-strain response of a material under a load can be simulated to produce the details of structure throughout the loading period.

The Itasca PFC2D software is used to investigate the structure of the force chains within a particle bed. A consolidation load is applied to a bed of particles and the contact forces between the particles are developed. The contact forces between the particles are connected through the contact points creating force chains as shown in Figure 5-11. In this figure the force chain structure for a high load and low load can be seen. The high load is a factor of ten greater than the low load. It can be seen that an increase in the load applied to a material increases the number and magnitude of the force chains. This implies that the spacing between the forces chains decreases and the number of major force chains increases. The increase in the number of major force chains increases the strength of the material.

The term granularity is used to describe the spacing between the major forces contributing to the cake strength. This parameter gives an indication of the size of the particle clusters between each contact force, i.e. the number of particles not associated with a major contact force. A decrease in the granularity implies that there exist a greater number of major force chains. The force chain images, as shown in Figure 5-11, are

analyzed using image analysis to determine the relative spacing between major force chains within the shear zone.

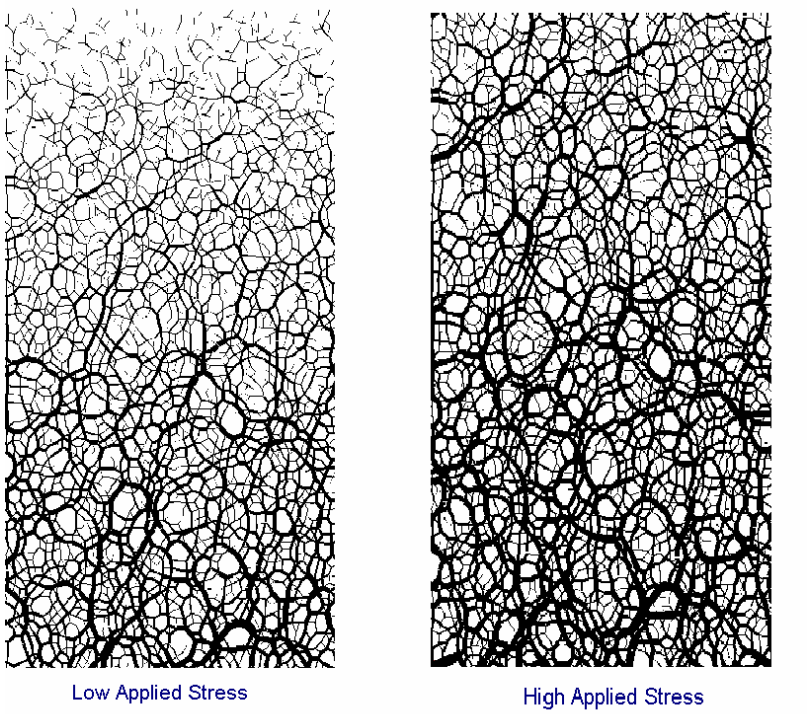

Figure 5-11. Force chain structure in a DEM simulated powder bed with a high applied load (right) and a low applied load (left).

A parametric study is conducted which includes varying the consolidation stress and friction coefficient between the particles. Before determining the granularity each image must be preprocessed to exclude the magnitude of the contact forces and insignificant contact forces which do not add to the strength. The magnitude of a contact force is represented by the thickness of the chains shown in Figure 5-11. The magnitude increases with increasing stress as illustrated by an increase in the thickness of the lines at each load. At higher loads, the increased chain thickness reduces the spacing between the chains, thus influencing the granularity. To eliminate this artifact each chain is reduced to a unit thickness such that they are consistent through every image. The major force

chains are those which are continuous through the particles until another force chain is contacted. Both ends of the force chain are connected to another force chain. The smaller contact forces not contributing to the strength are eliminated by introducing a threshold on the data such that these forces are not included.

After preprocessing, the images are analyzed using an imaging software package, ImageJ, to determine the granularity. There is a distribution of sizes representing the granularity as shown in Figure 5-12. Thus the median granularity is considered at each load.

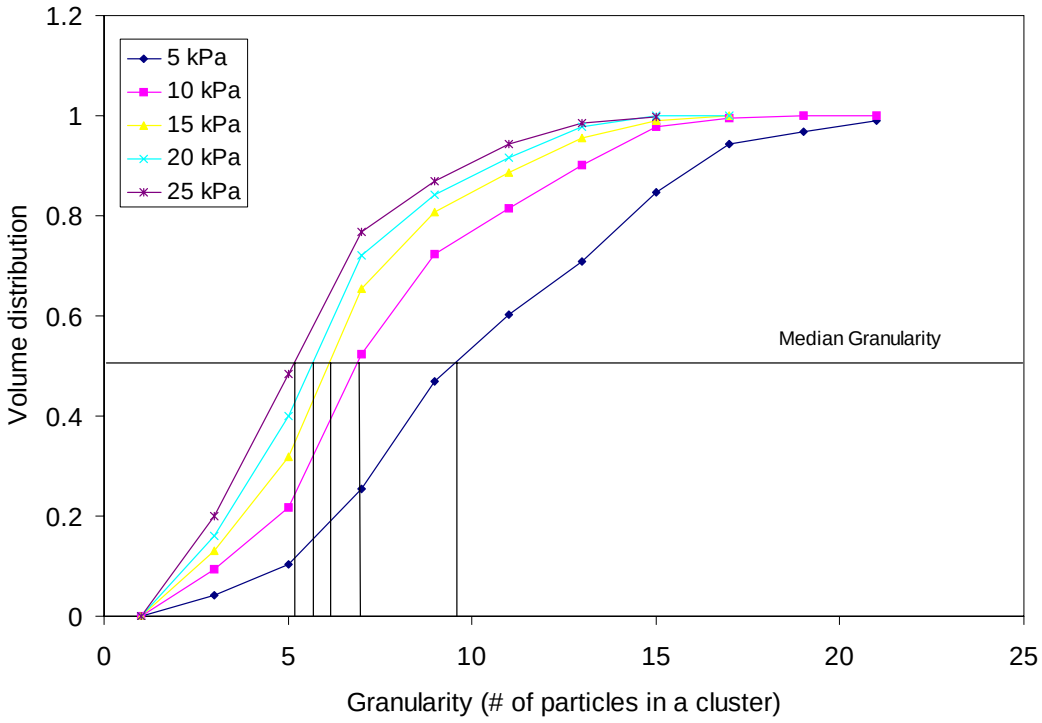

Figure 5-12. The cumulative distribution of the granularity at various consolidation loads.

The d_g, median granularity, is the size which splits the distribution into two equal parts. Half of the particle clusters are above this size and half of the particle clusters are below this size. If the d_g decreases with an increase in load this suggests that the spacing between the force chains decreases. It can be seen in Figure 5-13 that the granularity

decreases with a increase in the consolidation load applied to the material. Thus the granularity is inversely proportional to the unconfined yield strength. It can also be seen in Figure 5-13 that the granularity does change with the coefficient of friction.

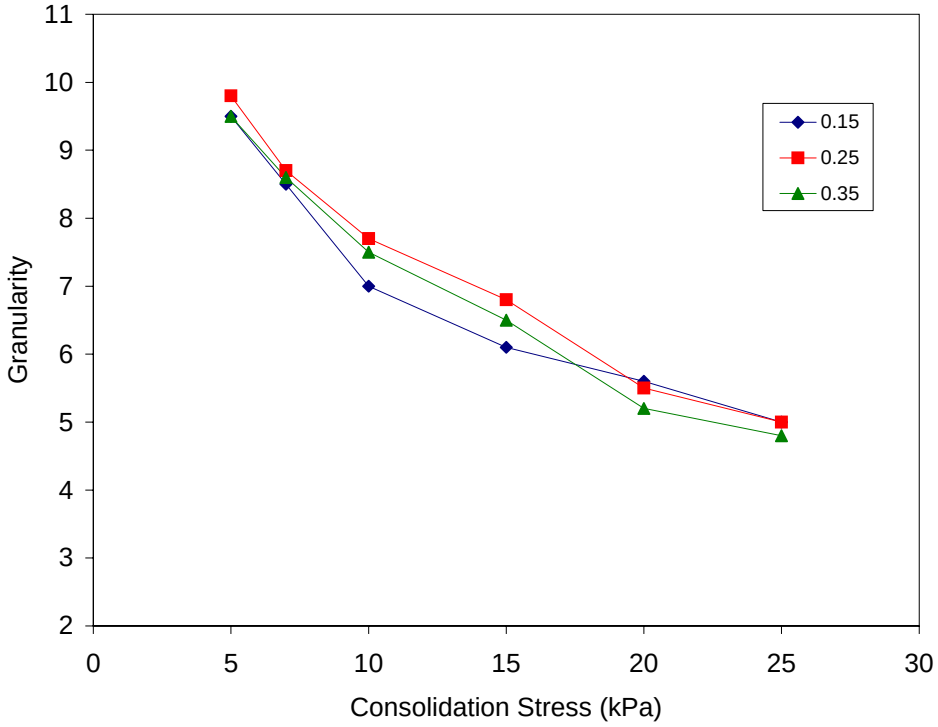

Figure 5-13. Granularity of the major force chains in a particle bed.

The granularity as a function of consolidation stress is related to the unconfined yield strength and incorporated into equation 5-25.

$$f_c = A(d_p, \%H_2O)\left(\frac{d_g}{d_{g_o}}\right)^3 \qquad (5\text{-}48)$$

In equation 5-48 d_{go} is a reference state of granularity. Because the granularity is defined as a length from a two dimensional image, this term must be raised to the third power to represent the volume of the particles. The cube of the ratio of the granularities, d_g/d_{go}, is then proportional to the strength. A approximate comparison of equation 5-48 with the experimental data is given by examining the ratio of strength at a high and low

stress. In chapter 2, the data indicate that the unconfined yield strength increases by a factor of 2.3 when the stress is increased from 10kPa to 17kPa.

$$\frac{f_{c,high}}{f_{c,low}} = 2.3 \tag{5-49}$$

In Figure 5-12 it is shown that the mean granularity d_f decreases by 1.5 when the stress is increased from 10kPa to 15kPa.

$$\left(\frac{d_{f,high}}{d_{f,low}}\right)^3 = 1.5 \tag{5-50}$$

The ratios from the experimental data and DEM simulation are the same order of magnitude. This shows that the concept of the granularity is a probable cause of the unconfined yield strength increasing with consolidation stress. Equation 5-50 is incorporated into the unconfined yield strength equation 5-25 and written in the final form as a function of particle size, moisture content and consolidation stress.

$$f_c = \left[\sigma_{f,tot}\frac{1+\sin\phi}{1-\sin\phi}\right]\left(\frac{d_f}{d_{f_o}}\right)^3 \tag{5-51}$$

Equation 5-51 is compared to experimental data shown in chapter 2. In Figure 5-14 it can be seen that the model predicts the trend of the data however the magnitude is not exact. The could be attributed to the use of spherical particles in the DEM simulations. If non spherical particles are used then the number of contacts would increase. Creating a greater number of force chains. Although the exact magnitude of the data is not predicted, this model provides a good base for the incorporation of strength as function as consolidation stress.

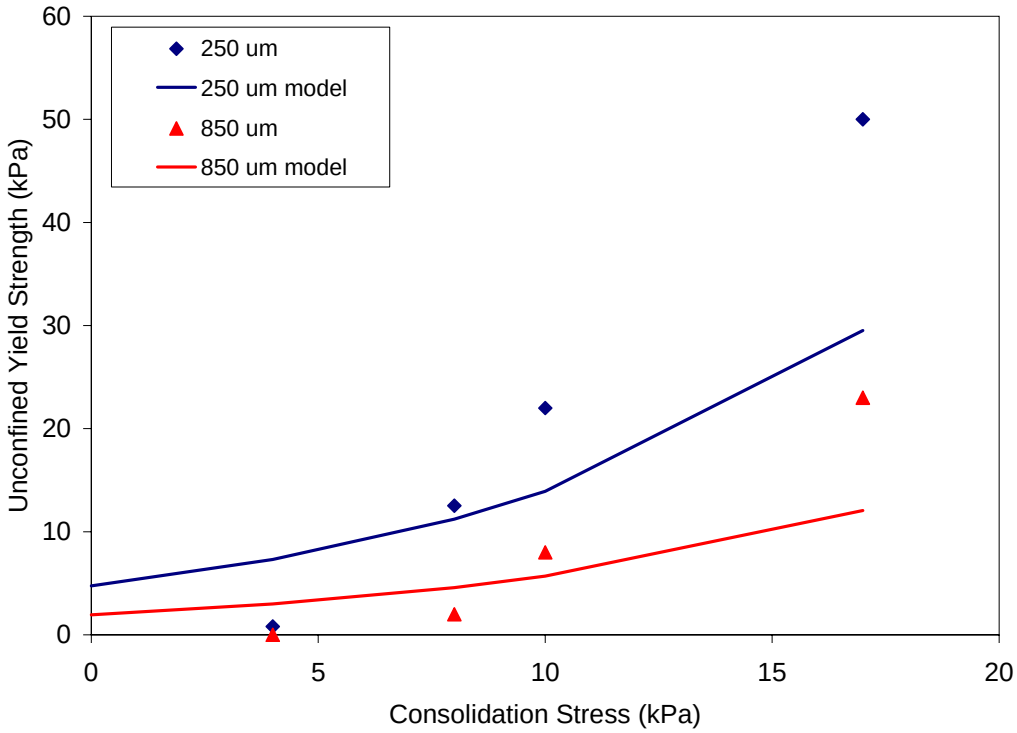

Figure 5-14. Unconfined yield strength as a function of the consolidation stress compared to the model of equation 5-51.

CHAPTER 6
CONCLUSIONS AND FUTURE WORK

The prevalence of granular materials is evident in many industries. Numerous plant operations involve the storage and handling of such materials. Thus the need to characterize and understand the behavior of granular materials is of great importance. The greatest challenge posed with granular materials is the ability to maintain and predict a continuous flow through process equipment. One phenomenon jeopardizing powder flow is powder caking. Powder caking is the process in which free flowing powder converts into agglomerates, preventing or reducing the flow of the powder.

In this research one particular mechanism of caking, moisture migration caking, is investigated. This type of caking involves materials which are soluble or slightly soluble in water. Moisture migration caking can be defined as the process by which free flowing materials are transformed into lumps and agglomerates due to changes in atmospheric or process conditions. An example of an atmospheric change is the temperature cycle from day to night. An example of a change in process condition is the introduction of warm material into a cold storage container. Caking is a time induced event, i.e., the longer a material is stored or not flowing the greater the likelihood of caking.

There are many variables that influence a caking event and the bulk cohesive strength of a caked material such as the particle size, consolidation stress, moisture content, relative humidity and time. Other researchers have studied the influence of some of these variables. However there lacks a complete understanding of the caking process

and the existence of a complete mathematical model which predicts the bulk cohesive strength of caking.

Several of the variables influencing the bulk cohesive strength are investigated in this research. The Johanson Indicizer® and the Schulze Shear cell are used to measure the unconfined yield strength as a function of particle size, moisture content, relative humidity and consolidation stress. The experimental work shows that an increase in the investigated variables causes an increase in the unconfined yield strength of the material. The measured data are used to verify the current strength models proposed by other researchers.

Rumpf (1958) proposed a theory to calculate the tensile strength of a material as a function of the particle size and moisture content. Later Kendall and Adams (1985) disputed the function of particle size and proposed a new theory based on fracture mechanics principles. It is shown in this dissertation that the model proposed by Kendall and Adams gives a better prediction of the strength. However it should be noted that the model by Kendall and Adams was developed for linear elastic materials, an ideal case. The models proposed by Rumpf and Kendall define the state of the art in regards to predicting cake strength. These models do not include an important variable which has a significant influence on the cake strength, consolidation stress.

In this dissertation a new model is presented to predict the unconfined yield strength as a function of the caking parameters: particle size, moisture content and consolidation stress. The elastic assumption made by Kendall is extended to include materials that exhibit plastic deformation during failure. Elastic-plastic fracture

mechanics principles are used to include the particle size in the caking model. Therefore this new model should be able to predict caking in a plastic system as well.

The impact of consolidation stress on the unconfined yield strength is determined using Discrete Element Method (DEM) modeling. It is proposed that increasing the consolidation stress increases the major force chains within the particle bed. This is shown by an analysis of the force chain structure in a particle bed after a consolidation load is applied. Using the images from the DEM simulation, the granularity of a powder bed is determined. The granularity is defined as the spacing between the major force chains. It is shown that the granularity is a function of the consolidation stress and is inversely proportional to the unconfined yield strength of the material. At lower consolidation stresses the granularity is larger than at higher consolidation stresses. The granularity function is incorporated into the new model for predicting the cake strength. It is found that the proposed caking model accurately predicts the trend of the unconfined yield strength and its magnitude is within 25% of the experimental data.

In order to initiate a moisture migration caking event, there must be a change in the water vapor content surrounding the particles. Thus the heat and mass transport in the system is an important factor in this type of caking. The migration of moisture through a particulate bed is also investigated. COMSOL Multiphysics, a commercial software, is used to describe the moisture migration with a finite element analysis. Many of the moisture migration models in literature suggest that free convection in the system is negligible. However, it is found in this research that the free convection plays a significant role in the heat and mass transport of the system. It is shown that the free convection speeds up the heat transfer process. This suggests that the storage life of a

material prone to caking is shorter due to faster transport processes. The adsorption isotherms and kinetics of moisture uptake of the material are also included in this analysis. The solids moisture content is determined after the material is exposed to a change in temperature. This data is used to predict the strength of the material using the model proposed in this research. The change in solids moisture content throughout a caking event is used to determine the increase in unconfined yield strength. An 18% increase in strength was predicted from the moisture migration analysis compared to a 40% increase observed with the experimental data. From this comparison, it can be concluded that the proposed model for cake strength combined with a moisture migration analysis can be used to estimate the unconfined yield strength of a material using the powder material properties and the process parameters.

Suggestions for Future Work

In this study one caking mechanism is investigated. To complete the understanding of caking the other caking mechanisms have to be investigated as well. The moisture migration analysis only included the kinetics of adsorption and desorption. When the moisture evaporates from the particle crystal bridges are formed. Thus this analysis can be extended to also include the kinetics of crystallization. The amount of moisture adsorbed by the particles are determined from the adsorption isotherm of the material. However this can also be predicted by estimating the amount of water vapor adsorbed by the particles using DEM simulations and a thin film approximation.

The DEM simulations in this research are simplified. The simulations are in two dimensions and the particles are spherical. The two dimensional simulations can be extended to three dimensions. The two dimensional simulations are qualitatively reliable i.e. it is possible to predict trends. However, the two dimensional simulations may not be

quantitatively reliable in predicting the actual values. The three dimensional simulations along with the incorporation of non spherical particles may provide a more accurate prediction of the granularity and unconfined yield strength.

The adhesion force model used in this research is the Hertzian contact model. However the proposed cake strength model should be included in these simulations. The DEM code should also include the rate of change of mass to determine the amount of material that will dissolve and contribute to caking and also the rate of crystallization to determine the crystal bridge formation. The moisture migration analysis can be incorporated into DEM simulations. Combining an improved moisture migration analysis with three dimensional DEM simulations would give a more complete and continuous analysis of cake strength.

APPENDIX A
NOMENCLATURE

β	Geometry factor of fracture mechanics
δ	Hertzian displacement
Γ	Interfacial energy
Γ_c	Fracture energy
ε	Porosity
ε_c	Porosity of recrystallized bridge
θ	Indicizer® cell angle
λ_s	Thermal conductivity
ν	Poisson's ratio
ρ	Density of solid
ρ_a	Denisty of gas phase
ρ_b	Denisty of the bulk
ρ_c	Density of cake
ρ_k	Density of dissolved species
ρ_s	Density of salt
ρ_w	Density of water
σ	Stress
σ_1	Major principle stress
σ_3	Minor principle stress
σ_{Ds}	Compressive strength of solid bridge

σ_f	Fracture stress
σ_k	Tensile strength of crystal bridge
$\bar{\sigma}_k$	Mean tensile strength of crystal bridge
σ_t	Tensile strength
τ	Shear stress
φ	Internal angle of friction
a	Length of crack (flaw)
A	Hertzian contact radius
A_{sp}	Specific transfer area
b	Narrowest width of bridge
c_{pa}	Specific heat of air
c_{ps}	Specific heat of solid
C	Concentration
C_e	Equilibrium concentration
d	Diameter of contact zone
d_p	Particle diameter
d_{50}	Mean particle diameter
D	Diffusion coefficient
D_e	Effective mass diffusivity
D_i	Inner piston diameter
D_l	Lower piston diameter
E	Young's modulus
E^*	Effective Young's modulus

F	Plastic modulus
f_c	Unconfined yield strength
F_a	Flow rate of inlet air
d_f	Median granularity
g	Gravity
$g(L)$	Granularity as function of consolidation stress
G	Elastic energy release rate
H_v	Enthalpy of water vaporization
H_w	Saturation humidity of air
J	J-integral
J_R	Fracture energy for EPFM
J_{Tot}	Total fracture energy
k	Heat transfer coefficient
k_f	Mass transfer coefficient
k_d	Dissolution rate
k_v	Drying rate
K_h	Parameter for humidity cycling model of cake strength
K	Stress intensity factor
K_c	Critical stress intensity factor
k_o	Coordination number
L	Applied load (consolidation stress)
m_{solid}	Mass of solid
M_p	Mass of agglomerate

M_s	Mass of salt
mw_{air}	Molecular weight of air
mw_{water}	Molecular weight of water
n	Strain hardening exponent
n_1	Number of shear layers
n_2	Number of contacts in a shear layer
N	Number of humidity cycles
p_{H2O}	partial pressure of water vapor
p_T	Total pressure
P	Consolidation load
P(b)	Probability of a bridge existing between particles
P(f)	Probability of a bridge contributing to the yield strength
q	Solids moisture content
q_E	Equilibrium moisture content
q_o	Initial moisture content
q_{tot}	Total moisture content
Q	Heat flow rate
R	Radius of sphere
R_c	Cleavage resistance
R_c^*	Effective cleavage energy
S	Surface area of the shear zone
t	Time
T_g	Glass transition temperature

V	Volume of water in liquid bridge
V_e	Volume at equilibrium
V_f	Stress function of unconfined yield strength
V_{sb}	Volume of solid bridge
V_s	Volume of bulk caked sample
V_t	Total volume of water possessed by a single particle
V_{to}	Initial total volume of water possessed by a single particle
w	Weight of dissolved solid
X	Heat and mass transport parameter
y_k	Concentration of dissolved species
Y_s	Solubility

APPENDIX B
MOISTURE MIGRATION PARAMETERS

The constants and boundary conditions listed in chapter 4 are calculated as follows.

$$permea = \frac{P\_diam^2 * porosity^3}{150 * (1 - porosity)^2}$$

$$R\_fluid = R\_gas * \left[\frac{c\_init}{(1 + c\_init) * mol\_w} + ((1 + c\_init) * mol\_a) \right]$$

$$c\_sat\_mol\_init = 1000 * \exp\left[a\_a - \frac{b\_b}{T\_init + c\_c} \right] / p\_init$$

$$c\_sat\_init = \frac{mol\_w * c\_sat\_mol\_init}{(mol\_w * c\_sat\_mol\_init) + (mol\_a * (1 - c\_sat\_mol\_init))}$$

$$RH\_init = \frac{c\_init}{c\_sat\_init} * 100$$

$$u\_init = A1 * \exp\left(-B1 * \left(1 - \frac{c\_init}{c\_sat\_init} \right) \right)$$

Constant Temperature

T=0

Axial Symmetry

r=0

Insulated (ht)

$$n \cdot (k \nabla T) = 0$$

Heat Flux

$$n \cdot (k \nabla T) = q_o + h(T_{\inf} + T) + const(T_{amb}^4 - T^4)$$

no slip

u=0

Normal Flow

$$\vec{t} \cdot \vec{n} = 0, \vec{n} \cdot \left(- p\vec{I} + \eta\left(\nabla \vec{u} + \left(\nabla \vec{u}\right)^T\right)\right) = -\vec{n} \cdot p_o$$

Insulated (cd)

$$\vec{n} \cdot \vec{N} = 0; \vec{N} = -D\nabla c + c\vec{u}$$

Neumann Boundary

$$-n \cdot \Gamma = G$$

LIST OF REFERENCES

Adams, M.J. (1985). The strength of particulate solids. Journal of Powder and Bulk Solids Technology, 9(4), 15-20.

Aguilera, J., del Valle, J., and Karel, M. (1995). Caking phenomena in amorphous food powders. Trends in Food Science and Technology, 6, 149-155.

ASTM (1996). Standard practice for maintaining constant relative humidity by means of aqueous solutions. in, Annual book of ASTM standards, no E 104-85. ASTM, West Conshoshocken.

ASTM (2002). Standard shear test method for bulk solids using the Schulze ring shear tester. in, Annual book of ASTM standards, 04.09 no D6773-02. ASTM, Philadelphia.

Brinkman, H.C (1947). A calculation of the viscous force exerted by a flowing fluid on a dense swarm of particles. Applied Science Research. Section A1, 27.

Briscoe, B. J., Adams, M. J. (1987). Tribology in Particulate Technology. Adam Hilger, Bristol, England.

Broek, D. (1974). Elementary Engineering Fracture Mechanics. Noordhoff International Publishing, Leyden, The Netherlands.

Broek, D. (1988). The Practical Use of Fracture Mechanics. Kluwer Academic Publishers, Dordrecht, The Netherlands.

Cleaver, J. A. S., Karatzas, G., Louis, S., Hayati, I. (2004). Moisture-induced caking of boric acid powder. Powder Technology, 146(1-2), 93-101.

Down, G. R. B., McMullen, J. N. (1985). The effect of interparticulate friction and moisture on the crushing strength of sodium chloride compacts. Powder Technology, 42(2), 169-174.

Farber, L., Tardos, G. I., Michaels, J. N. (2003). Evolution and structure of drying material bridges of pharmaceutical excipients: Studies on a microscope slide. Chemical Engineering Science, 58(19), 4515-4525.

Greenspan, L. (1977). Humidity fixed points of binary saturated aqueous solution. Journal of Research of the National Bureau of Standards-A. Physics and Chemistry, 81A(1), 89-96.

Griffith, A.A., (1921). The phenomena of rupture and flow in solids. Philosophical Transactions of the Royal Society of London A, 221, 163-167.

Hancock, B. C., Dalton, Chad R. (1998). The effect of temperature on water vapor sorption by some amorphous pharmaceutical sugars. Pharmaceutical Development and Technology, 4(1), 125-131.

Hancock, B. C., Shamblin, S. L. (1998). Water vapour sorption by pharmaceutical sugars. Pharmaceutical Science & Technology Today, 1(8), 345-351.

Iglesias, H., Chirife, J. (1976). Prediction of the effect of temperature on water sorption isotherms of food material. Journal of Food Technology, 11, 109-116.

Irwin, G.R. (1957). Fracture I. Handbuch der Physik. VI, 558-590.

Jenike, A. W. (1964). Storage and flow of solids. University of Utah, Salt Lake City.

Johanson, J. R. (1992). The Johanson Indicizer® system vs. Jenike shear tester. Bulk Solids Handling, 12(2).

Johanson, J. R., Paul, B. (1996). Eliminating caking problems. Chemical Processing: 71-75.

Kendall, K. (1988). Agglomerate strength. Powder Metallurgy, 31(1), 28-31.

Knight P., J., S. (1988). Measurement of powder cohesive strength with penetration test. Powder Technology, 54, 279-283.

Kuu, W.-Y., Chilamkurti, R., Chen, C. (1998). Effect of relative humidity and temperature on moisture sorption and stability of sodium bicarbonate powder. International Journal of Pharmaceutics, 166(2), 167-175.

Leaper, M., Bradley, M., Cleaver, J., Bridle, I., Reed, A., Abou-Chakra, H., and Tuzun, U. (2002). Constructing an engineering model for moisture migration in bulk solids as a prelude to predicting moisture migration caking. Advanced Powder Technology, 13(4), 411-424.

Leaper, M., Berry, M., Bradley, M., Bridle, I., Reed, A., Abou-Chakra, H., and Tuzun, U. (2003). Measuring the tensile strength of caked sugar produced from humidity cycling. Journal of Process Mechanical Engineering, 217, 41-47.

Mathlouthi, M., Roge, B. (2003). Water vapor sorption isotherms and the caking of food powders. Food Chemistry, 82, 61-71.

Merrow, E.W. (1998). Estimating the startup times for solids processing plants. Chemical Engineering, 95(15), 89-92.

Mullier, A., Seville, J., and Adams, M. (1987). A fracture mechanics approach to the breakage of particle agglomerates. Chemical Engineering Science, 42(4), 667-677.

Nedderman, R.M. (1992). Statics and Kinematics of Granular Materials. Cambridge University Press, Cambridge, UK.

Noel, T.R., Ring, S.G. and Whittam, M.A. Glass transition in low moisture foods. Trends in Food Science and Technology, 1, 62-67.

Perry, R. (1997). Perry's Chemical Engineers' Handbook. McGraw-Hill, New York.

Persson, B.N. (2000). Sliding Friction. Springer, New York.

Pietsch, W. (1969a). The strength of agglomerates bound by salt bridges. The Canadian Journal of Chemical Engineering, 47, 403-409.

Pietsch, W. (1969b). Adhesion and agglomeration of solids during storage, flow and handling- a survey. Journal of Engineering for Industry, 435-.

Purutyan, H., Pittenger, B., and Tardos, G. (2005). Prevent caking during solids handling. Chemical Engineering Progress, 22-27.

Rastikian, K., Capart, R. (1998). Mathematical model of sugar dehydration during storage in a laboratory silo. Journal of Food Engineering, 35, 419-431.

Rennie, P., Dong Chen, X., Hargreaves, C., and Mackereth, A. (1999). A study of the cohesion of diary powders. Journal of Food Engineering, 39, 277-284.

Rumpf, H. (1958). Grundlagen und methoden des granulierens. Chemie-Ing.-Techn., 30(3), 144-158.

Schubert, H. (1981). Principles of agglomeration. International Chemical Engineering, 21(3), 363-377.

Schweiger, A., and Zimmermann, I. (1999). A new approach for the measurement of the tensile strength of powders. Powder Technology, 101, 7-15.

Tanaka, T. (1978). Evaluating the caking strength of powders. Industrial & Engineering Chemistry Product Research & Development, 17(3), 241-246.

Tardos, G. I. (1996). Ingress of atmospheric moisture in bulk powders: Application to caking of fine crystalline powders. Powder Handling and Processing, 8(3), 215-220.

Tardos, G. I., Gupta, R. (1996). Forces generated in solidifying liquid bridges between two small particles. Powder Technology, 87(2), 175-180.

Tardos, G. I., Nicolaescu, I.V., and Ahtchi-Ali, B. (1996). Ingress of atmospheric moisture into packed bulk powders. Powder Handling and Processing, 8(1), 7-15.

Teunou, E., and Fitzpatrick, J.J. (2000). Effect of storage time and consolidation on food powder flowability. Journal of Food Engineering, 43, 97-101.

Teunou, E., Fitzpatrick, J. J. (1999). Effect of relative humidity and temperature on food powder flowability. Journal of Food Engineering, 42(2), 109-116.

Tomas, J. a. S., H. (1982). Modeling of the strength and the flow properties of moist soluble bulk materials. Aufbereitungs-Technik(9), 507-515.

York, P., and Pilpel, N. (1973). The effect of temperature on the mechanical properties of powders: Presence of liquid films. Materials Science and Engineering, 12, 295-304.

Zhang, J., Zografi, G. (2000). The relationship between "BET" - and "Free volume" - derived parameters for water vapor absorption into amorphous solids. Journal of Pharmaceutics, 89(8), 1063-1072.

BIOGRAPHICAL SKETCH

Dauntel Wynette Specht was born in Houston, Texas, on the 23rd of July 1979. She attended Jesse H. Jones high school. After high school, Dauntel enrolled at Trinity University in San Antonio, Texas, where she received a Bachelor of Science in engineering science. Upon graduation from Trinity, she was admitted into the Chemical Engineering Department at the University of Florida. Dauntel will receive her Doctorate of Philosophy in May of 2006.